

Uncovering the Hidden Glycan Structures in Metastatic Melanoma

Jodie Louise Abrahams

BSc (Hons) Biomedical Science, University of Essex

A thesis presented for the degree of

Doctor of Philosophy



MACQUARIE
University

Department of Chemistry and Biomolecular Sciences
Macquarie University, Sydney, Australia

April 2016

Declaration

I hereby certify that the work presented in this thesis entitled “Uncovering the hidden glycan structures in metastatic melanoma” has not previously been submitted for a degree nor has it been submitted as part of the requirements for a degree to any other university or institution other than Macquarie University. This thesis is an original piece of research and is the result of my own work except where appropriately acknowledged. Human ethics (approval number: 5201200519, appendix) and biosafety (approval number: LIK270412BHA, appendix) approval has been duly obtained to use human samples for research purposes only. I consent to a copy of this thesis being available in the Macquarie University library for relevant consultation, loan and photocopying forthwith.

Jodie Louise Abrahams
April 2016

Acknowledgements

I would like to thank my supervisor Prof. Nicki Packer for her guidance and support throughout my PhD. Thank you to the Glyco@MQ group past and present members with a special thanks to Matthew, Kat, Zeynep, Vignesh, Kathrin, Wei, Terry, Maja, Chi-Hung, Morten and Robyn. Thanks to Yukie, Edward and Zhiping for being great office mates over the last three years.

Thank you to Prof. Pauline Rudd and Dr. Louise Royle for my introduction to glycobiology and all of their help and encouragement over the years. I would like to thank Prof. David Harvey and Dr. Weston Struwe for their invaluable help, training and advice.

This work would not have been possible without the financial support from Macquarie University and the Northern Translational Cancer Research Unit. I would also like to acknowledge my collaborators at The Melanoma Institute Australia and Curtin University for providing samples.

To my family, without your support and patience over the last four years this thesis would not have been possible.

Abstract

In the search for glycan disease biomarkers current glycoanalytical methods may not be revealing a complete picture of precious biological samples, and we may be missing potentially valuable information on structures that fall outside of current analysis approaches. The separation capabilities of porous graphitized carbon liquid chromatography with electrospray ionization mass spectrometry (PGC-LC-ESI-MS) is a powerful tool for the detailed characterisation and relative quantitation of glycans released from glycoproteins in human cells, tissues and body fluids. However the limitations of this approach have not been fully explored and much of the data analysis can only be achieved by expert manual annotation.

This thesis expands on the capabilities of the PGC-LC-ESI-MS glycoanalysis and develops new approaches that facilitate the interpretation of the resultant data to enable the discovery of glycan structures that may be hidden from view. In this thesis, *N*-linked glycan structures released from proteins were assigned based on PGC elution order, and MS fragmentation patterns in the negative ESI mode. To further validate assignments the released glycans were treated with a full array of exoglycosidase enzymes to confirm monosaccharide linkage and terminal epitopes.

Subsequently, the improved PGC-LC-ESI-MS analytical approach was used to fully characterise the *N*-glycosylation profile of melanoma lymph node tumour tissue and cultured cell samples. Metastasis accounts for the majority of mortality associated with melanoma, as limited treatment options exist for advanced stages of the disease. Alterations in cell surface protein glycosylation, in particular, increase the highly branched *N*-glycan structures that contribute to the invasive and metastatic potential of melanoma cells. Despite a growing understanding of the role of *N*-linked oligosaccharides in melanoma biology, there has been little progress in using glycosylation changes as a predictor of prognosis for patients with metastatic melanoma.

The global membrane *N*-glycosylation profile of lymph node melanoma tumour tissue of good and poor prognosis patient samples from stage III and IV patient cohorts was compared. Glycan structures were quantitated by LC-MS before and after selected exoglycosidase combinations to confirm differences in structural features including the degree of branching, sialylation and fucosylation. Over 90 glycan structures were identified, including high mannose, pauci mannose, hybrid and complex type glycans. In addition, the glycosylation

profile of a human melanoma cell line was compared to the glycosylation of the known melanoma prognostic marker, cell adhesion glycoprotein MCAM. Here we identified a group of bi-antennary structures with the LacdiNAc epitope and a high abundance of tetra-antennary glycans in the profile of MCAM that were not seen in the total cell membrane profile.

By reducing the complexity of glycan pools using specific exoglycosidase enzymes it was shown that the abundance of tri- and tetra-antennary glycans were severely underrepresented in an undigested profile. Therefore a targeted strategy was developed combining PGC-LC-ESI-MS with exoglycosidases to improve the relative quantitation of tri- and tetra-antennary glycan classes. This method was applied to determine if the abundance of tetra antennary *N*-glycans could be correlated with clinical outcome.

The use of this strategy provided additional valuable structural information on the length of poly LacNAc chains present, degree of sialylation, linkage of sialic acid residues and previously unreported epitopes including LacdiNAc carried by cell surface proteins, which may play a role in melanoma metastasis.

This is the first in-depth characterisation of melanoma samples enabled by the extension and optimisation of PGC-LC-ESI-MS/MS. Our findings contribute to the understanding of glycosylation alterations in melanoma metastasis and suggest the complementary use of specific glycosylation changes as prognostic markers.

List of Publications

This thesis contains material that has been published, submitted or prepared for publication, as follows:

1. Christiansen MN*, Chik J*, Lee L*, Anugraham M*, **Abrahams JL***, Packer NH*. Cell surface protein glycosylation in cancer. *Proteomics*. 2014; 14(4-5):525-46. Review article**Equal contribution*
2. Everest-Dass AV, **Abrahams JL**, Kolarich D, Packer NH, Campbell MP. Structural features for distinguishing N- and O-linked glycan isomers by LC-ESI-IT MS/MS. *J Am Soc Mass Spectrom*. 2013. 24(6):895-906.
3. **Abrahams JL**, Campbell MP, Packer NH. Using standard glycoproteins to build a PGC-LC-MS retention library and retention mapping resource. *Prepared manuscript*
4. Gotz L, **Abrahams JL**, Mariethoz J, Rudd PM, Karlsson NG, Packer NH, Campbell MP, Lisacek F. GlycoDigest: a tool for the targeted use of exoglycosidase digestions in glycan structure determination. *Bioinformatics*. 2014 1; 30 (21):3131-3.
5. **Abrahams JL**, Packer NH, Campbell MP. Quantitation of multi-antennary N-glycan classes: combining PGC-LC-ESI-MS with exoglycosidase digestion. *Analyst*. 2015. 140(16):5444-9

Publications obtained during PhD candidature, which are not included in this thesis:

1. Campbell MP, Peterson R, Gasteiger E, Zhang, J, Akune, **Abrahams, JL**, Mariethoz J, Hayes CA, Karlsson NG, Aoki-Kinoshita KF, Kolarich D, Lisacek F, Packer NH. *UniCarbKB: First Year Report Card*. 3rd International Beilstein Symposium on Glyco-Bioinformatics, 2014.

Presentations

- Abrahams JL, Campbell MP, Packer NH. The N-glycosylation Profile of Metastatic Melanoma Lymph Node Tissue. The Society for Glycobiology Annual Meeting, 16-19 November 2014. Honolulu, Hawaii. **Poster**
- Abrahams JL, Wong CW, Dye DE, Coombe DR, Packer NH. Characterisation of the N-glycosylation profile of MCAM in Metastatic Melanoma. 2nd Proteomics and Beyond symposium, 12 November 2014. Macquarie University, Sydney, Australia. **Poster**
- Abrahams JL, Campbell MP, Packer NH. Uncovering Sialylated Tetra-antennary N-glycans in Metastatic Melanoma. Sialoglyco 2014, 7-10 September. Gold Coast, Australia. **Poster**
- Abrahams JL, Campbell MP, Packer NH. Uncovering the Hidden Structures in Metastatic Melanoma. 5th Warren Workshop. August 6-9 2014. Galway, Ireland. **Selected Oral and poster**
- Abrahams JL, Wong CW, Dye DE, Coombe DR, Packer NH. Characterisation of the N-glycosylation profile of MCAM in Metastatic Melanoma. The 9th International Symposium on Glycosyltransferases (GlycoT), 18-21 June 2014. Porto, Portugal. **Poster**
- Abrahams JL, Parker B, Packer NH. Quantitative Analysis of Nucleotide Sugars Involved in Protein Glycosylation by Capillary Electrophoresis. 17th Lorne Proteomics Symposium. 2-5th February 2012. Lorne, Australia. **Poster**

Awards

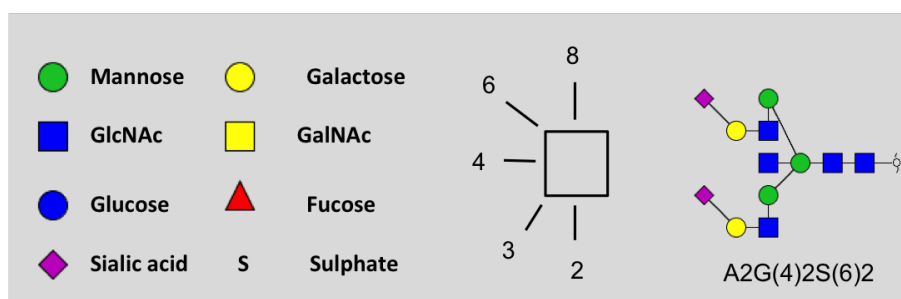
- Poster award: 2nd Proteomics and Beyond symposium, November 2014. Macquarie University, Sydney, Australia.
- Macquarie University Postgraduate Research Fund 2014
- Northern Translational Cancer Research Unit Research Scholar Award 2013
- International Macquarie University Postgraduate Research Excellence Scholarship (MQRES) 2011

Symbols and Nomenclature

Glycan nomenclature

All *N*-glycans have two core GlcNAcs; F at the start of the abbreviation indicates a core $\alpha(1-6)$ fucose linked to the inner GlcNAc; M_x, number (x) of mannose on core GlcNAcs; A_x, number of antenna (GlcNAc) on trimannosyl core; A2, biantennary with both GlcNAcs as $\beta(1-2)$ linked; A3, triantennary with a GlcNAc linked $\beta(1-2)$ to both mannose and a third GlcNAc linked $\beta(1-4)$ to the $\alpha(1-3)$ linked mannose; A3', triantennary with a GlcNAc linked $\beta(1-2)$ to both mannose and a third GlcNAc linked $\beta(1-6)$ to the $\alpha(1-6)$ linked mannose; A4, GlcNAcs linked as A3 with additional GlcNAc $\beta(1-6)$ linked to $\alpha(1-6)$ mannose; B, bisecting GlcNAc linked $\beta(1-4)$ to $\beta(1-3)$ mannose; G_x, number (x) of $\beta(1-4)$ linked galactose on the antenna; S_x, number (x) of sialic acids linked to galactose; Round brackets are used to indicate the linkage type for example the number 3 or 6 in parentheses after S indicates whether the sialic acid is in an $\alpha(2-3)$ or $\alpha(2-6)$ linkage. Square brackets indicate either the $\alpha(1-3)$ or $\alpha(1-6)$ mannose arm of the glycan core.

Symbols and nomenclature



Glycan structures have all been created using GlycoWorkbench¹ version 1.1.3 using CFG monosaccharide symbols with oxford linkage placement notation in compact view and exported with reducing end indicator. Linkages after a bracket drawn in default 1-4 position are undefined.

Abbreviations

2AA	2-amino-benzoic acid
2AB	2-aminobenzamide
2AP	2-aminopyridine
AJCC	American Joint Committee on Cancer
ALM	Acral lentiginous melanoma
ANTS	8-aminonaphthalene-1,3,6-trisulfonic acid
APTS	8-aminopyrene-1,3,6-trisulfonic acid
CE	Capillary electrophoresis
CFG	Consortium for Functional Glycomics
CID	Collision-induced dissociation
CM	Cutaneous melanoma
EIC	Extracted ion chromatogram
ER	Endoplasmic reticulum
ESI	Electrospray ionization
FAB	Fast atom bombardment
Fuc	Fucose
FUT8	Fucosyltransferase 8 (alpha (1,6) fucosyltransferase)
GalNAc	<i>N</i> -acetylgalactosamine
Gal	Galactose
Glc	Glucose
GnT	<i>N</i> -acetyl-glucosamine transferase
HILIC	Hydrophilic interaction-liquid chromatography
HPLC	High performance liquid chromatography
IMMS	Ion mobility mass spectrometry
IT	Ion Trap
MALDI	Matrix-assisted laser desorption ionization
MAPK	Mitogen-activated protein kinase
L1-CAM	L1 Cell Adhesion Molecule
LDH	Lactate dehydrogenase
LMM	Lentigo maligna melanoma
Man	Mannose
MCAM	Melanoma cell adhesion molecule
MS	Mass spectrometry
NeuAc	<i>N</i> -acetylneuraminic acid
NM	Nodular melanoma
NMR	Nuclear magnetic resonance
OST	Oligosaccharidetransferase
PGC	Porous graphitized carbon
PHA-E	<i>Phaseolus vulgaris</i> erythroagglutinin
PHA-L	<i>Phaseolus Vulgaris</i> Leucoagglutinin
PNGase A	Peptide- <i>N</i> -glycosidase A
PNGase F	Peptide <i>N</i> -glycosidase F
PVDF	Polyvinylidene difluoride
PSA	Polysialic acid
Q-TOF	Quadrupole time-of-flight
RP	Reversed phase
RT-PCR	Reverse transcriptase-polymerase chain reaction
SDS-PAGE	Sodium dodecyl sulfate-polyacrylamide gel electrophoresis
SSM	Superficial spreading melanoma

UPLC	Ultra-performance liquid chromatography
UV	Ultra violet
VCAM-1	Vascular cell adhesion protein 1
WAX	Weak anion exchange

Table of Contents

Declaration	III
Acknowledgements	IV
Abstract	V
List of Publications	VII
Presentations and Awards	VIII
Symbols and Nomenclature	IX
Abbreviations	X
Chapter 1	1
Introduction	3
1.1 Melanoma	3
1.1.1 Cutaneous melanoma	3
1.1.2 Melanoma staging and prognosis	4
1.1.3 Current Biomarkers	4
1.1.4 Cell adhesion molecules in melanoma development and progression	6
1.2 Glycosylation	7
1.2.1 Protein glycosylation	7
1.2.2 <i>N</i> -glycosylation	7
1.2.3 <i>N</i> -glycan diversity	9
1.3 Cell surface protein glycosylation in cancer	11
Cell surface protein glycosylation in cancer (Publication1)	12
1.4 Glycan analysis strategies	34
1.4.1 Glycoproteomics	34
1.4.2 Glycomics	34
1.4.2.1 Glycan release	34
1.4.2.2 Derivatisation of glycans	35
1.4.2.3 Separation of released glycans	36
1.4.2.4 LC Separation of Glycans	36
1.4.2.5 Mass spectrometry	39
1.4.2.6 Quantitation	42
1.4.2.7 Bioinformatics	42
1.5 Glycan analysis strategies applied to melanoma research	43
1.6 Thesis Aims	46
Chapter 2	47
Structural feature ions for distinguishing N- and O-linked glycan isomers by LC-ESI-IT MS/MS (Publication 2)	51
Supplementary Figures	63

Chapter 3	69
Building a PGC-LC-MS <i>N</i>-glycan retention library and elution mapping resource (Publication 3)	73
Supplementary Tables	97
Chapter 4	103
GlycoDigest: a tool for the targeted use of exoglycosidase digestions in glycan structure determination (Publication 4)	107
4.2 Exoglycosidase examples	110
4.3 Data interpretation example: Analysis of IgG <i>N</i> -glycans by PGC-LC-MS with exoglycosidase digestions	118
Chapter 5	119
<i>N</i>-glycosylation in metastatic melanoma: confirmation of β1-6 branched <i>N</i>-glycans	123
5.1 Introduction	123
5.2 Materials and Methods	127
5.3 Results	130
5.4 Discussion	143
5.5 Supplementary Figures	146
Chapter 6	149
Relative quantitation of multi-antennary <i>N</i>-glycan classes: combining PGC-LC-ESI-MS with exoglycosidase digestion (Publication 5)	153
Supplementary Material	159
Chapter 7	169
The glycosylation profile of metastatic melanoma lymph node tumours	173
7.1 Introduction	173
7.2 Materials and Methods	175
7.3 Results	176
7.4 Discussion	197
7.5 Supplementary Figures	200
Chapter 8	207
Summary and Future Directions	209
8.1 Summary	209
8.2 Melanoma glycosylation	211
8.3 Future directions	215
References	217
Appendix 1: Patient clinical information	229
Appendix 2: Ethics approval	231
Appendix 3: Biosafety approval	232

Chapter 1

Introduction

1.1 Melanoma

Melanoma, considered as one of the most aggressive human cancers, originates from the melanin producing melanocytes. Primary melanoma tumours can develop in any tissue where melanocytes are found and can be divided into two classes depending on whether the origin is in either the epidermal skin layer (cutaneous melanoma) or elsewhere (non-cutaneous melanoma). Although cutaneous melanoma is the most common form of the disease, non-cutaneous melanomas do occasionally form in the eye, respiratory, gastrointestinal, and genitourinary mucosal surfaces, or the meninges². The work presented in this thesis focuses on cutaneous melanoma.

1.1.1 Cutaneous melanoma

Cutaneous melanoma (CM) can be further divided into four major subgroups depending on their clinical features: superficial spreading melanoma (SSM), nodular melanoma (NM), acral lentiginous melanoma (ALM), and lentigo maligna melanoma (LMM)²⁻⁴. Over 80% of melanomas are classified as either SSM or NM and are distinguished by radial (SSM) or vertical (NM) growth within the dermis. SSM is the most common form of cutaneous melanoma (approximately 65% of cases) and grows horizontally in the epidermis, usually with an asymmetric appearance. NM melanoma (20%) is the most aggressive of the subtypes as it has no radial growth phase but instead invades vertically into the epidermis^{4,5}. Nodular melanomas are characterised by a raised nodular lesion with an irregular border. LMM is generally considered the least aggressive of the subtypes as it has a long radial growth phase. This type of melanoma is most common amongst older people in areas of chronic UV exposure. LMM presents as slowly enlarging pigmented patches, usually on the head and neck. Lesions are characterised by an asymmetric appearance, an irregular peripheral border, variegated colour, enlarging diameter, and change in appearance over time⁶. ALM occurs on the palms, soles of feet and nails. ALM is the least common of the four major subtypes in people with lighter skin, accounting for between 4 and 10% of primary melanomas, whereas it is the most common subtype in darker skin populations who have a lower overall incidence of melanoma. ALM is a distinct subclass due to its development in often sun-protected areas of the body, and occurs in all races at the same rate⁷.

1.1.2 Melanoma staging and prognosis

Staging of melanoma is determined by the guidelines outlined by the American Joint Committee on Cancer (AJCC) staging and classification system that incorporates tumour thickness, ulceration, mitotic index and the lymph node status^{3,8}. Melanoma is classified into four stages from the development of the primary tumour (Stages I and II), metastasis to regional lymph nodes (stage III) and distant metastasis to other organs (stage IV) including the lung, liver, brain and bone⁸⁻¹⁰. Despite significant advances in treatment of melanoma during the past decade, the survival rate has not improved for late stage disease¹¹. The five year survival rate for AJCC stage I and II melanoma patients ranges from 97 to 53%, but once metastasis to regional lymph nodes has occurred the five year survival rate decreases to between 70 to 39% (AJCC stage III) and 18 to 6% for patients with distant metastases (AJCC stage IV)⁸.

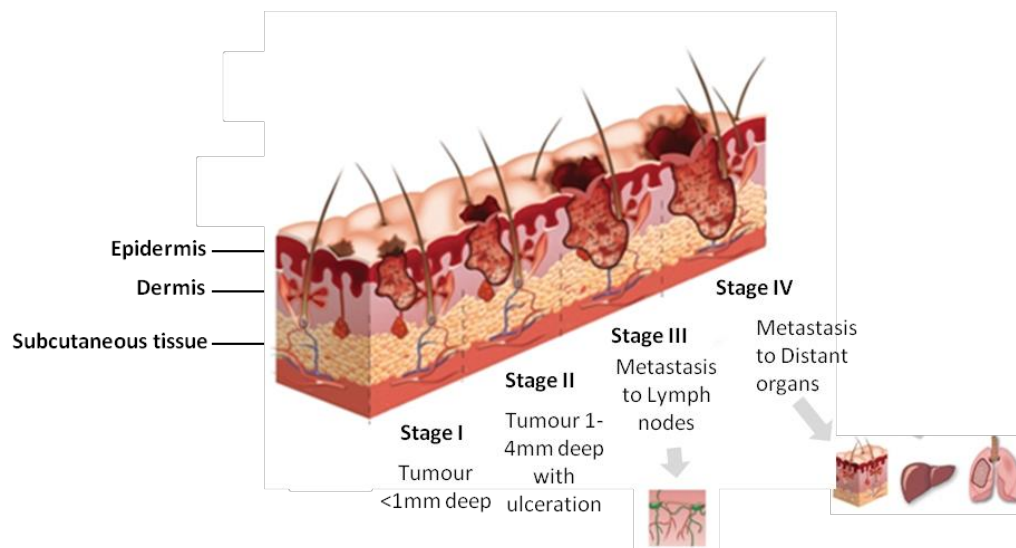


Figure 1. Melanoma stages. Characteristics of melanoma progression from primary stages I/II to lymph node metastasis Stage III and distant organ metastasis stage IV. Image taken and modified from¹².

1.1.3 Current Biomarkers

A contributory factor to the poor outcome for melanoma patients is a lack of sensitive and specific diagnostic, prognostic and therapeutic response biomarkers¹¹. To date the search for biomarkers has focused on serum, cell lines and tissue analysis, and although candidate melanoma biomarkers have been identified, only a limited number have been validated for use in a clinical setting.

Several clinical factors (patient age, the location of the tumour, the number of cancerous lymph nodes and the presence of distant metastases) and histopathological factors (including the depth of the tumour and the presence of ulceration) are currently used as the main

prognostic factors¹¹. However, recent advances in the genetic analyses of melanoma tumours have led to a better understanding of the molecular pathways involved in the onset and progression of the disease leading to the development of molecular subtype classification systems^{13,14}. Oncogenic mutations in melanomas involving the mitogen-activated protein kinase signal transduction (MAPK), Kit receptor (c-KIT), G protein (GNAQ), and Neuroblastoma RAS (NRAS) signalling pathways have been identified and are the basis for molecular classification as well as therapeutic targets¹⁵. The most common mutations observed in metastatic melanoma and typical phenotypic associations are summarised in Table 1. BRAF mutations in the MPAK pathway are the most frequently observed and are associated with a poorer prognosis in metastatic melanoma patients compared to other known gene mutations¹⁵.

Table 1. Molecular classification scheme for metastatic melanoma (*Table taken from*^{13,15})

Gene Mutation	Signalling Pathway	Percentage of melanomas with mutation	Phenotypic associations
<i>BRAF</i>	MAPK	50%	Young patient age Intermittent sun-exposed primary site Trunk and limb primary locations High neavus count Few freckles Tan easily Superficial spreading histogenetic type
<i>NRAS</i>	NRAS	15-20%	Intermittent sun-exposed sites (weak association) Low or absent upward spreading into the epidermis Peripheral circumscription
<i>c-KIT</i>	c-KIT	2% (10-20% of acral and mucosal melanomas)	Acral and mucosal lentiginous histogenetic melanoma types
<i>GNAQ</i>	GNAQ	50% of Uveal melanomas blue naevus-like melanomas	Uveal melanoma

The most valuable serum protein markers for melanoma to date are lactate dehydrogenase (LDH) and S100 calcium-binding protein B (S100B). Although high LDH and S100B levels have been correlated with poor prognosis in AJCC stage III/IV melanoma patients^{16,17}, poor sensitivity and specificity are major limitations for their routine use in all stages of disease¹⁰.

Despite these limitations, elevated serum LDH is the only molecular biomarker that was included in the classification of stage IV CM by the AJCC 6th edition as a predictor of survival outcome^{8,18}, and S100B is used to monitor treatment response in patients with metastatic disease as levels are linked to tumour burden, clinical stage and tumour progression^{11,19}.

1.1.4 Cell adhesion molecules in melanoma development and progression

A characteristic of invasive melanoma tumour cells which have migrated to form metastatic tumours distant from the primary site is a change in the properties and expression of glycosylated adhesion molecules belonging to the integrin, cadherin and immunoglobulin superfamilies^{20,21} (Figure 2).

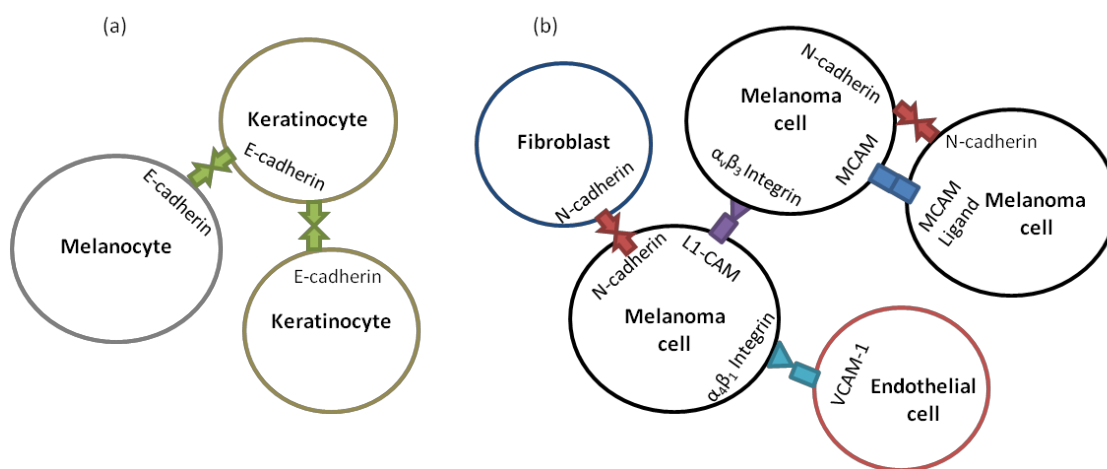


Figure 2. Cell-cell adhesion of melanocytes and melanoma cells. (a) Normal cell-cell contact between melanocytes and keratinocytes through E-cadherin. (b) Interactions between melanoma cells, fibroblasts and endothelial cells during melanoma progression via N-cadherin, MCAM, L1-CAM, VCAM-1 and Integrin. Figure adapted from Hass *et al*²².

The melanoma cell adhesion molecule, also referred to as MCAM, MUC18 or CD146, is a cell surface glycoprotein belonging to the immunoglobulin superfamily class of proteins²³. MCAM expression is regulated by direct cell-to-cell contact with keratinocytes these interactions are diminished in advanced primary and metastatic melanoma cells²⁴. It is therefore frequently over-expressed on the surface of advanced and metastatic melanoma cells and has been used as a biomarker of melanoma progression since 1989. Increased cell surface expression correlating with disease progression and poor prognosis of patients^{25,26}.

Genomics and proteomics have so far not identified biomarkers with the necessary specificity and sensitivity for the prognosis and treatment response for metastatic melanoma. Therefore, since glycosylation of proteins is known to alter in cancer²⁷⁻²⁹ and evidence for significant

involvement of cell surface glycoproteins in the progression of melanoma^{23,30,31} this thesis investigates changes in the membrane glycome of metastatic melanoma.

1.2 Glycosylation

Glycosylation is one of the most abundant posttranslational modifications and is of great importance for the correct folding of proteins, protein stability and function, and also for interactions between cells and the extracellular environment^{32,33}. Alteration in glycosylation can upset the normal functioning of proteins and cells and is implicated in many disease states including Alzheimers, cancer, and autoimmunity. Glycans exist either as free molecules or conjugated to other molecules. Glycans can be attached to proteins or lipids and these glycoconjugates can be divided into the classes of glycoproteins (including *N*-linked or *O*-linked), proteoglycans, glycosylphosphatidylinositol (GPI) anchored proteins and glycosphingolipids^{34,35}. Glycosylation is an enzymatic process involving the action of glycosyltransferases, glycosidases, glycan-modifying enzymes, nucleotide sugar donors and transporter molecules³².

1.2.1 Protein glycosylation

Glycoproteins can be membrane bound or secreted. *N*-linked glycans are attached to the nitrogen of asparagine residues of the consensus sequence: asparagine followed by any amino acid except proline ending with serine or threonine (Asn-X-Ser/Thr)³². *O*-linked glycans are linked to the oxygen of OH groups of serine/threonine residues³⁶. A range of monosaccharides exist in *N*- and *O*- linked glycans on mammalian glycoproteins; most commonly *N*-acetylgalactosamine (GalNAc), *N*-acetylglucosamine (GlcNAc), galactose (Gal), mannose (Man), fucose (Fuc) and *N*-acetylneuraminic acid (NeuAc)³². Protein *N*-glycosylation is the main focus of this thesis and described further below.

1.2.2 *N*-glycosylation

The synthesis of *N*-glycans is a complicated process involving the building of a precursor that is then transferred to a protein, trimmed back and then rebuilt to a specific glycoform structure. The assembly of the dolichol-linked precursor begins on the cytoplasmic side of the endoplasmic reticulum (ER) membrane and terminates in the lumen^{32,37}. Glycosyltransferases encoded by the *ALG* (asparagine linked glycosylation) genes build a 14-residue glycan, consisting of the chitobiose *N*-glycan core, plus nine mannose and three glucose residues (Glc₃Man₉GlcNAc₂)³⁸, which once assembled, is transferred to the polypeptide catalysed by the action of oligosaccharyltransferase (OST)^{39,40}. Once transferred to the protein backbone, terminal glucosidase enzymes remove the three glucose residues⁴¹. After the glycan has been

trimmed to the $\text{Man}_8\text{GlcNAc}_2$ structure the glycoprotein is then transferred to the Golgi apparatus where further trimming of the mannose residues and rebuilding of hybrid and complex glycans takes place. This is initiated by transfer of GlcNAc to $\text{Man}_5\text{GlcNAc}_2\text{Asn}$ by GlcNAcT-I^{32} (Figure 3). *N*-glycans can be divided into four subclasses, paucimannose, high mannose, hybrid and complex type. High mannose, hybrid and complex consist of a common chitobiose core (Figure 4). Hybrid and complex type glycans can be elongated and modified with different structural features including branching, bisecting GlcNAc (Figure 5), galactose, fucosylation (Figure 7) and sialylation and sulphation (Figure 8)³⁸.

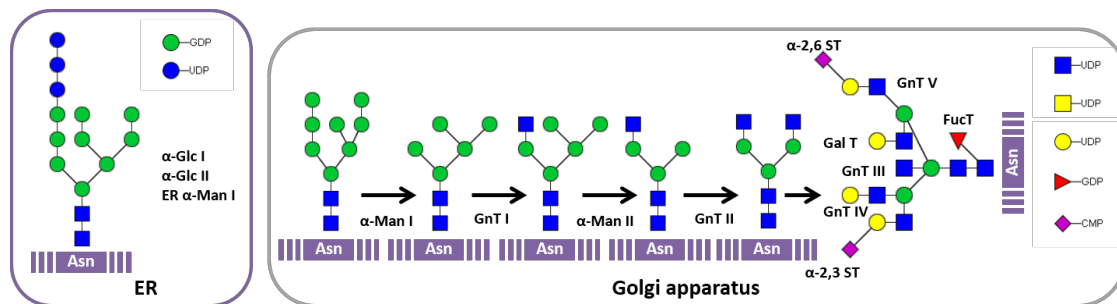


Figure 3. Mammalian *N*-glycosylation pathway. The precursor $\text{Glc}_3\text{Man}_9\text{GlcNAc}_2$ glycan is initially trimmed in the ER before maturation in the Golgi apparatus. In the ER glucosidases I and II remove two terminal Glc residues, which allows the lectins calnexin and calreticulin to bind to the nascent glycoprotein promoting correct folding of proteins⁴². The final Glc residue is hydrolysed by glucosidase II followed by the removal of one mannose residue. The newly processed glycoprotein is then transported to the Golgi apparatus and subjected to both further trimming and elongation. This highly ordered maturation process can generate a diverse repertoire of glycans using a range of nucleotide sugar substrates, the specificity of glycosidases and glycosyltransferases as shown.

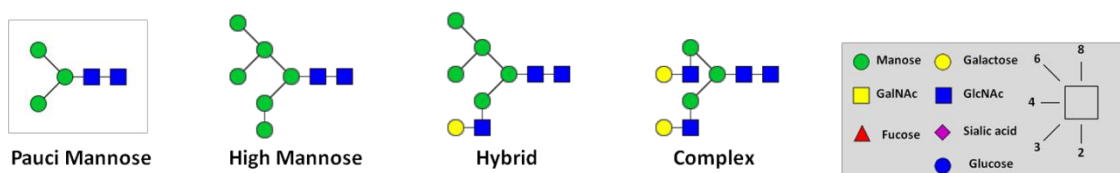


Figure 4. The four common *N*-glycan sub-classes. All *N*-glycans are based on the common chitobiose core ($\text{Man}_3\text{GlcNAc}_2$) that is further processed in the Golgi apparatus. Mammalian high-mannose glycans contain between five and nine mannose residues and are denoted as M5-M9. Pauci mannose glycans contain between one and four mannose residues with or without core fucosylation. Hybrid glycans contain a mannose residue on the 6-arm and a

GlcNAc residue linked to the 3-arm mannose. The addition of the GlcNAc residue and resulting hybrid glycoforms initiates the synthesis of complex structures by providing the substrate for α -mannosidase II. Complex glycans are characterised by the presence of GlcNAc residues on both the 3- and 6-mannose arms, which are typically then extended with other monosaccharide residues. Complex glycans exist in bi-, tri-, and tetra- and (less reported non-human) penta-antennary forms.

1.2.3 *N*-glycan diversity

Complex-type *N*-glycans exist in bi-, tri-, and tetra-antennary structures (Figure 5), which are formed by the action of *N*-acetyl-glucosamine transferase enzymes, GnT I-V. The addition of GlcNAc linked to the core 3- and 6- arm mannose residues by the action of GnT I and II, respectively, results in the bi-antennary class of structures. Tri-antennary structures exist with either a β 1-4 linked GlcNAc attached to the 3-arm mannose (GnT IV) or with a β 1-6 linked GlcNAc attached to the 6- arm mannose residue (GnT V)⁴³. Tetra antennary structures are formed by the action of both Gnt IV and V on the bi-antennary structure. GlcNAc can also be β 1-4 linked to the core mannose by GnT III to produce the bisected class of *N*-glycans structures⁴⁴.

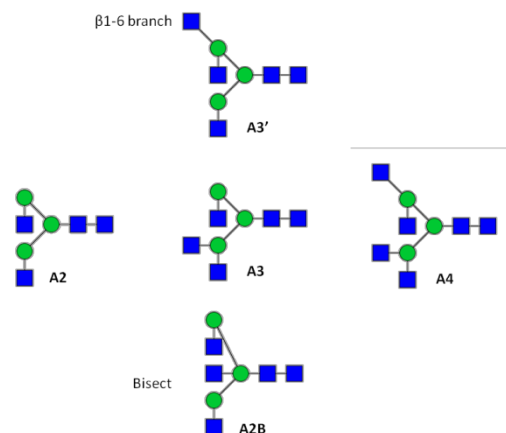


Figure 5. *N*-glycan core branching.

Complex bi- to tetra- antennary branching are then elongated by the addition of galactose residues β 1-4/3 linked to GlcNAc (LacNAc). Antennae can be further elongated by the addition of multiple LacNAc repeats β 1-3 linked to galactose (polylactosamine extension).

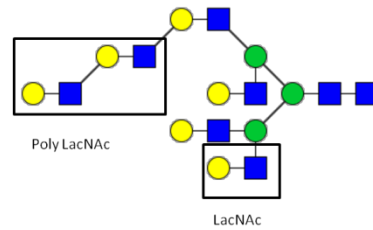


Figure 6. The addition of β 1-4 linked galactose residues to form the LacNAc unit (GlcNAc-Gal) present on hybrid and complex type glycans and multiple lactosamine repeats (poly LacNAc).

Fucose residues can either be linked to the *N*-glycan core (α 1-6) or linked to GlcNAc (α 1-3) and galactose (α 1-2) residues of the antennae (Lewis antigens) (Figure 7). Core fucosylation is catalysed by the action of the FUT8 α 1,6-fucosyltransferase which transfers a fucose in a α 1-6 linkage to GlcNAc⁴⁵. The addition of outer arm fucosylation is catalysed by α 1-3/ α 1-4- and α 1-2 fucosyltransferases which result in the Lewis blood group antigens⁴⁶.

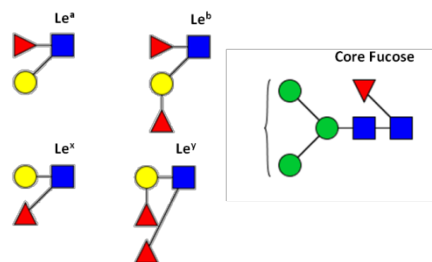


Figure 7. Core and outer arm Fucosylation.

Sialic acid can be either α 2-3 or α 2-6 linked to galactose. α 2-3 linked sialic acid is the precursor for α 2-8 linked polysialic acids (PSA)⁴⁷(Figure 8).

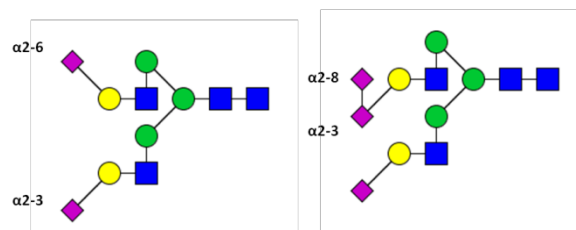


Figure 8. Sialic acid linkages to galactose.

Terminal β -linked GalNAc can also be added to antennae GlcNAc of *N*-glycan structures, referred to as the LacdiNAc epitope (Figure 9). This epitope can be further modified by the addition of α 2-6 linked sialic acid, fucose and or sulphate⁴⁶.

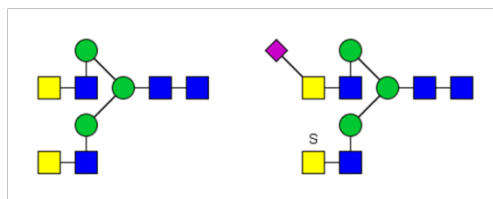


Figure 9. LacdiNAc. *N*-glycan structures with terminal GalNAc.

Alterations in the *N*-glycan features described above seen in cancer are discussed in the following review article.

1.3 Cell surface protein glycosylation in cancer (publication 1)

The cell surface protein glycosylation alterations observed in melanoma were reviewed from the published literature and the resultant manuscript was an equal contribution to a comparative review on the changes in glycosylation occurring in five different cancers:

Review article: Christiansen MN, Chik J, Lee L, Anugraham M, **Abrahams JL**, Packer NH. Cell surface protein glycosylation in cancer. *Proteomics*. 2014; 14(4-5):525-46.

Author contributions: All authors contributed equally to the concept, design and preparation of the manuscript. I prepared the sections on melanoma, branching and bisecting GlcNAc.

1.4 Glycan analysis strategies

Glycans can be analysed as either part of an intact protein, as glycopeptides, released glycans or hydrolysed monosaccharides. Many different methods exist for the analysis of glycans including high/ultra-performance liquid chromatography (HPLC/UPLC), capillary electrophoresis (CE), nuclear magnetic resonance (NMR) and mass spectrometry (MS)⁴⁸ (Figure 10). No single universal method is available for the complete glycosylation analysis of complex biological samples, therefore the most appropriate method or combination of methods providing complementary information must be chosen for each individual research goal⁴⁹.

1.4.1 Glycoproteomics

Glycoproteomics is the site-specific analysis of the glycoproteome⁵⁰. Although glycoproteomic analysis remains relatively immature compared to glycomics due to the higher level of complexity, it is becoming increasingly popular as it yields a more detailed picture of an individual glycoprotein; including information on the protein itself, site occupancy and site-specific glycosylation patterns. Glycopeptides are more frequently analysed than intact glycoproteins because of the available technologies. Challenges in glycopeptide analysis include the resistance of glycoproteins to tryptic digestion, missed cleavages and the production of large glycopeptides, which could potentially contain multiple glycosylation sites⁵¹. The glycopeptide analysis of multiple glycoproteins simultaneously from a complex biological sample is a lot more challenging compared to a single purified glycoprotein therefore when looking at biological samples including serum and tissue glycans are often analysed after removal from proteins.

1.4.2 Glycomics

Glycomics based approaches are used to analyse the total glycan population released from biological samples⁵².

1.4.2.1 Glycan release

Glycans can be released from glycans either enzymatically or chemically. For the release of *N*-glycans several endoglycosidases exist including the widely used Peptide *N*-Glycosidase F (PNGase F), which cleaves the bond between the glycan core and asparagine residue of the protein. A second member of the PNGase family of enzymes, Peptide *N*-Glycosidase A (PNGase A) is used for *N*-glycan structures containing α 1,3 linked core fucosylation seen on plant and insect glycan structures as PNGase F is ineffective at cleaving glycans with this structure⁵³. Endoglycosidase H (endo H) cleaves glycan structures between the two GlcNAc

residues of the chitobiose core of high mannose and selected hybrid structures but does not have activity toward complex glycan classes⁵⁴.

For the release of *O*-linked glycans so far only one *O*-glycanase is available which is highly specific for the cleavage of the core 1 *O*-glycan structure (Gal β 1-3GalNAc) but not to any extended *O*-glycans⁵⁵. Enzymatic release of glycans has the advantage of keeping the protein intact for further analysis whereas the chemical release needed for samples with *O*-glycosylation results in degradation of the protein. These methods include reductive and non-reductive alkaline β - elimination, and hydrazinolysis^{56,57}. The harsh chemical reaction conditions can cause degradation or “peeling ” reactions of *O*-glycans⁵⁸ unless they are rapidly reduced using sodium borohydride that reduces the free reducing end of the glycan to an alditol⁵⁹. Ammonia-based non-reductive β - elimination can be a useful technique when a free reducing end is required for derivatisation⁴⁹. Hydrazinolysis procedures can also be used to release glycans with a free reducing end at high yield, and by using milder conditions degradation can be minimised⁵⁶.

Glycans can be released from proteins successfully under different conditions; including after immobilisation on PVDF membranes⁶⁰, from SDS-gel separated protein bands/spots^{61,62}, in gel block⁶³ or in solution. Each technique has distinct advantages depending on the sample type. For the analysis of both *N*-and *O* -glycans from the same sample, immobilisation onto PVDF membrane either directly or by electro-transfer of proteins after SDS-PAGE is the method of choice as *N*-glycans can first be released using PNGase F, followed by reductive β -elimination to release *O*-glycans⁶⁴.

1.4.2.2 Derivatisation of glycans

Enzymatically released sugars contain a single reactive carbonyl group at the reducing end,⁶⁵ to which fluorophores or chromophores can be attached using reductive amination to enable fluorescence or UV detection. Fluorescent amine tags including 2-aminobenzamide (2AB), 2-aminopyridine (2AP) and 2-amino-benzoic acid (2AA) are successfully used for HPLC analysis and 8-aminopyrene-1,3,6-trisulfonic acid (APTS) or 8-aminonaphthalene-1,3,6-trisulfonic acid (ANTS) for CE analysis of released *N*-glycans. On the other hand, permethylation is the replacement of all the hydrogen atoms of -OH, -NHAc and -COOH groups with a methyl group and results in uniform ionisation and reduced polarity of both acidic and basic oligosaccharides which can improve the reproducibility of LC separation and MS analysis⁵⁷.

1.4.2.3 Separation of released glycans

Due to the high complexity and varying abundances of glycan pools released from valuable biological sample sources including patient biopsies, powerful separation techniques are necessary to maximise the information that can be obtained from a single sample run. These methods include liquid chromatography (LC), capillary electrophoresis (CE) or ion mobility (IM) separations coupled with either electrochemical, optical, or mass spectrometric (MS) detection. LC separation coupled to MS was the chosen method for the analysis of released glycans in this thesis.

1.4.2.4 LC Separation of Glycans

There are a number of different chromatographic separation phases used in HPLC, UPLC or chip-based systems combined with either fluorescence or mass spectrometry detection that are commonly used in the analysis of sugars released from proteins.

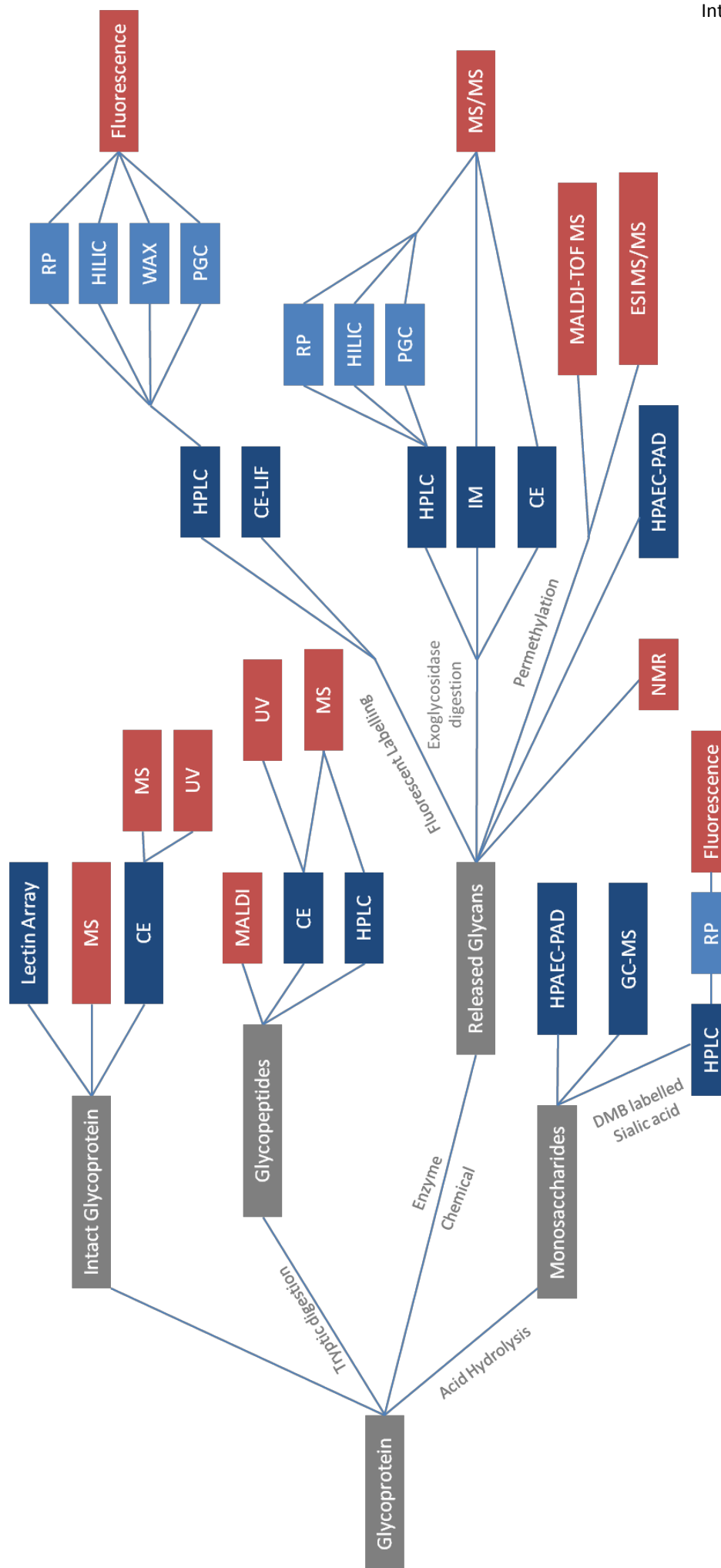
Reversed Phase (RP)

Reversed phase separation is based on hydrophobicity using a non-polar stationary phase and a polar mobile phase. RP materials generally do not retain the hydrophilic non-derivatised native glycans but this can be overcome by derivatisation to increase hydrophobicity and allow sensitive detection^{48,66}, for example by the addition of the fluorescent label aminobenzoic acid (2-AA).

Hydrophilic Interaction Liquid Chromatography (HILIC)

Hydrophilic interaction liquid chromatography offers selectivity based on a polar stationary phase and non-polar mobile phase⁶⁷. The separation of derivatised glycans using HILIC is a reproducible method for the analysis of *N*-glycans based on polarity and size⁶⁸. This reproducibility and development of a retention based elution mapping based on comparison to a hydrolysed similarly derivatised dextran ladder has led to the development of databases and bioinformatics resources to aid the assignment of structures and has increased in popularity^{63,69}. Used in combination with fluorescence detection HILIC has successfully been shown to be compatible with high throughput analysis using robotic platforms, desirable for the fingerprint analysis of large sample cohorts⁷⁰⁻⁷².

Figure 10. Glycan analysis strategies. Approaches to analysis of intact glycoproteins, glycopeptides, released glycans and monosaccharides. Figure modified from Domann *et al*⁷³.



Weak Anionic Exchange (WAX)

Weak anionic exchange chromatography is used to separate glycan classes based on charge and is often used in combination with HILIC separation to pre-fractionate derivatised glycans in order to simplify the profile of complex glycan pools and increase the confidence of structural assignment of samples analysed with fluorescence detection. It is also useful for the relative quantitation of charged glycan classes within a sample. Assignment of separated fractions is based on the number of sialic acid residues by retention time comparison to a standard of *N*-glycans released from fetuin, that is run in parallel with each sample batch⁶². With the improvement of columns available and separation conditions it is now also possible to separate each charged fraction further to collect peaks which are separated based on both charge and size. This technique has been valuable for the analysis of samples like erythropoietin with a high degree of sialylation and lactosamine extensions that are more difficult to assign when using HILIC alone^{68,74}.

Porous graphitised carbon (PGC)

Porous graphitised carbon offers unique properties as a liquid chromatography stationary phase. It is stable over a wide pH and temperature range, and is robust with longer column lifetime and regeneration capabilities⁷⁵. PGC shares characteristic behaviours with reversed phase material in its strong retention of non-polar analytes, but unlike RP materials PGC also shows exceptional retention towards polar compounds^{76,77}. These retention behaviours combined with its ability to separate structurally similar isomeric non-derivatised glycans offers advantages over other LC phase materials when applied to the analysis of sugars.

Although the retention mechanisms and influencing factors of PGC chromatography for glycan analysis are not fully understood it nevertheless has become a valuable tool for on-line LC-ESI-MS analysis of complex glycan samples. PGC has the ability to separate glycan classes including bisecting and tri-antennary, galactose arm isomers and α 2-3 and α 2-6 sialic acid linkage isomers⁷⁸⁻⁸¹. The separation of *N*-glycans by PGC combined with MS detection is the main method used through this thesis work. PGC elution behaviour and isomer separation is further explored in chapters 2 and 3.

Mixed mode columns

Recently mixed mode columns for the analysis of glycans combining WAX with HILIC or RP materials have become available⁸². This has allowed for more efficient analysis by removing the need for a multistep approach, which involves pre-fractionation of samples based on charge using WAX columns and then further separation by either HILIC or PGC HPLC. This

eliminates various salt removal steps and potential sample loss and speeds up analysis times. The column and mobile phase conditions are also compatible with both fluorescence and MS detection.

Columns on CHIP

A recent advancement in LC-MS glycan analysis was the introduction of the chipLC system⁸³. The chipLC format includes a miniaturised trapping column, switching valve, and LC column in the form of a microfluidic chip interfaced directly to the inlet of an ESI source for MS detection^{53,84}. Integrated LC microchips have the advantage of online sample enrichment prior to chromatographic separation, simplified operation, higher sensitivity and improved reproducibility^{85,86}. Chips are now available with RP⁸⁷, HILIC⁸⁸ and PGC⁸⁹⁻⁹¹ micro separation columns and have been used in numerous glycomic studies. A more advanced chip design includes an immobilised PNGase F reactor for online glycan release after short incubation (6s for IgG)⁹².

1.4.2.5 Mass spectrometry

Mass spectrometry (MS) is a widely used technique for the analysis of glycans either alone or in combination with pre-separation techniques as discussed above, of which LC is most widely used. MS not only provides a link between mass and composition but can also yield valuable information required to assign structure based on fragment ion patterns.

Ionisation methods

Matrix assisted laser desorption ionisation (MALDI) and electrospray ionisation (ESI) are the most frequently used ionisation techniques for the analysis of glycans^{93,94}. These are both soft ionisation techniques imparting lower amounts of energy to the samples and minimising the risk of fragmentation during the ionisation process compared to other methods such as fast atom bombardment (FAB)⁶⁶. Glycans can be analysed in positive or negative ion mode using either of these techniques depending on the sample type. Samples containing acidic groups such as sialic acids, are usually analysed in negative mode⁶⁶. These methods are very good for giving an initial picture of a sample but in order to elucidate the structures present further fragmentation of the parent ion (MS/MS) is required⁹⁵.

MALDI produces mainly singly charged ions, which means the spectra produced are less complex than ESI spectra that contain multiply charged ions, and for neutral glycans the ionisation efficiency is consistent even for larger masses^{65,66}. MALDI is more tolerant to contaminants than ESI. However, acidic residues including sialic acid, sulphate, and phosphate are easily lost during MALDI⁹³ and for this reason samples analysed by MALDI are often

desialylated or permethylated to stabilise the acidic groups (detailed above) prior to analysis⁴⁹. ESI produces better-resolved peaks than MALDI due to the absence of peaks from matrix adducts⁹³, but is less tolerant to salts and contaminants than MALDI and generates multiply charged states that have to be taken into account when quantitating structures^{65,96}. ESI may be used either by direct infusion of samples or coupled to LC⁹³. Advantages of combining ESI with chromatography separation include the removal of salts and contaminants and also separation of isomeric structures which allows individual fragmentation spectra to be acquired⁵⁴.

Mass analysers

Types of mass analysers currently used for glycomic analysis include ion-traps, Quadrupole Time-of-Flight (Q-TOF) and Orbitrap instruments. Each has its advantages and disadvantages in terms of sensitivity, mass accuracy, resolution, speed of data acquisition and tandem MS capabilities⁴⁸. Instruments used for MS/MS include Q-TOF (ESI) and TOF-TOF(MALDI) and ion traps for multistage MS^{54,97}. Q-TOF and Orbitrap are favoured because of their high mass accuracy that can distinguish phosphate from sulphate groups, which cannot be achieved using ion-traps⁴⁸ such as was used in this study.

Fragmentation of released glycans

Fragmentation of glycans is dependent on a number of factors including the fragmentation mode, the type of mass analyser used, ion polarity, use of adducts and derivatisation method^{48,98}. There are two types of fragmentation commonly observed for glycans; glycosidic bond cleavage between neighbouring sugar residues and cross-ring cleavage of one or more of the monosaccharide sugar rings⁶⁵. Glycosidic cleavages give sequence and composition information, whilst cross-ring cleavages give details on linkage types⁹⁸. The glycan fragmentation nomenclature proposed by Domon and Costello⁹⁹ is the most widely used to describe observed glycan fragment ions (Figure 11).

Collision-induced dissociation (CID)

Collision-induced dissociation (CID) remains the most common choice for tandem mass spectrometric fragmentation of glycan parent ions⁴⁸. Positive mode CID produces mainly glycosidic cleavages, which yields sequence information but no linkage information with the use of metal adducts resulting in more cross-ring cleavages⁶⁵. Negative mode CID however produces A-type crossring cleavage ions and more C-type than B and Y-type fragments⁵⁴. Structural features that can be determined from negative ion spectra include the absence or presence of core fucose, antennae composition and the presence of bisecting GlcNAc.

Common diagnostic ions (Figure 12) for the assignment of the detailed sequence and linkages of *N*-glycans are obtained by negative mode tandem mass fragmentation and are further discussed and reviewed in Chapter 2.

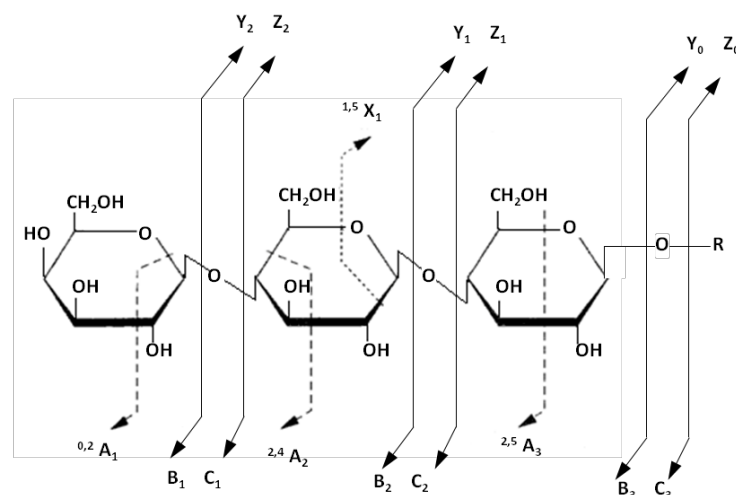


Figure 11. The Domon and Costello nomenclature system for labelling glycan fragment ions commonly observed in tandem mass spectra including the cross-ring X and A ions, B and Y type ions and C and Z type ion fragments. The systematic representation is taken and modified from⁹⁹.

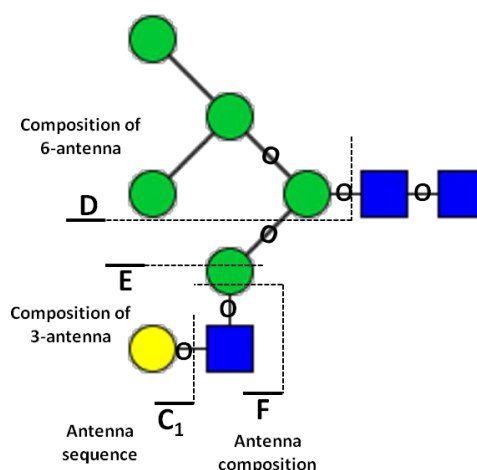


Figure 12. Hybrid glycan showing the major fragment ions used for assigning antenna sequence and composition. These well-established ions diagnostic of specific fragmentation cleavages were proposed by Harvey *et al*¹⁰⁰⁻¹⁰³. The D ion: 6-antenna and the branching mannose residue, E ion: ^{0,4}A and F ion: ^{1,3}A cleavage of the mannose residues attached to the core branching mannose. Figure taken and modified from¹⁰⁰.

1.4.2.6 Quantitation

It is important to accurately determine the identity of glycans present within biological samples but also to accurately quantitate changes in the abundance of glycans between individual samples. Methods for the quantitative analysis of glycans are less established than that for proteins or peptides but recent advances are providing both label and label-free options¹⁰⁴. These include the use of isotopically labelled glycan standards of known concentration¹⁰⁵ or incorporation of stable isotopes via permethylation⁵³. Determining the quantity of each individual glycan within a sample (absolute quantitation) is a difficult task especially when using MS based analysis approaches. This is due mainly to differences in the ionisation efficiency of different glycan species within a sample and instrument response. For these reasons relative quantitation is still the best strategy for glycan samples analysed using MS techniques, although this method is still susceptible to errors from ionisation efficiency, instrument performance variability and sample handling⁶⁶. However by calculating the relative abundance of glycans with a sample, a comparison can be made with other samples analysed in the same manner⁵².

1.4.2.7 Bioinformatics

The availability of databases and tools to aid data interpretation and assignment of glycan structures from both LC and MS data has significantly improved in recent years. These resources can be categorised into integrated databases which provide curated published data and associated information, structural databases and tools for annotation (Table 2). Tools and databases used to assist data analysis throughout this thesis include Glycomod¹⁰⁶, GlycoWorkbench¹, GlycoSuiteDB¹⁰⁷, UnicarbKB¹⁰⁸ and Unicarb-DB¹⁰⁹.

Table 2. Glyco databases and electronic resources and tools.

Type	Name	URL
Integrated databases	UnicarbKB	http://unicarbkb.org
	GlycomeDB	http://www.glycome-db.org/
	EUROCarbDB	http://www.ebi.ac.uk/eurocarb/
	CFG	http://functionalglycomics.org/
	GlycoSuiteDB	http://glycosuitedb.expasy.org/glycosuite/glycodb
	Glycosciences DE	http://www.glycosciences.de/index.php
	JCGGDB	http://jcgddb.jp
Glycan biosynthetic and catabolic pathways	KEGG-Glycan	http://www.genome.jp/kegg/glycan
	CazyDB	http://www.cazy.org
	GGDB	http://riodb.ibase.aist.go.jp/rcmg/ggdb
Structural glycan characterisation	Unicarb-DB	http://www.unicarb-db.com
	GlycoMob	http://www.glycomob.org
	GlycoBase (Oxford/Dublin/NIBRT)	http://glycobase.nibrt.ie/glycobase.html
	CCSD (CarbBank)	http://boc.chem.uu.nl/sugabase/carbbank.html
	GMDB (Glycan Mass Spectra Database)	http://riodb.ibase.aist.go.jp/rcmg/glycodb/Ms_ResultSearch
	BCSDB (Bacterial Carbohydrate Structural Database)	http://www.glyco.ac.ru/bcsdb3/
Tridimensional structure	Glycoconjugate databank	http://www.glycoconjugate.jp
Analysis Tools	Glycan Pathway Predictor (GPP) Tool	http://www.rings.t.soka.ac.jp/
	GlycoWorkbench	https://code.google.com/p/glycoworkbench/
	GlycoMod	http://web.expasy.org/glycomod/

Table updated and adapted from⁴⁹

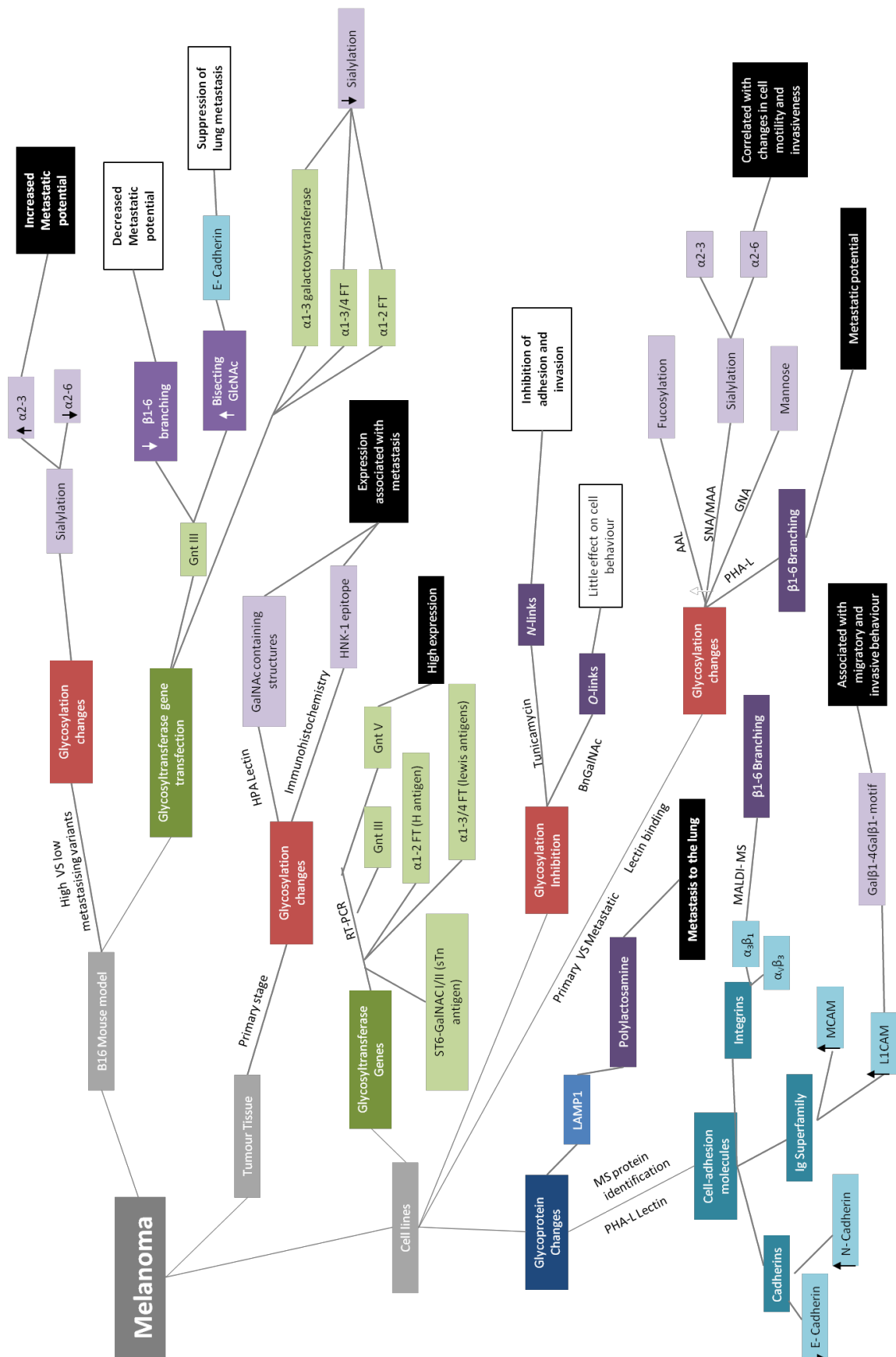
1.5 Glycan analysis strategies applied to melanoma research

Important components of functional glycomics are the in-depth characterisation of the repertoire of glycan structures found on proteins in cells and tissues, and the heterogeneity of these glycans that results from their non-template-driven biosynthesis. Establishing connections between glycan structure and biological functions are important research goals; to this end various glycoanalytical methodologies have been developed over recent years including mass spectrometry and high-performance liquid chromatography, as described above. However, regardless of the method, a balance is needed between complete structure determination (explicitly assigning monosaccharide residues, branching and linkages) and high-throughput analysis. No single robust method is available for the rapid and reliable identification of all glycan structures.

Aberrant changes in glycosylation have been reported to contribute towards the invasive and metastatic potential of melanoma cells. Most of these studies have focused on

glycosyltransferase expression profiling, the use of lectins to probe glycan changes, sialic acid profiling with HPLC, and targeted tandem mass spectrometry of glycans released from isolated glycoproteins, summarised in Figure 13. The majority of studies to date have involved the use of cell line and B16 Mouse models to evaluate glycosylation changes between primary and metastatic disease at both the global and glycoprotein level. The limited studies involving tumour tissue from patients have so far only provided potential glycan epitope biomarkers at the primary tumour levels using lectin and immunohistochemistry techniques, these candidates have yet to be verified using MS based methods. Cell line models combined with targeted lectin approaches have provided some potential targets for further investigation including the abundance of fucose, sialic acid and β 1-6 branched containing glycans from cell lysates of different disease stages. Although these glycan features have been identified and correlated with changes in cell motility and invasiveness, the structures carrying these features have yet to be confirmed. Investigations at the glycoprotein level have mainly focused on the identity of proteins carrying β 1-6 branched glycans by L-PHA lectin isolation and mass spectrometry analysis has also been carried out^{110,111}. Glycans released from individual glycoproteins isolated from cell lines including Integrin subunits have also been characterised by MALDI MS/MS^{112,113}, and more recently HILIC-HPLC analysis of 2AB labelled glycans with exoglycosidase digestion of the glycans on the glycoprotein L1CAM isolated from melanoma cell lines of different metastatic potential has been described¹¹⁴.

Figure 13. Summary of specific observations on glycosylation changes in melanoma from cell line, tumour tissue and mouse models. Figure generated from the following references^{29,110-112,114-124}.



1.6 Thesis Aims

Overall aim

The overall aim of this thesis work was to optimise new strategies for the comprehensive membrane protein glycomic characterisation combining Porous Graphitised Carbon (PGC) separation, mass spectrometry fragmentation and exoglycosidase digestion, and to apply these techniques to the analysis of metastatic melanoma cells and tissues to identify potential new biomarkers.

Specific aims

- To investigate and optimise analysis parameters for the facilitated detection and relative quantitation of multi-antennary *N*-glycan structures in complex biological samples.

To this end

- To map the PGC elution behaviour of *N*-glycans and build a retention time library covering a full spectrum of biologically significant *N*-glycans from pauci mannose to sialylated tetra-antennary classes.
- To produce high quality annotated mass spectrometry data sets in order to facilitate the development of bioinformatics tools and resources to aid future glycan analysis.
- To characterise the membrane *N*-glycosylation profile of metastatic melanoma cell line models, prognostic marker protein and lymph node tumour tissues.

To this end

- To confirm glycosylation characteristics associated with metastatic melanoma including β 1-6 branched structures documented in the literature and to identify new glycan features.
- To characterise the *N*-glycosylation profile of the melanoma cell adhesion molecule (MCAM) prognostic biomarker.
- To investigate potential glycosylation features associated with melanoma stage, prognosis and primary subtype in patient lymph node tissues.

Chapter 2

Negative ion CID MS spectra of released *N*-glycans contain ions that are diagnostic for specific structural features such as antennae composition, the presence of bisecting GlcNAc and the location of fucose residues. Previous studies have shown that negative ion CID fragmentation can provide more detailed structural information than corresponding positive ion spectra^{101,102,125}. This difference is due to the abundance of C-type glycosidic cleavages formed following deprotonation and A-type cross-ring cleavages rather than the B- and Y-type glycosidic cleavages that are common to the fragmentation of positive ions.

In this chapter we present a PGC-LC-ES-MS/MS (negative mode) strategy that can be used to carry out in-depth structural analysis of mixtures of glycans released from proteins in complex biological samples. We investigate the fragmentation of these glycans and demonstrate that informative structural information can be obtained by producing abundant cross ring fragmentation products, and that improvements in isomer recognition can be further obtained by porous graphitised carbon chromatography in combination with exoglycosidase treatment. The method was developed on the heavily *N*- and *O*- linked glycosylated human salivary glycoproteins and characterized over 200 *N*- and *O*- released glycans; thereby validating the method and providing an information rich spectra resource of annotated glycan structures.

Publication: Everest-Dass AV, **Abrahams JL**, Kolarich D, Packer NH, Campbell MP. Structural feature ions for distinguishing *N*- and *O*-linked glycan isomers by LC-ESI-IT MS/MS. J Am Soc Mass Spectrom. 2013. 24(6):895-906.

Author contributions: Experimental design- AD, JA and MC, data collection and analysis- AD and JA, manuscript preparation- AD, MC and JA, editing and reviewing- NP and DK.

I was responsible for the design, data collection and interpretation of exoglycosidase digestion experiments.

Chapter 3

In Chapter 2 we demonstrated that negative ion mode PGC-LC-ESI-MS/MS can be efficiently applied to analyse the structural details of released, reduced *N*-glycans. An important feature of this study was the efficient mapping of various diagnostic MS/MS ions to confidently assign many glycan structures. For complex samples the analytical challenge lies in the discrimination of the numerous isomers and elongated structures that cannot be easily distinguished by MS alone. One of the advantages of using PGC-LC is the high separation power for structural and linkage isomers, which complements MS analyses as isobaric compounds exhibiting exactly the same m/z can be separated and analysed.

Analysing the *N*-glycans released from well characterised glycoprotein standards provides the opportunity to elucidate and understand not only the unique fragmentation properties of individual glycans compared to their corresponding isomers, but also to determine their retention behaviours using PGC chromatographic retention. Little work has been published on the retention order of *N*-glycans (on PGC) and, consequently, in this chapter we demonstrate its usefulness for inferring structural features that are difficult to identify by mass spectrometry alone. By analysing a full range of *N*-glycan classes the retention order of different glycan structures was mapped and a comprehensive knowledge base created with supporting MS/MS spectra. In addition, we show that an efficient mapping of various isomeric fucosylated, sialylated and complex branched glycans by negative ion mode PGC-LC-ESI-MS/MS of glycans released from cells and tissues can benefit from the resource described (Chapters 5 and 7).

Prepared Manuscript: Abrahams JL, Campbell MP, Packer NH. Using standard glycoproteins to build a PGC-LC-MS retention library and retention mapping resource.

Author contributions: Experimental design- JA and MC, data collection and analysis- JA, manuscript preparation- JA and MC, editing and reviewing- NP.

Chapter 4

Exoglycosidase enzymes are an important resource available to glycobiologists to aid in the elucidation of glycan structures. The results of exoglycosidase treatment provide information on the type and linkage of the cleaved monosaccharide residues. Used alone or in array format, exoglycosidases can reveal a wealth of information on a specific glycan species or mixture, including the sequence of a glycan and quantitative assessment of the abundance of sialylation, fucosylation, the degree of branching. Traditionally exoglycosidases have been used in combination with HPLC combined with fluorescence detection to confirm glycan structures, but their use with other platforms including CE and LC-MS is becoming increasingly popular.

As demonstrated in the previous two chapters, combining PGC-LC-MS analysis with exoglycosidase digestions is a powerful strategy for the characterisation of complex samples. By using knowledge of known enzyme specificities and the number of monosaccharide residues removed, terminal glycan moieties and linkages can be determined. Most importantly experimental evidence such as is available in the database GlycoBase (for 2AB labelled glycans analysed by HILIC-U/HPLC) and the data described here for MS/MS analysis of reduced glycans in Chapters 2 and 3 (integrated into the MS/MS spectral database, UniCarb-DB) enables the establishment of a defined set of controlled digestion rules, which can be used to aid glycan analysis. Here, we present a bioinformatics tool, called GlycoDigest, which simulates the exoglycosidase treatment of *N*-glycans and predicts digestion products for individual glycans treated with either a single or panel of exoglycosidases. This chapter details the resulting prediction tool, user guides and examples, and demonstrates how this tool can be used to tailor a panel of exoglycosidases for the full characterisation of separated glycans. The development of this tool was designed to further facilitate the detailed structural characterisation of glycans released from complex mixtures of glycoproteins derived from cell lines and tissues.

Publication: Gotz L, **Abrahams JL**, Mariethoz J, Rudd PM, Karlsson NG, Packer NH, Campbell MP, Lisacek F. GlycoDigest: a tool for the targeted use of exoglycosidase digestions in glycan structure determination. *Bioinformatics*. 2014 1; 30 (21):3131-3.

Author contributions: Experimental design- MC, JA and NP, Bioinformatics- LG, JM and MC, data collection, analysis and supplementary material- JA, manuscript preparation- MC, editing and reviewing- NP, NK, PR and FL.

Chapter 5

It has been suggested that abnormal expression of specific glycosyltransferases might serve as useful biomarkers for cancer. In fact, many studies of melanoma have implicated the importance of beta1,6-*N*-acetylglucosaminyltransferase V (GnT V) activity in the progression of the disease and the functional roles that the enzyme product, β 1-6 branched *N*-glycans, on cell surface glycoproteins have as important factors in the migration of primary melanoma cells. To date, most studies have utilised lectin-based approaches (PHA-L) to recognise and assess changes in specific glycan branched epitopes; however, detailed structural characterisation of this class of β 1-6 branched *N*-glycan structures has not yet been reported.

The melanoma cell adhesion molecule, also referred to as MCAM, MUC18 or CD146, is a cell surface glycoprotein frequently over expressed on the surface of advanced and metastatic melanoma cells, however, its expression is rare in benign nevi. Previously, it has been reported that over-expression of MCAM plays an important role in progression of metastatic melanoma, however the structural glycosylation on this prognostic biomarker has not been determined.

Using the techniques described in Chapters 2, 3, and 4, the global *N*-glycosylation profiles of the membrane glycoproteins, and of the immunoprecipitated metastatic glycoprotein marker MCAM, from a metastatic melanoma cell line (MM253; lymph node derived) were analysed by PGC-LC-MS/MS and structures determined, notably with focus on the identification and relative quantitation of β 1-6 branched structures.

***N*-glycosylation in metastatic melanoma: Investigating the presence of β 1-6 branched *N*-glycans**

5.1 Introduction

Melanoma is the greatest cause of skin cancer-related deaths worldwide despite only accounting for 4% of all skin cancers. The only established curative treatment is the early detection and removal of melanoma lesions at an early stage; unfortunately, once a patient develops metastatic disease the prognosis is poor^{127,128}. There are five defined stages of melanoma progression, starting with the development of a congenital nevus, then dysplastic nevus, a radial growth phase (early primary melanoma), radial growth phase (advanced primary melanoma) and metastasises first to the lymph nodes and then to distant organs²⁴. Metastasis accounts for the majority of mortality associated with melanoma, as limited treatment options exist for advanced stages of the disease¹²⁹.

Cells within the epidermal environment, mainly surrounding keratinocytes, tightly regulate melanocyte growth and behaviour²⁴. Changes that upset this delicate homeostatic balance between melanocytes and their environment can lead to the altered expression of cell-cell adhesion and communication molecules. This has been demonstrated by the culturing of normal melanocytes in isolation leading to the expression of melanoma-associated antigens^{24,130}, but when co-cultured with keratinocytes, cell-to cell expression of melanoma-associated antigens disappear^{131,132}. Various types of adhesion molecules including integrins, cadherins and members of the immunoglobulin (Ig) superfamily have been shown to undergo significant changes in expression levels during progression of melanoma¹³³. Examples of altered cell surface proteins include a shift from the E-cadherin to N-cadherin and an increase in MCAM expression that benefit melanoma cell-melanoma cell interactions¹³⁴.

An important role in cancer pathogenesis is attributed to *N*-glycans with bisecting GlcNAc and β 1-6 branches^{29,43,135}, but the exact mechanisms still remain unknown. To date, the role of glycosylation in the progression of melanoma has focused on glycoproteins bearing glycans with a β 1-6 branched GlcNAc linkage. Much of this work has been driven by Litynska and colleagues who have shown a correlation between the presence of the β 1-6 branch (confirmed by lectin-based methods) and the invasive and migratory behaviour of melanoma cells in culture^{20,110,111,119,129}. The addition of β 1-6 linked GlcNAc residues to the six arm of the tri-mannosyl core to form tri – and tetra-antennary glycan structures is catalysed by the action

of the GlcNAc transferase V enzyme (GnT V) encoded by the *MGAT 5* gene⁴³. The β 1-6 GlcNAc branch is a preferred substrate for the addition of poly-lactosamine extensions (β 1-3 GlcNAc- β 1-4 Gal)⁴⁶ (Figure 1).

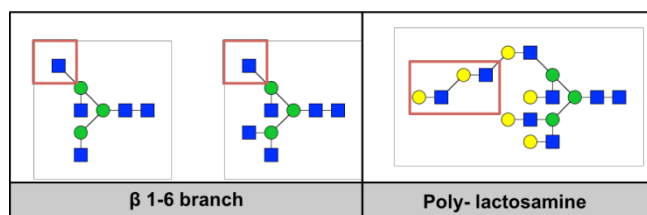


Figure 1. Products of GnT V activity. Tri- and tetra-antennary glycans with β 1-6 branching, and tetra-antennary with modification of the β 1-6 branch by poly-lactosamine extensions.

Candidate glycoproteins, expressing β 1-6 branching glycans, have been isolated by lectin-affinity chromatography using *Phaseolus vulgaris* agglutinin (PHA-L) and identified by tandem mass spectrometry. These proteins include integrin, L1CAM, Mac-2 binding protein, melanoma cell adhesion molecule (MCAM), intercellular adhesion molecule, melanoma associated antigen, tumour rejection antigen-1, melanoma-associated chondroitin sulfate proteoglycan 4 and lysosome-associated membrane protein (LAMP- 1)¹¹¹. Characterisation by MALDI-MS of glycans released from the integrin subunits α_3 and β_1 isolated from melanoma cell lines representing different stages of disease has shown that the glycosylation profile of this protein differs in the abundance of branched and sialylated species between disease classifications¹¹². An important observation is the increased abundance of branching for more aggressive melanoma cell lines¹¹⁹. Recently, *N*-glycans released from the L1 cell adhesion molecule (L1CAM) isolated from different stages of melanoma have been characterised by HPLC with fluorescence detection combined with exoglycosidase digestion¹³⁶. To date, this is the most comprehensive glycan analysis of a potential melanoma glycoprotein prognostic marker, and reports a novel mono-antennary structure containing a β Gal-Gal epitope with a terminal polysialic acid unit of variable length. This study also observed a loss of α 2-3, and an increase in α 2-6, linked sialic acid residues on L1CAM glycans associated with metastasis. Although L1CAM has been reported as a candidate protein for β 1-6 branching glycans by previous studies^{111,129} (as confirmed by lectin-binding studies), only two tetra-antennary species were reported in this study, which were identified using HPLC with fluorescence detection and confirmed by MALDI-MS. In addition, tri-antennary and polylactosamine species were reported but the GlcNAc linkages were not fully defined¹¹⁴.

The expression of the cell surface glycoprotein MCAM is known to be a prognostic indicator of melanoma. MCAM was originally identified on the surface of melanoma cells but absent on normal melanocytes²⁵, however it is now known to be involved more generally in development, signal transduction, cell migration, mesenchymal stem cell differentiation, angiogenesis and immune responses¹³⁷. MCAM has been used as a biomarker of melanoma progression since 1989 with its increased cell surface expression correlating with disease progression and poor prognosis of patients²⁶. Furthermore, increased MCAM expression has also been linked to the progression of other cancers including breast, prostate and ovarian^{23,138,139}. The mechanism of MCAM expression has been extensively studied. In brief, MCAM expression is regulated by direct cell-to-cell contact with keratinocytes in normal melanocytes, nevus, and early primary melanoma cells. Such interactions are diminished in advanced primary and metastatic melanoma cells, in turn leading to up regulation of MCAM²⁴. Consequently, investigating the differences between normal melanocyte and metastatic melanoma cell homeostasis, especially the physical properties of key cell surface proteins, is vital to a better understanding of how melanoma cells escape the microenvironment created by the epidermal keratinocytes.

MCAM, also known as MUC18, CD146, A32 antigen or S-Endo-1, is a 113 kDa member of the immunoglobulin superfamily^{137,140}. It has many names as several independent research groups identified it. Originally it was cloned and sequenced from a human melanoma cDNA library and demonstrated to be a cell adhesion molecule and subsequently it was given the name MCAM to reflect its function^{140,141}. It consists of five characteristic Ig-like extracellular domains in the configuration V-V-C2-C2-C2, a short transmembrane region and a cytoplasmic tail. Two isoforms exist that differ in the length of the cytoplasmic domain. The long form (CD146-l) is the main isoform expressed by melanoma cells compared with endothelial cells that express both the long and short form (CD146-s). MCAM exists as a monomer and dimer on the cell surface, with dimerisation mediated through a disulphide bond between cysteine residues in the Ig domains²³. In addition to the membrane-associated form of MCAM a soluble form also exists (sCD146) which has been detected in cell culture supernatant and serum from normal healthy individuals²³. MCAM has five potential protein kinase recognition motifs in the cytoplasmic domain suggesting its involvement in cell signalling¹⁴², and it was identified as a sialylated glycoprotein after observation of a shift in molecular mass after treatment with neuraminidase²⁵. It has eight potential *N*-glycosylation sites located at positions 56, 418, 449, 467, 508, 518, 527 and 544²⁶. Approximately 35% of its molecular mass is composed of

carbohydrates, including the abundant expression of sialic acid bearing glycans and evidence for the HNK-1 epitope (3-O-sulfated glucuronic acid (GlcA) α 1–3 linked to galactose) verified by reactivity with a monoclonal antibody specific for the HNK-1 epitope¹⁴³⁻¹⁴⁵.

Cell lines from different stages of melanoma progression have helped in our understanding of the stepwise progression from primary melanoma to metastases. Such investigations have been facilitated by the accessibility of melanoma lesions and the fact that melanoma can be adapted to tissue culture. There are an abundance of cell lines available for studying melanoma from different stages of the disease, with an estimated 5000 types available for research. Of these, approximately 200 established human cell lines have been thoroughly characterised for genetic aberrations, global gene expression patterns, and biological properties including invasion *in vitro*, and tumour and metastasis formation in immunodeficient mice¹⁴⁶. Notably, most studies have focused on understanding the genetic etiology of disease.

Despite the importance of glycosylation in the progression of melanoma only a few studies have investigated the glycan profiles of cell lines and/or individual glycoproteins^{112,113,115,136}. Glycans on specific glycoproteins are recognised to play key roles in cell adhesion and signaling⁴³. It has been suggested by several reports that MCAM plays an important role as a signalling molecule in human melanoma²⁶, therefore, a change in the glycosylation profile of MCAM as well as increased expression may contribute to the metastatic phenotype by changing signaling behavior and adhesion properties.

Studies in recent years have confirmed that MCAM is a target substrate for GnT-V activity and that its glycosylation profile includes glycans bearing β 1-6 linked GlcNAc branching that is the product of GnT-V activity, as was shown by PHA-L lectin reactivity^{110,111,147}. The effect of induced over expression of N-acetylglucosaminyltransferases III and V (GnT III and V) on the *N*-glycosylation profile of MCAM have recently been investigated in relation to its interaction with endothelial cells¹⁴⁷. Surprisingly, although this glycan characteristic has been confirmed, along with information on the presence of terminal sialylation, the complete glycosylation profile of MCAM has not yet been analysed.

In this chapter we characterise the *N*-glycosylation profile of the MM253 cell line (derived from metastatic melanoma of the lymph node), as well as the glycosylation profile of MCAM

isolated from this cell line, with a focus on the detailed characterisation of structures bearing the β 1-6 linked GlcNAc branch.

5.2 Materials and Methods

The human melanoma cell line MM253 (axillary lymph node metastasis) and MCAM purified from MM253 cells were provided by Prof. Deirdre Coombe, Curtin University, Australia.

MCAM was immunoprecipitated using a mouse anti-human melanoma cell adhesion molecule (MCAM) monoclonal antibody (mAb CC9) and provided in the form of 1D SDS gel bands for *N*-glycan analysis.

Cell culture of MM253 cells

MM253 cells were cultured in RPMI 1640 media supplemented with 2 mM L-glutamate, 10 mM HEPES, 1 mM sodium pyruvate (all from Gibco BRL, USA) and 10% foetal calf serum (CSL Limited, Melbourne, Australia) (RPMI/10%) in a humidified incubator equilibrated with 5% CO₂ at 37°C. Cells were grown to 70 - 80% confluence in Nunclon tissue culture flasks (Nalge Nunc International, USA) as monolayers and harvested with 0.05% (w/v) trypsin/0.53 mM EDTA (TE) (Gibco BRL). All cultures were free of *Mycoplasma*. Cell pellets (1×10^7 cells) were washed three times with PBS and pelleted by centrifugation prior to membrane protein enrichment.

Enrichment of membrane proteins from MM253 cell pellets

Total cell membranes were enriched by cell lysis and ultracentrifugation. Cell pellets were homogenised on ice in 0.5 mL of lysis-buffer (50 mM Tris-HCl (pH 7.4), 0.1 M NaCl, 1 mM EDTA and protease inhibitor cocktail (Roche Diagnostics, Mannheim, Germany) using a Polytron homogenizer (Omni TH, Omni International Inc, Kennesaw, GA). Cellular debris and un-lysed cells were removed by centrifugation at 2000 x g for 20 mins at 4 °C. The supernatant was diluted with 2.5 ml of Tris binding buffer (20 mM Tris-HCl, and 0.1 M NaCl, pH 7.4) and sedimented at 120,000 x g for 80 min at 4° C. Pellets were resuspended in 100 μ L of 20 mM Tris-HCl, 0.1 M NaCl, pH 7.4 and proteins precipitated by acetone overnight at -20° C. proteins were centrifuged at 1000g for 3 min and the resulting pellets resolubilised in 4 M urea¹⁴⁸.

N-glycan release

N-glycans were enzymatically released with PNGase F (Roche) from either PVDF membrane (MM253 membrane proteins) or from SDS gel bands (MCAM) after reduction and alkylation. Fetuin or IgG were used as positive controls to test the success of each release.

MM253 cell membrane proteins

N-glycans were released from immobilised proteins as previously described⁶⁴. Approximately 10 µg of protein was immobilised onto PVDF membrane (Millipore). Protein spots were dried overnight to ensure maximum binding and stained with Direct Blue 71 (Sigma) before being excised and transferred to a flat bottom 96 well plate. To prevent non-specific binding of PNGase F, sample wells were blocked with 1% PVP 40 and washed with water. *N*-glycans were released by overnight incubation with PNGase F (2.5 U in 10 µl water) at 37 °C. Released glycans were recovered after sonication for 5 min and washing each sample well with 2x20 µl of water. Samples were then dried in a vacuum centrifuge.

MCAM

N-glycans were released from 1D SDS-PAGE gel bands as previously described⁶². Gel bands were excised and cut into 1mm³ pieces. The gel pieces were washed alternately with 500 µl of acetonitrile (x3) and 100 mM ammonium bicarbonate buffer (x2) while shaking on an orbital platform shaker for 15 min each. After washing, PNGase F (3 U in 30 µl buffer) was added to the gel pieces. The gel pieces were left for 5 min before adding enough buffer to cover the gel pieces (~100 µl). Samples were incubated at 37°C overnight. The released glycans were extracted from the gel pieces by sonication for 15 min alternate water and acetonitrile washes (200 µl each). All extractions were combined and filtered using 0.45 µm PTFE syringe filters (Millipore) before being dried in a vacuum centrifuge.

Reduction and desalting of N-glycans

Released *N*-glycans and glycan standards were treated with 10 µl of 100 mM ammonium acetate for 1 h at room temperature and dried. Glycans were reduced to alditols with 0.5 M NaBH₄ in 50 mM KOH for 3 hours at 50°C. reduction was quenched by adding 2 µl of glacial acetic acid. The reduced *N*-glycans were desalted using AG 50W X8 strong cation exchange resin (30 µl bed volume) packed in C18 tips (Stage tips, Thermo) and dried in a vacuum centrifuge. Samples were washed three times with methanol to evaporate residual borate⁶⁴.

Exoglycosidase digestion

Aliquots of reduced *N*-glycans were dried by vacuum centrifugation before being digested with an array of exoglycosidase enzyme combinations including ABS, ABS+BTG, ABS+BTG+BKF.

All reactions were carried out in a total volume of 10 µl including 2 µl of 5X incubation buffer (50 mM sodium acetate pH 5) enzyme and water at 37 °C for 16 h^{62,63}. Enzymes were used at

the concentrations described in Chapter 4. Enzymes were removed by carbon clean up before being analysed by PGC- LC-ESI MS/MS.

Carbon clean up

Samples were subjected to carbon solid phase extraction before analysis by LC-MS.

Spin columns were prepared in-house by packing material from a carbon SPE cartridge into C18 Stage tips (Thermo Fisher Scientific). Samples were eluted in 40% Acetonitrile containing 0.05% (vol/vol) TFA and dried in a vacuum centrifuge⁶⁴.

Instruments and processing software

Glycans were analysed using Agilent 1260 capillary HPLC with Agilent LCD/ MSD Trap XCT Ultra (Agilent Technologies Inc., USA). Instrument control, data acquisition and processing were performed with Bruker DataAnalysis software version 4.0 (Bruker Daltonics, Germany).

Porous Graphitized Carbon (PGC) LC of N-glycans

N-glycans were separated using PGC (Hypercarb KAPPA Capillary Column; Thermo Fisher Scientific) 0.18 mm inner diameter × 100 mm either 3 or 5 µm particle size. Separations were performed at 2 µl/min. Mobile phase A was 10 mM ammonium bicarbonate pH 8 and mobile phase B 10 mM ammonium bicarbonate in 45% (vol/vol) acetonitrile. Samples were run for 85 min using the following gradient; 0-8 min 100% buffer A, 5-35% B over 45 min, 35-100% B over 20min, the column was then washed with 100% B for 5 min before equilibrating with 100% A for 10 min⁸¹.

IT-ESI-MS/MS

Glycan masses were detected using an Agilent 6330 ESI ion trap (Agilent Technologies Inc., CA, USA) The MS spectra were acquired in the negative ion mode over mass range of 440 to 2200 m/z. The following MS settings were used: drying gas temperature: 300°C, drying gas flow: 6 L/min, nebulizer gas: 12 psi, skimmer, trap drive and capillary exit were set at -40 V, -99.1 V and -166 V, respectively. Ions were detected in ion charge control (ICC) (target: 30,000 ions) with an accumulation time of 200 ms. Induced collision was performed at 35 % normalized collision energy and an isolation window of 4 m/z.

5.3 Results

Previous studies of metastatic melanoma using cultured cell models and lectin-based methods have implicated an increased expression of cell surface tri- and tetra-antennary *N*-glycans with a β 1-6 branch in the progression of melanoma. In order to assess the degree of antennae branching and to identify *N*-glycans containing this structural feature we enriched the membrane proteins of a metastatic melanoma cell line (MM253; lymph node derived) by ultracentrifugation, released the *N*-glycans using PNGase F and analysed the structures present by PGC-LC-MS/MS. Compositional glycan assignments were made after manual interpretation of MS profiles and database matching with UniCarbKB (<http://unicarbk.org>) using the GlycoMod tool (<http://web.expasy.org/glycomod/>). Structural assignments were made after further analysis of negative mode MS/MS fragmentation, PGC elution behaviour and exoglycosidase digestion (Chapters 2 and 3).

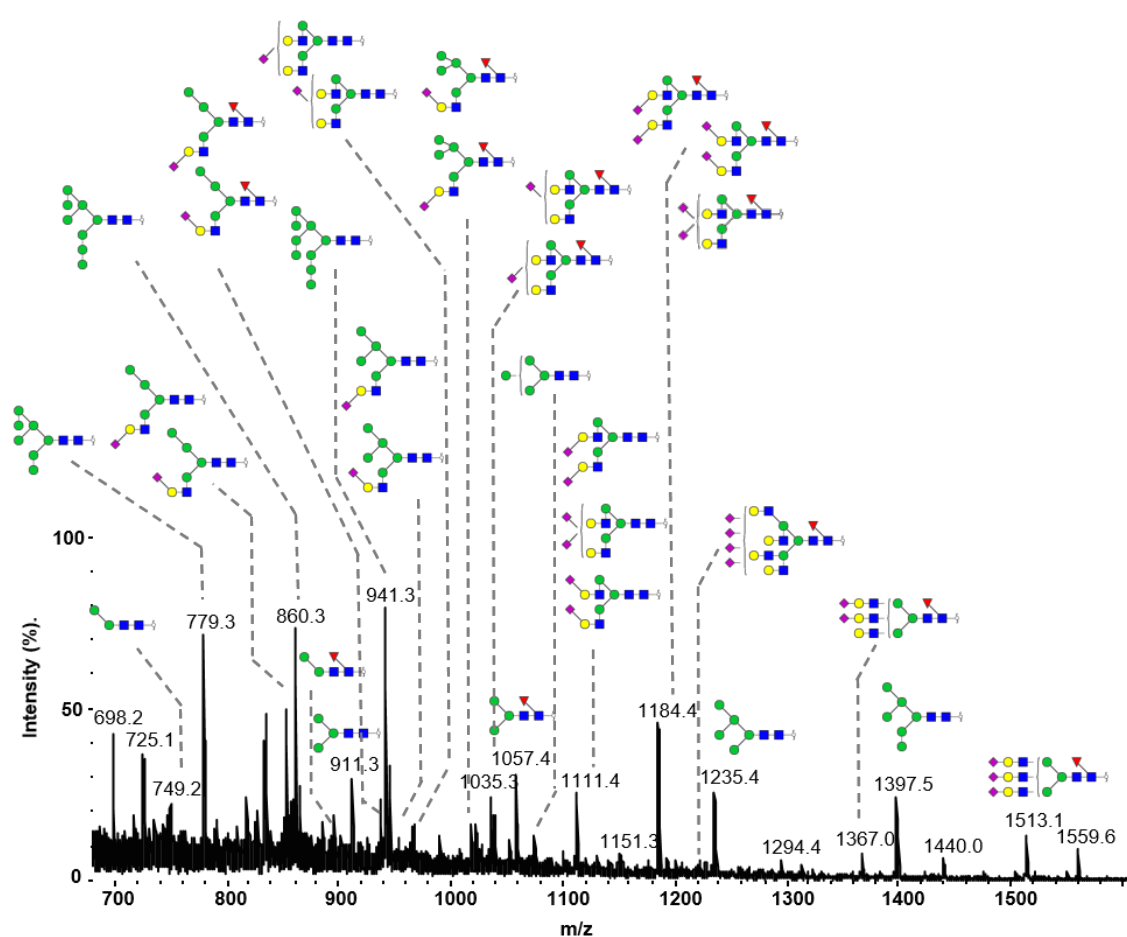
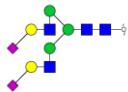


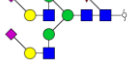
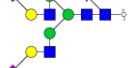
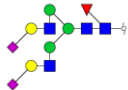

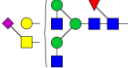

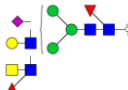
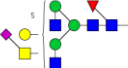
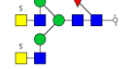
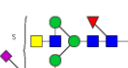




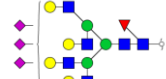
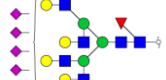
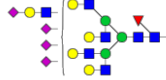
Figure 2. PGC-LC negative ion MS profile of *N*-glycans released from the enriched membrane protein fraction of MM253 cells. Details of the structures are shown in Table 1. Structures are drawn using CFG notation with linkage placement.

Table 1. Structural assignments and relative percentage abundances of identified *N*-glycans released from the membranes and MCAM of the metastatic melanoma cell line MM253.

Structure			Mass (m/z)			Relative % Abundance		
			[M-H] ¹⁻	[M-2H] ²⁻	[M-3H] ³⁻	MM253 (n=3) Mean ±SD	MCAM	
Pauci Mannose	M2		749.3			0.93 ± 0.30	-	-
	M3		911.3			1.36 ± 0.37	-	-
	FM2		895.3			2.30 ± 0.35	-	-
	FM3		1057.4			1.89 ± 1.50	-	-
	M4		1073.3			1.00 ± 0.17 0.43 ± 0.04	-	-
High Mannose	M5		1235.4			1.72 ± 0.59	0.86	2.76
	M6		1397.5	698.3		1.12 ± 0.24 11.99 ± 1.39	11.59	13.61
	M7		1559.5	779.3		15.60 ± 1.43 3.54 ± 0.78	5.23	8.90
	M8			860.3		15.98 ± 2.57	2.03	3.29
	M9			941.3		16.80 ± 2.90	-	-
	M9 Glc1			1022.3		1.12 ± 0.26	-	-
Hybrid	M4A1G1S(6)1			864.3		1.35 ± 0.45	-	-
	M4A1G1S(3)1			864.3		0.27 ± 0.24	-	-
	FM4A1G1S(6)1			937.3		1.64 ± 0.67	-	-

Structure			Mass (m/z)			Relative % Abundance				
			[M-H] ¹⁻	[M-2H] ²⁻	[M-3H] ³⁻	MM253 (n=3)			MCAM	
						Mean ±SD			Rep 1	Rep 2
Hybrid	FM4A1G1S(3)1		937.3			0.51	±	0.31	-	-
	M5A1G1S(6)1		945.3			2.50	±	0.33	0.64	0.77
	M5A1G1S(3)1		945.3			0.79	±	0.13	0.44	0.41
	FM5A1G1S(6)1		1018.4			0.64	±	0.48	-	-
	FM5A1G1S(3)1		1018.4			0.22	±	0.07	-	-
Mono-antennary	FA1G1S1		856.3			0.51	±	0.48	-	-
			856.3			0.53	±	0.20	-	-
Neutral Bi-antennary	FA2		731.3			-		-	3.34	4.93
	FA2G1		812.3			-		-	7.51	7.26
	FA2G2		893.3			-		-	1.00	1.04
Bi-antennary	A2G2S(6)1		965.8			0.84	±	0.26	4.11	6.74
	A2G2S(3)1		965.8			0.41	±	0.18	-	-
	A2G2S(6)2		1111.4			0.69	±	0.27	5.06	4.36
	A2G2S(6,3)2		1111.4			1.45	±	0.60	-	-

Structure		Mass (m/z)			Relative % Abundance		
		[M-H] ¹⁻	[M-2H] ²⁻	[M-3H] ³⁻	MM253 (n=3) Mean ±SD	MCAM	
Bi-antennary	A2G2S(3)2		1111.4		0.21 ± 0.06	9.48	7.45
	FA2G2S(6)1		1038.9		1.07 ± 0.79	2.37	3.59
	FA2G2S(3)1		1038.9		0.32 ± 0.12	0.23	0.75
	FA2G2S(6)2		1184.4		1.54 ± 0.46	4.48	3.18
	FA2G2S(6,3)2		1184.4		3.03 ± 0.99	4.69	5.84
	FA2G2S(3)2		1184.4		0.39 ± 0.11	0.76	1.33
LacdiNAc	F(6)A2GalNAc2S(6)1		1079.9		-	0.62	1.13
	F(6)A2G1GalNAc1S(6)1		1059.4		-	0.47	0.60
	F(6)A2G1GalNAc1S(3,6)2		1204.9		-	0.97	1.21
	F(6)A2G1F(3)1GalNAc1S1		1132.4		-	0.46	0.47
	F(6)A2G1GalNAc1S1+sulph		1099.4		-	3.26	2.87
	F(6)A2GalNAc2+sulph2		1014.3		-	0.75	1.34
	F(6)A2GalNAc2S1+suph		1119.9		-	1.32	0.91

Structure		Mass (m/z)			Relative % Abundance		
		[M-H] ¹⁻	[M-2H] ²⁻	[M-3H] ³⁻	MM253 (n=3) Mean ±SD	MCAM Rep 1	Rep 2
Tri-antennary	FA3G3S2 		1366.9		0.61 ± 0.11	1.06	1.72
	FA3G3S3 		1512.5		2.70 ± 0.79	7.56	3.18
Tetra-antennary	FA4G4S3 		1695.1		-	2.84	1.49
	FA4G4S4 		1840.6		2.02 ± 0.48	12.52	5.13
	FA4G4Lac1S4 			1348.5	-	2.64	2.09

MM253 N-glycome

The annotated summed MS PGC-LC-ESI-MS spectra of *N*-glycans released from the enriched membrane protein fraction of MM253 cells are shown in Figure 2. The structures identified included pauci mannose, high mannose, hybrid and complex *N*-glycan classes. A total of 23 *N*-glycan compositions were detected and 36 structures assigned. Relative quantitation of individual structures and structural classes were calculated from triplicate glycan releases and summarised in Table 1 and Figure 3. High mannose glycans (M5-M9Glc1) were the most abundant class of structures (69.3%) and pauci mannose with and without core fucosylation (M2-M4) accounted for (6.5%) of the total pool. The rest of the glycan profile consisted of sialylated hybrid (7%) and sialylated complex type glycans (16.3%).

Complex-type glycans ranged from mono- to tetra-antennary sialylated structures with and without core fucose. The most abundant complex-type class was the family of bi-antennary glycans (10%) that include fully galactosylated forms with and without core fucose, and either one or two terminal sialic acid residues. Multiple mass peaks corresponding to sialylated hybrid and bi-antennary structures revealed the presence of sialic acid linkage isomers. By using the previously defined PGC elution order of sialic acid linkages (described in Chapter 4), it was possible to assign both α 2-3 and α 2-6 linkages for S1 (single sialic) structures and α 2-3, α 2-6 and a mixture of linkages for S2 (disialic) structures. Quantitation of structures with defined sialic acid linkages showed an overall higher abundance of α 2-6 linked sialic acids compared to α 2-3 linked sialic acids (Figure 4).

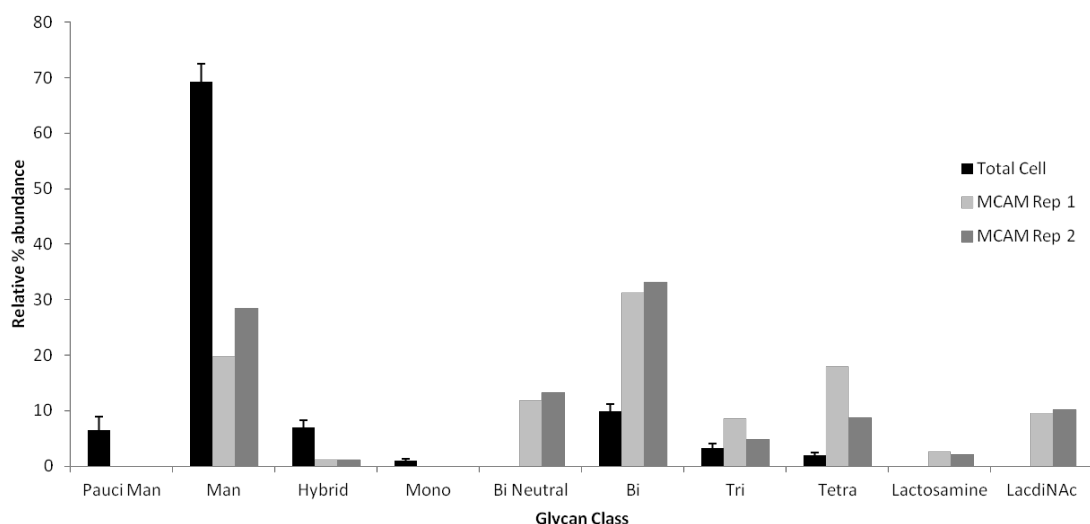


Figure 3. Relative abundance of different classes of *N*-glycans released from MM253 cells and MCAM. Error bars represent the standard deviation of triplicate cell membrane preparations from three separate cultures. Duplicate immunoprecipitation preparations of MCAM are represented separately as it was considered that there were too many variables in the sample preparation to confidently apply statistical analyses.

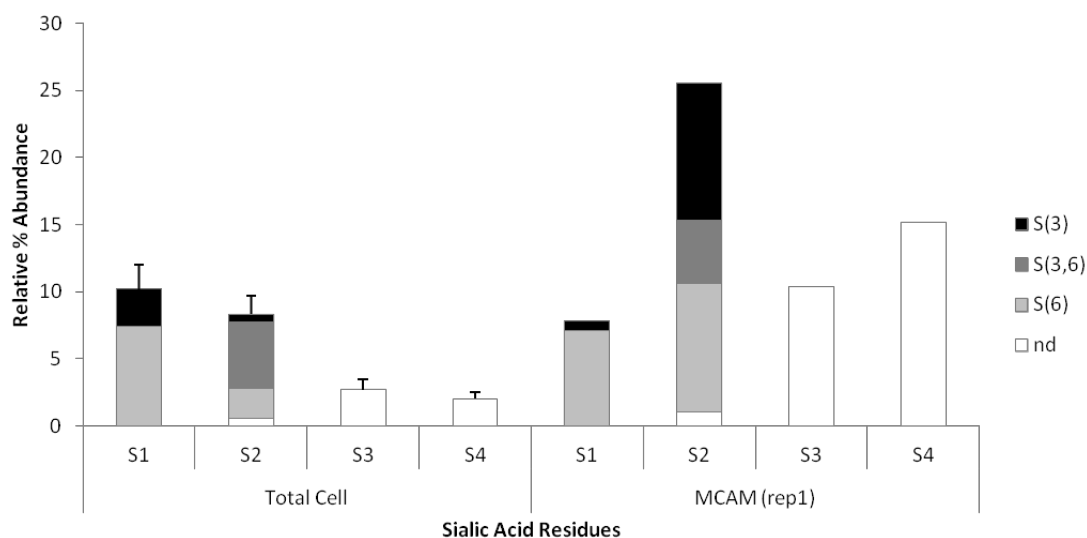


Figure 4. Relative abundance of sialylated *N*-glycans released from MM253 cells and MCAM. S1-4= number of sialic acid residues, S(3) = α 2-3 linked sialic acid, S(6) = α 2-6 linked sialic acid, S(3,6) = S2 structures with one α 2-3 and one α 2-6 linked sialic acid residue, nd = sialic acid linkages not determined. Sialic linkages were assigned based on PGC elution order for hybrid and bi-antennary glycans, but could not be determined for structures with three or more sialic acid residues. Graph shown is of representative data from a replicate analysis of one sample of MCAM.

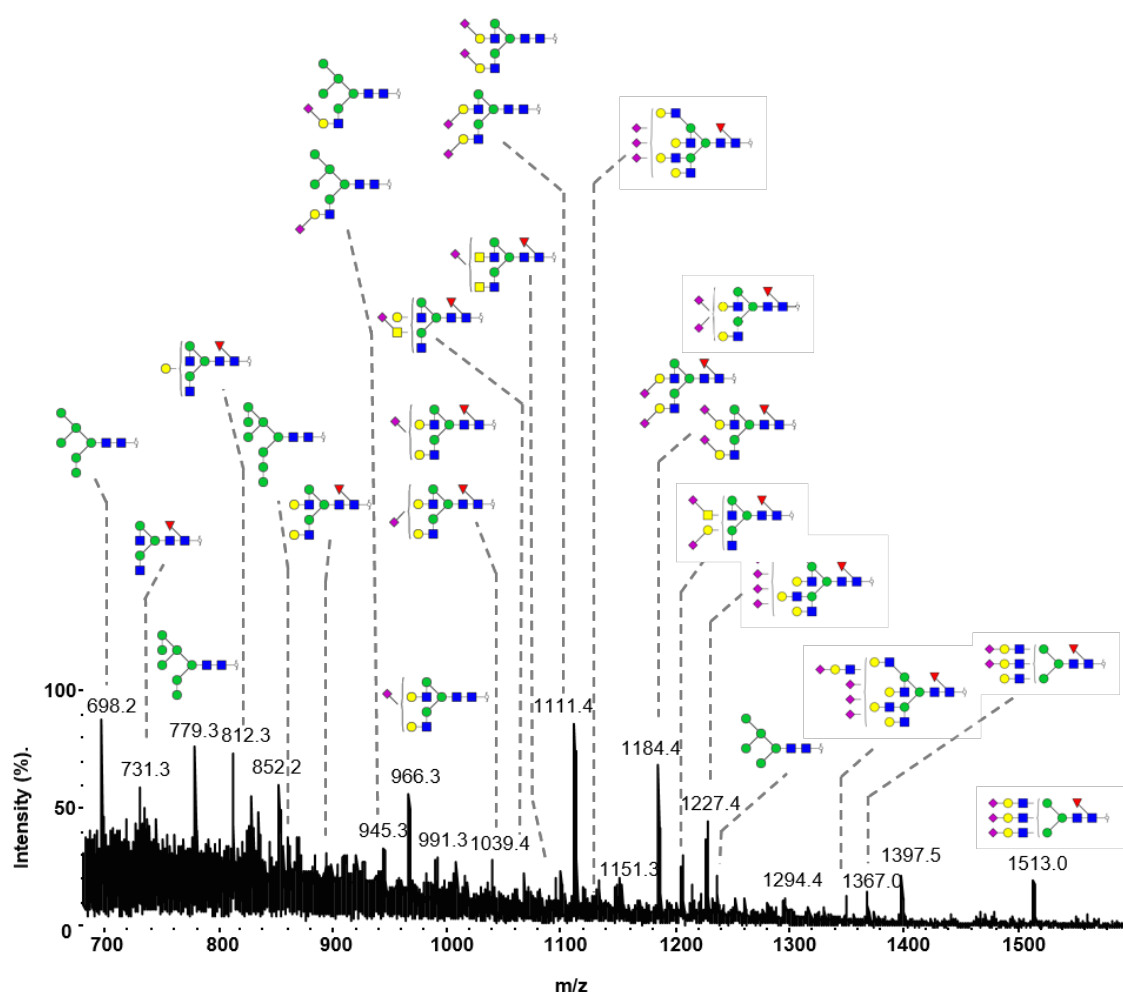


Figure 5. PGC-LC negative ion MS profile of MCAM *N*-glycans released from purified MM253 cells. A summary of the determined structures is shown in Table 1.

MCAM N-glycome

To characterise the specific glycoprotein implicated in melanoma metastasis, MCAM was immunoprecipitated from MM253 cell lysate using a mouse anti-human melanoma cell adhesion molecule (MCAM) monoclonal antibody (mAb CC9) and its precipitation was confirmed by western blotting. The total glycan profile released from MCAM is shown in Figure 5 and the relative abundance of each structure is summarised in Table 1 from duplicate preparations of MCAM. A total of 38 individual structures were identified including structural isomers spanning high-mannose, hybrid, neutral complex and sialylated complex-type glycans. The relative abundance of glycan classes are shown in Figure 3.

Unlike the total cell membrane glycome, the most abundant class of structures on MCAM were bi-antennary structures (~45% compared to 10%) which includes both neutral and sialylated structures the majority of which are core fucosylated. No pauci mannose glycans

were detected on MCAM and only a selection of high-mannose species were present (M5-M8) which account for 20-30% of the glycan pool compared to the 68% high mannose structures seen on the total cell membrane glycome (Figure 3).

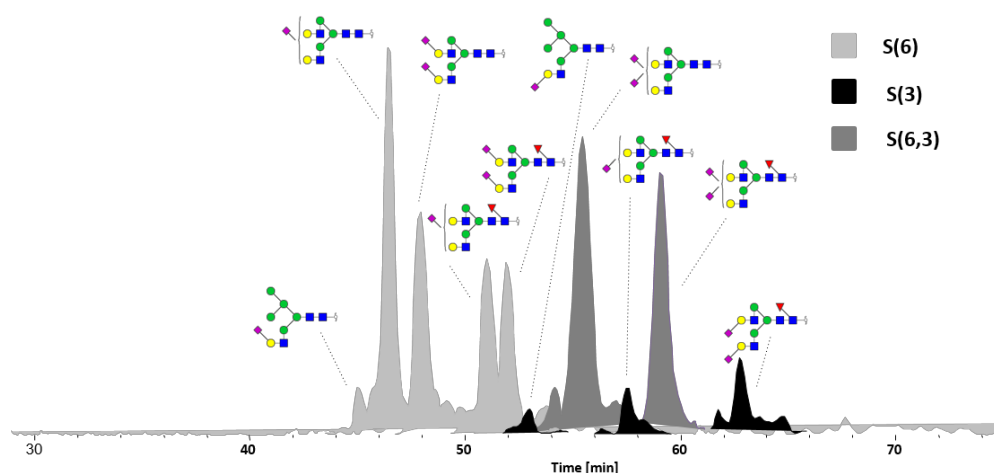


Figure 6. PGC separation of hybrid and bi-antennary sialic acid linkage isomers released from MCAM. Isomers were assigned based on elution order and time relative to M5 as described previously in Chapter 3 $S(3)$ = $\alpha 2$ -3 linked sialic acid, $S(6)$ = $\alpha 2$ -6 linked sialic acid, $S(3,6)$ = S2 structures with one $\alpha 2$ -3 and one $\alpha 2$ -6 linked sialic acid residue.

Sialic acid linkages of hybrid and bi-antennary structures were assigned by PGC elution order as shown in Figure 6. As observed for the total membrane protein glycome there was a higher overall abundance of $\alpha 2$ -6 (18.5%) compared to $\alpha 2$ -3 (10%) linked sialic acid residues to hybrid and bi-antennary structures (Figure 4), however, a higher abundance of the $\alpha 2$ -3 linkage was observed in disialic S2 structures of MCAM compared to the total cell membrane. Interestingly, an abundant group (~10%) of bi-antennary structures containing the LacdiNAc (GalNAc-GlcNAc) epitope was also confirmed by MS² fragmentation (Figure 7) on MCAM, but were not detected in the global cell membrane glycome. These structures were further modified with sialic acid residues, sulphation and outer arm fucose residues (Table 1).

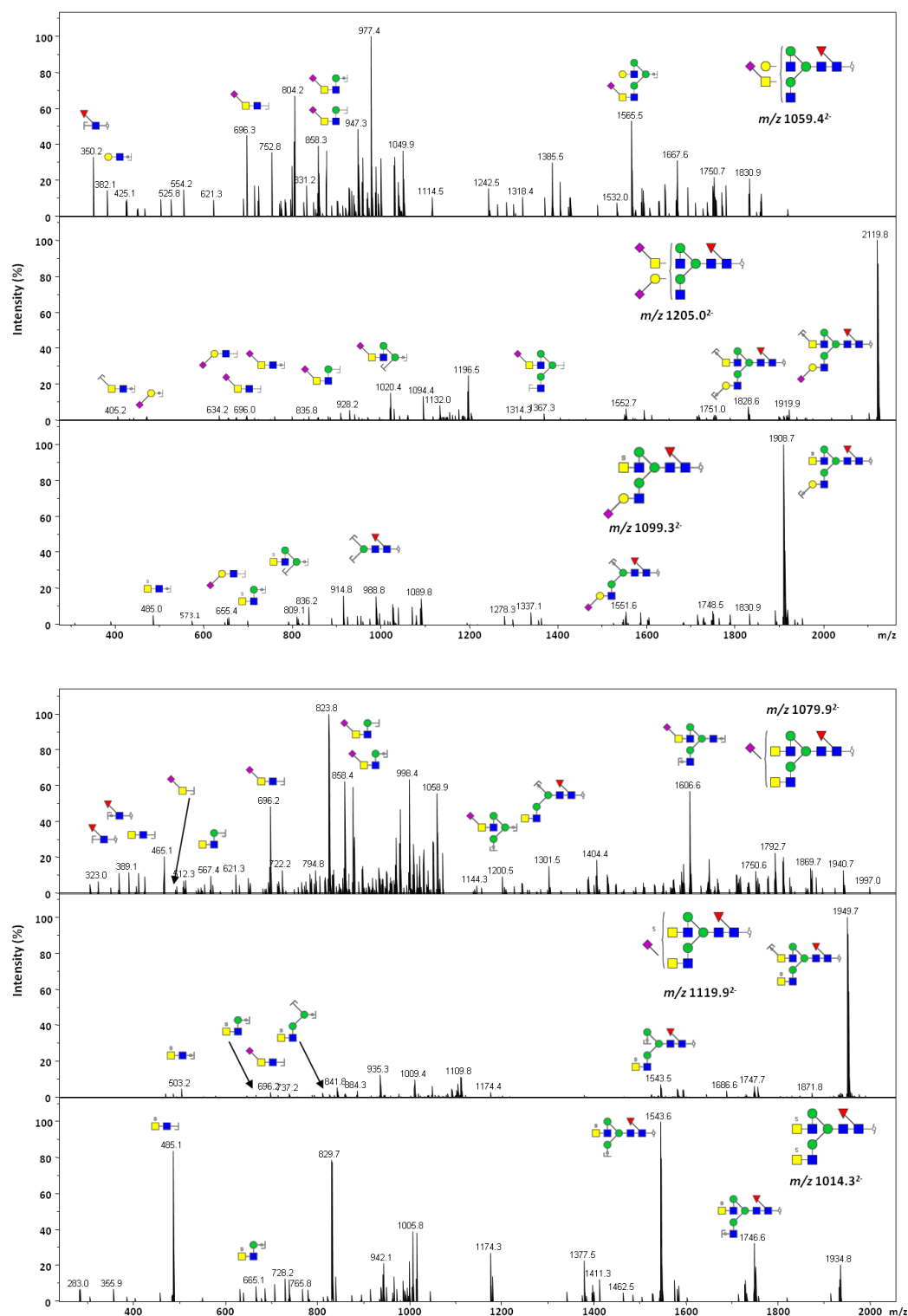


Figure 7. MS² fragmentation spectra of bi-antennary N-glycans containing the LacdiNAc epitope identified on MCAM. To confirm the presence of the epitope the diagnostic ions for identification of a sialylated LacdiNAc m/z 696 and the HexNAc-HexNAc disaccharide m/z 465 were used^{81,100}.

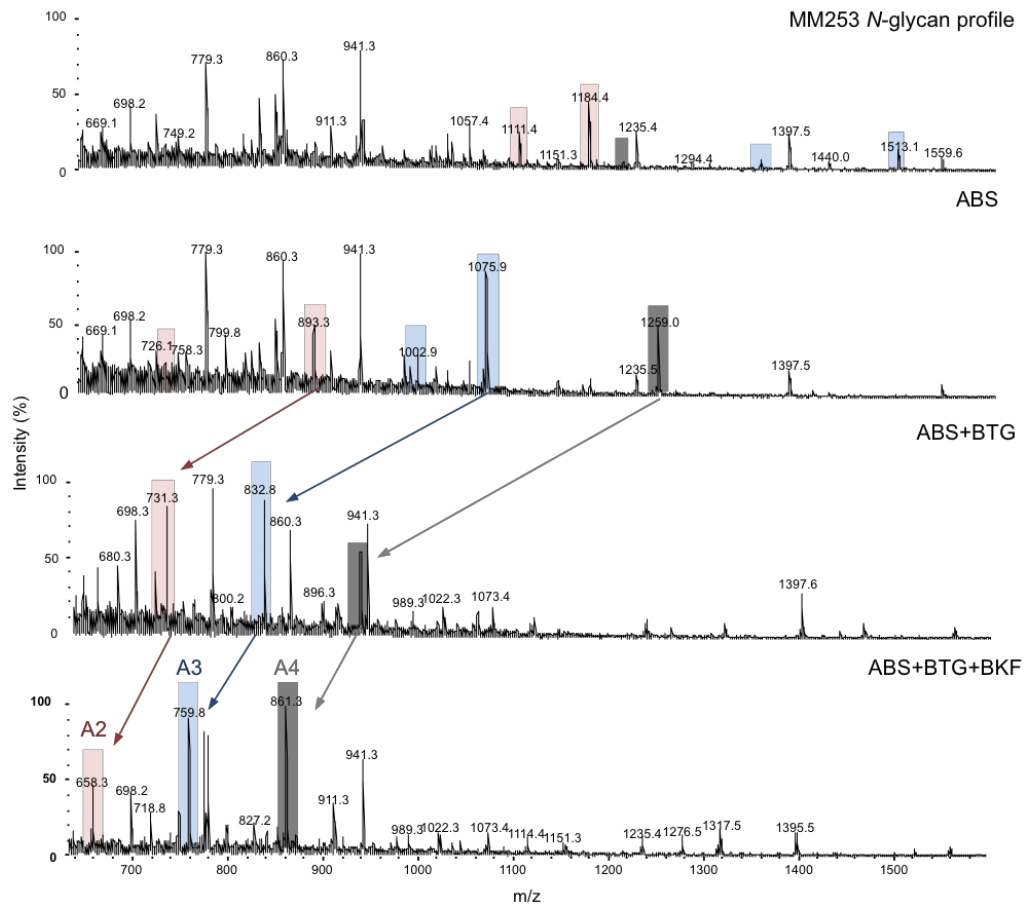


Figure 8. PGC-LC- negative ion MS profile of *N*-glycans released from the enriched membrane protein fraction of MM253 cells before and after digestion with an array of exoglycosidase enzymes to confirm the presence of bi-, tri- and tetra-antennary glycan classes. ABS (α 2-3,6,8 sialidase), ABS+BTG (α 2-3,6,8 sialidase and β 1-3,4 galactosidase), ABS+BTG+BKF (α 2-3,6,8 sialidase, β 1-3,4 galactosidase and α 1-6 fucosidase). Highlighted masses represent the collapse of bi- (red), tri- (blue) and tetra- (grey) antennary classes to single mass peaks (A2, A3 and A4) after removal of sialic acid, galactose and fucose residues.

β1-6 branched N-glycans

Masses corresponding to sialylated tri- and tetra-antennary structures were detected at only low abundance in the total membrane protein profile, 3.31% and 2.02% respectively. MCAM however had a much higher abundance of these structures compared to the total cell profile with tri- and tetra-antennary structures contributing 5-8% and 9-18% of the total glycans on the two samples of MCAM respectively. These masses were detected as multiple peaks in the MCAM profile, which could be due to the presence of polylactosamine units attached to the bi- and tri-antennary structures. For example, the mass of the *N*-glycan core with five lactosamine groups, one fucose residue and four sialic acids was detected (m/z 1348.5³⁻); this mass was assigned as a core fucosylated, fully sialylated, tetra-antennary with one lactosamine extension (~2.5%) Table 1.

Due to the heavy sialylation of these tri- and tetra-antennary masses, MS fragmentation did not provide informative diagnostic ions for the composition of the 6-antennae (D ion¹⁰⁰), therefore it was not possible to accurately confirm the presence of the β1-6 linked GlcNAc residues connected to the *N*-glycan core from MS² data alone. In order to confirm the identity and abundance of structures with β1-6 linked GlcNAc and thus to distinguish multi-antennary structures from polylactosamine (β1-3 linked) GlcNAc extensions, the total glycan pool was digested with an array of exoglycosidase enzymes in the following combinations; 1) α2-3,6,8 sialidase (ABS), 2) α2-3,6,8 sialidase and β1-3,4 galactosidase (ABS,BTG), 3) α2-3,6,8 sialidase, β1-3,4 galactosidase and α1-6 fucosidase (ABS,BTG,BKF). The masses corresponding to tri- and tetra-antennary glycans and their predicted digestion products based on enzyme specificities were monitored in the summed MS and PGC elution profiles after each digestion step (Figure 8 and 9). Once sialic acid and galactose residues had been removed, the composition of the 6-antennae could be determined using MS² fragmentation spectra (Figure 10) and compared to a commercial standard (Supplementary Figure 2). By using the results of exoglycosidase digestion both the tri- and tetra-antennary classes with β1-6 linked GlcNAc branch were confirmed in the *N*-glycosylation profile of MM253 melanoma cell membrane proteins. These structures were assigned as fully galactosylated, highly sialylated and core fucosylated (Table 1).

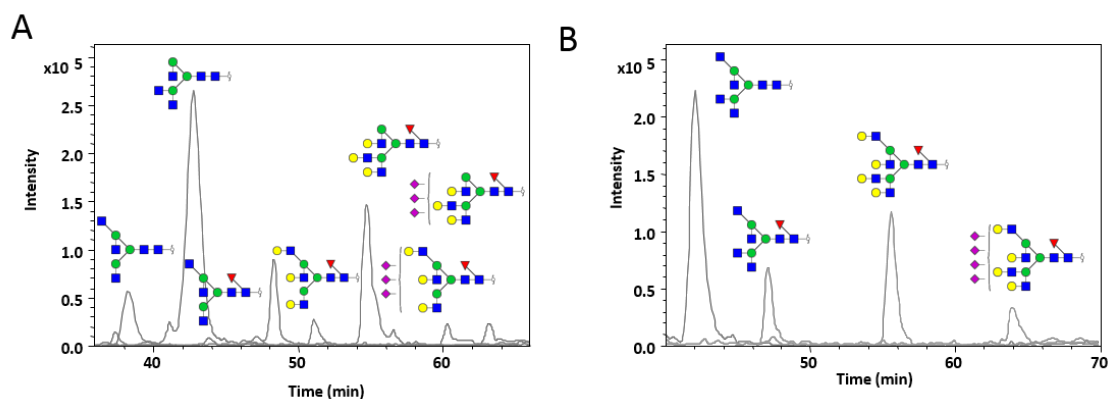


Figure 9. Overlay of extracted ion chromatograms generated for the masses of (A) tri- and (B) tetra-antennary glycans released from MM253 cells before and after exoglycosidase digestion. Two peaks for each mass in (A) confirm the presence of both tri-antennary linkage isomers. Structures were confirmed as core fucosylated, fully galactosylated and sialylated by monitoring exoglycosidase digestion products.

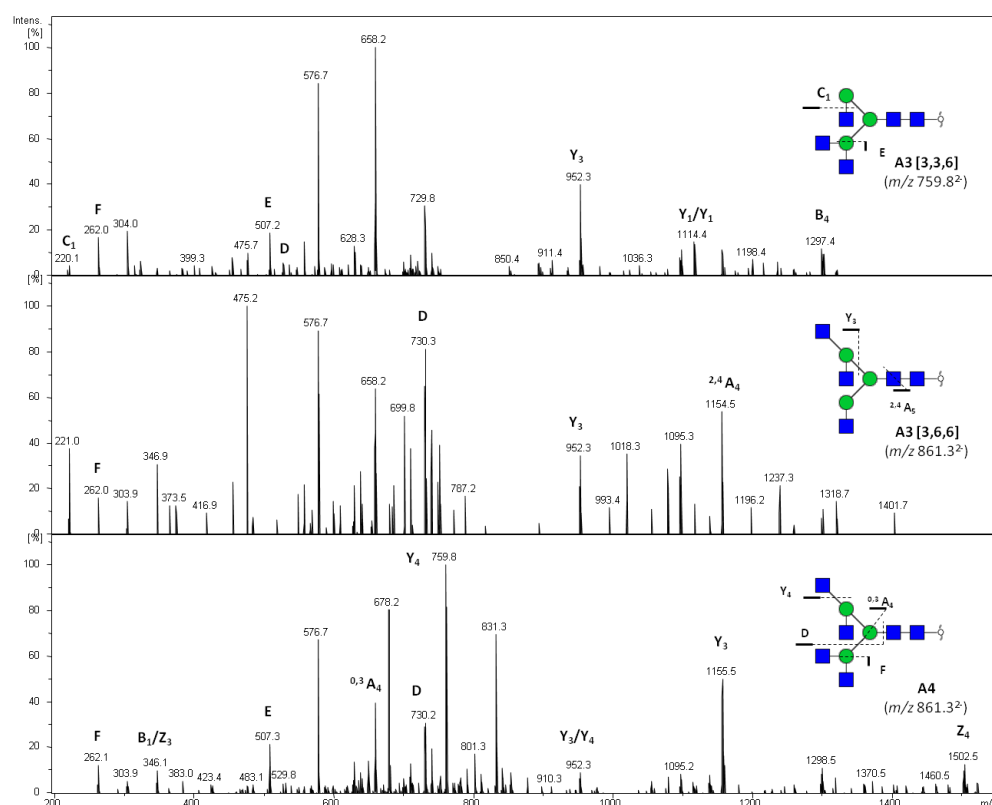


Figure 10. MS² negative ion fragmentation spectra for the tri- (m/z 759.8²⁻) and tetra- (m/z 861.3²⁻) antennary digestion products following cleavage of terminal sialic acid, galactose and core fucose residues.

PGC separation of the sialidase treated glycan pool revealed the presence of multiple isomers of mass (m/z 1075.9²) corresponding to the core fucosylated and fully galactosylated tri-antennary structure (Figure 9, panel A). These isomers were confirmed as one structure with two lactosamine groups linked to the 3-antennae mannose and one structure with two lactosamine groups linked to the 6-antennae mannose of the *N*-glycan core. Only one isomer was observed for the glycan mass (m/z 1258.5²) corresponding to the core fucosylated, fully galactosylated tetra-antennary structure (Figure 9, panel B) and MS fragmentation confirmed two lactosamine groups attached to each mannose antennae of the glycan core (Supplementary Figure S1). Complete removal of galactose residues after sialidase and galactosidase treatment confirmed that the structures did not contain polylactosamine extensions.

Unfortunately, due to a limited amount of material, it was not possible to digest the MCAM glycans with exoglycosidase enzymes to fully elucidate all structures but the information generated from the PGC elution behaviour, comparison to the total membrane glycosylation analysis, tissue analysis (Chapter 7) and MS fragmentation allowed us to confidently assign the glycans present.

5.4 Discussion

Changes in cell surface glycosylation have been identified in the progression of early to metastatic stages of melanoma; in particular the expression of proteins bearing β 1-6 linked branched *N*-glycans^{110,119,121,129,149}. In this study we aimed to profile the total membrane *N*-glycosylation profile of a metastatic melanoma cell line MM253 and purified cell surface glycoprotein MCAM from the same cell line to determine the degree of antennae branching and identify the particular structures with β 1-6 linked GlcNAc. By using a combination of information generated by PGC isomer separation, exoglycosidase digestion to remove sialic acid and galactose residues and MS² fragmentation to determine 6 arm antennae composition we confirmed that tri- and tetra-antennary glycans containing a β 1-6 linked GlcNAc branch are a relatively minor glycan feature of the membrane glycosylation profile of the metastatic melanoma MM253 cells. The specific structures were characterised as core fucosylated fully sialylated species F(6)A3[3,6,6]G3S3 and F(6)A4G4S4 (Table 1). Other features of the membrane glycome included a high abundance of mannose (pauci and high mannose) and hybrid type compared to complex type structures. The relative abundance of the tetra-antennary structure (m/z 1226.8³) was very low (2%) in comparison to high mannose, hybrid

and bi-antennary structures. However, when the glycans released from the whole cell membranes were treated with an array of exoglycosidase enzymes to confirm the identity of structures with the underlying β 1-6 linked GlcNAc, we observed an increase in intensity of mass ions corresponding to the tri- and tetra-antennary digest products, compared to the high mannose and bi-antennary glycan masses (Figure 8). This increase in the relative abundance of these structures made us question which profile represented the true relative abundance of these particular high mass, charged structures, and whether they were being accurately detected in the LC-MS/MS conditions used to determine the total cell membrane glycome. Therefore we investigated method parameters for the detection and quantitation of these multi-antennary structures. This work is detailed in the following chapter (Chapter 6) including an analysis of the optimal conditions for accurately determining the relative abundance of these highly branched glycan classes.

Increased expression of these Gnt V and tri- and tetra-antennary glycan products have been implicated in various cancer metastases including melanoma^{29,43,135}. Therefore the identity of protein targets for Gnt V activity and also the characterisation tri- and tetra-antennary glycans are of great importance to advance our understanding of the role and regulation of glycosylation in melanoma. Previous studies of total cell lysate and MCAM isolated from lymph node derived metastatic cell lines identified MCAM as a target protein for Gnt V activity using the PHA-L lectin^{111,150}. Consistent with these results we confirm the presence of masses corresponding to tri- and tetra-antennary glycans as well as evidence for bi-, tri- and tetra-antennary structures with lactosamine extension on MCAM. We also identified a high proportion of complex bi-antennary structures with and without core fucosylation. An interesting observation was the presence of a group of bi-antennary core fucosylated structures with a HexNAc-HexNAc disaccharide on one or both antennae modified with sialic acid, sulphate or fucose. These structures have not been previously reported on MCAM however, bi-antennary glycans containing the LacdiNAc (GalNAc β 1-4GlcNAc) motif, with or without sulphation/ α 2-6 sialylation, have been identified on Bowes melanoma tissue plasminogen activator^{144,151}.

Both the glycosylation profile of MCAM and total cell membrane exhibited a number of sialylated structures. The presence of highly sialylated branched structures on the cell surface are characteristic of a highly invasive variant of the murine melanoma model B16¹²¹. The expression and distribution of sialic acid linkage has been investigated in non-melanoma skin

cancer. Lectin histochemistry showed a difference in linkage between both stage and tumour origin¹⁵². Analysis of another member of the Ig superfamily cell adhesion molecules L1CAM identified a loss of α 2-3, and an increase in α 2-6, linked sialic acid residues that was associated with metastasis¹¹⁴. We also observed a higher overall abundance of α 2-6, compared to α 2-3 linked sialic acid residues in both the total membrane and MCAM profiles.

Comparison of the MCAM and total cell membrane revealed that individual protein glycosylation is not consistent with total membrane glycosylation. The total cell membrane profile contained a high abundance of mannose glycans especially M9 and M9Glc1, which may be derived from intra-cellular membrane proteins that were not present in the glycosylation profile of MCAM. Additionally, there were glycan features only present in the MCAM profile, including glycans with an LacdiNAc epitope and/or a polylactosamine extension. This data suggests that glycans present on low abundant membrane proteins are being masked by the less processed glycans released from internal cell membranes in a global cell analysis approach. Therefore, in a total membrane sample preparation we are not seeing a complete representation of the cell surface glycosylation and in order to identify changes that relate to specific or low abundant protein targets that accompany metastasis we need to enrich for cell surface and individual protein candidates.

5.5 Supplementary Figures

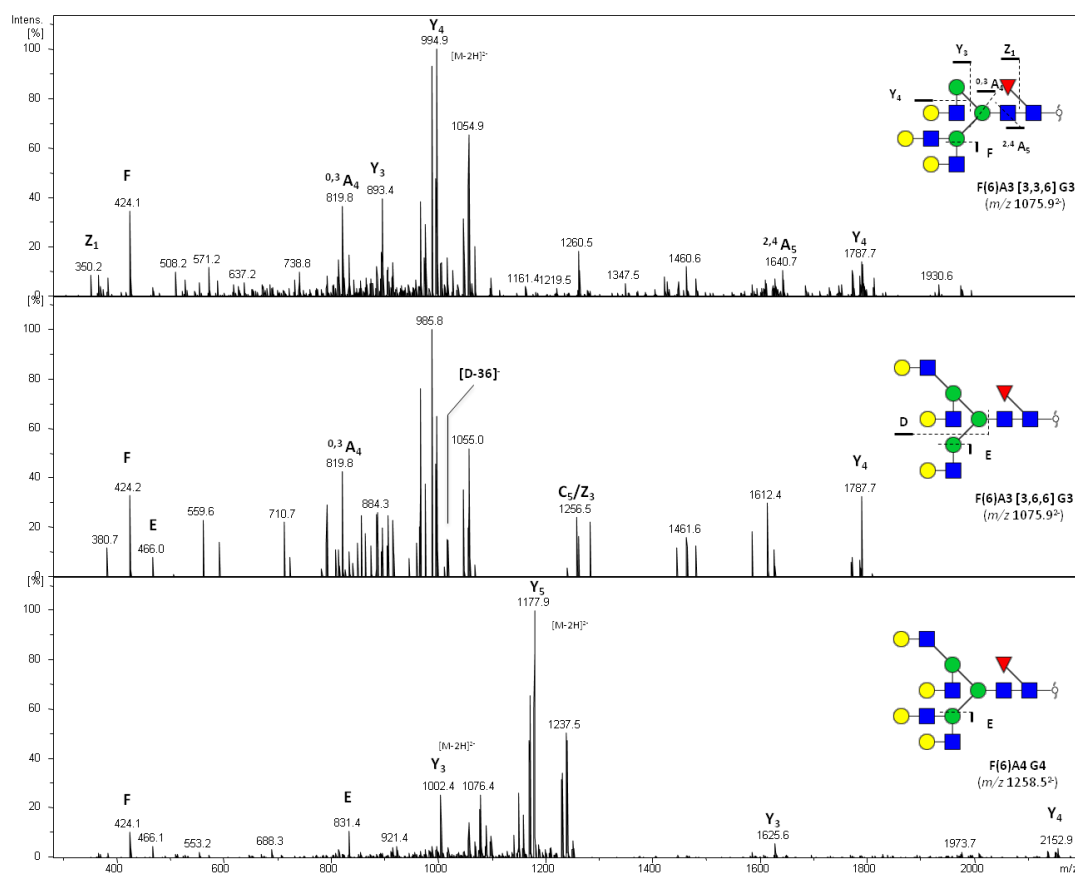


Figure S1. MS² negative ion fragmentation spectra of the masses of tri- (m/z 1075.9²⁻) and tetra- (m/z 1258.5²⁻) antennary digestion products after removal of terminal sialic acid residues.

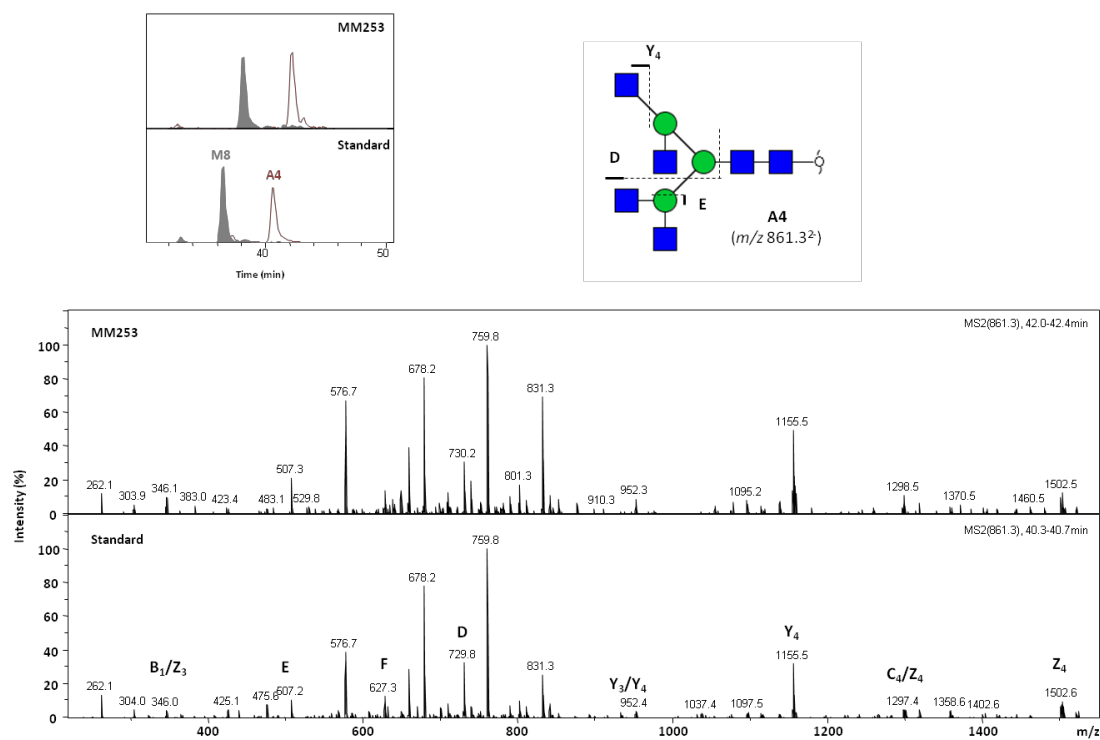


Figure S2. PGC retention and MS² fragmentation spectra comparison of the tetra-antennary digestion product (m/z 861.3²⁻) from MM253 released glycans compared to a commercial glycan standard containing β 1-6 linked GlcNAc. PGC elution is compared relative to the elution of the Man 8 (M8) structure.

Chapter 6

Following the previous study of a melanoma cell line (Chapter 5) it was observed that the existing analysis method used was not optimal for the quantitation of tri- and tetra-antennary *N*-glycan structures.

PGC-LC-MS is a powerful tool for glycomic studies yielding both qualitative and quantitative information. Although this method allows for a reliable representation of the relative abundance of bi- and tri- antennary structures, changes in the more highly branched and extended *N*-glycans can be lost in complex samples as they are retained longer on the PGC matrix and ionise less favourably. The under-representation of these larger glycan classes may be a limiting factor in the clinical application of this platform, such as for biomarker discovery and for monitoring the glycosylation profiles of bio-therapeutic proteins. Exoglycosidase enzymes are not only useful for determining linkage information and confirming terminal epitopes but can also be used to reduce the complexity of glycan mixtures to quantitate specific glycan features.

Here, we focus on how a targeted method combining PGC-LC-MS with exoglycosidase digestion can be used for the relative quantitation of tetra-antennary glycans released from metastatic melanoma tissue and cultured cell samples. In order to determine the degree of branched structures within the *N*-glycan pool, released glycans were treated with a combination of sialidase and beta-galactosidase to trim structures back to the antennae GlcNAc residues. The method described was initially optimised with commercially available glycan standards, then used for the quantitative analysis of the melanoma cell line MM253 and tissue samples from patient cohorts to include whether the abundance of tetra antennary *N*-glycans can be correlated with clinical outcome (Chapter 7).

Publication: Abrahams JL, Packer NH, Campbell MP. Quantitation of multi-antennary N-glycan classes: combining PGC-LC-ESI-MS with exoglycosidase digestion. *Analyst*. 2015. 140(16):5444-9

Author contributions: Experimental design, data collection and analysis- JA, Manuscript preparation- JA, Editing and reviewing- MC, NP.

Chapter 7

Cell surface glycoproteins are known to play an important role in the development and progression of melanoma. The prognosis of patients with melanoma lymph node metastasis varies significantly and there is a need to identify improved prognostic markers to better predict an individual's outcome. The *N*-glycans attached to the cell surface proteins of surgically excised lymph node tissue from stage III/IV melanoma patients were analysed by PGC-LC-MS in order to characterise and quantitate the glycosylation profile of tumour tissue and to investigate potential glycan markers of prognosis.

Structures were assigned using the optimised methods developed in Chapters 2 and 3, and quantitated before and after exoglycosidase digestion as detailed in Chapter 5 and further developed in Chapter 6.

The Glycosylation Profile of Metastatic Melanoma Lymph Node Tumours

7.1 Introduction

Melanoma is considered one of the most aggressive human cancers, increasing in worldwide incidence faster than any other cancer in recent decades¹⁵³. If diagnosed early the best treatment option is surgical removal of the primary tumour (American Joint Committee on Cancer, AJCC stages I/II) resulting in a 97% five-year survival rate⁸. Metastasis occurs very early in disease progression and accounts for the majority of mortality associated with melanoma, as limited treatment options exist for advanced stages of the disease. Once metastasis to distant organs has occurred (stage IV) the five-year survival rate dramatically decreases (18 to 6%). The first stage of melanoma metastasis is to regional lymph nodes; the prognostic outcome for patients diagnosed at this stage (AJCC stage III) differs widely ranging from 70% to 39%^{8,154} five-year survival. Due to the variability in survival within this population of patients, there is a critical need to identify the subset of individuals most likely to benefit from available chemo- and immune-therapy treatment options^{11,155}.

Cutaneous melanoma can be divided into four major subgroups depending on their clinical histology: superficial spreading melanoma (SSM), nodular melanoma (NM), acral lentiginous melanoma (ALM), and lentigo maligna melanoma (LMM)^{2,3}. Current classification of patients is based on clinical and histological parameters but it has been shown that tumours with identical classification can have strikingly different mRNA expression profiles, which could account for the variability in patient prognosis^{14,155-157}. Clinical, histological, serum and more recently gene and protein expression profiles have been investigated in an attempt to find informative prognostic markers for these patients^{11,154,155,158}. Serum has been a limited source of biomarkers to date, with only one validated for use as a prognostic factor for stage IV melanoma (serum lactate dehydrogenase)¹⁸.

Aberrant cell surface protein glycosylation is a well-established event in oncogenesis and cancer progression. An in-depth overview of literature on the changes of cell surface protein glycosylation for five different cancer types originating from the breast, colon, liver, skin and ovary is provided in Chapter 1. In brief, there are key similarities and differences between the glycosylation profile of these cancers that reflect the importance of glycan structural changes including sialylation, fucosylation, and degree of branching. In particular, increases in highly

branched tetra-antennary *N*-glycan structures on cell adhesion proteins appears to correlate with increased invasive and metastatic potential of melanoma cells¹²⁹. As yet there has been little progress towards the identification of prognostic glycan markers of melanoma despite growing evidence for the role of cell surface glycoproteins in the progression from primary to metastatic disease^{20,21,129}.

Several tissue biomarkers have been identified by immunohistochemistry-based studies that change in expression during melanoma progression. Many of these proteins are cell surface glycoproteins, with notably increased expression of three glycosylated cellular adhesion molecules, melanocyte-specific MCAM/MUC18, neuron-specific L1-CAM, and glandular tissue-associated CEACAM-1, which are significantly associated with worse case prognosis¹⁵⁵.

Studies of melanoma cell lines have also implicated the importance of cell surface glycosylation and expression of glycoproteins in metastasis. Typically, lectin based and gene manipulation methods have been used to investigate glycosylation features including β 1-6 branching, lactosamine repeats, sialylation, and bisecting GlcNAc, Lewis-type and HNK-1 epitopes from cells representing different stages of disease. We have further extended these findings by performing an in-depth mass spectrometry analysis of glycans released from the MM253 cell line (Chapter 5). In addition, the role of glycosylation, (in particular β 1-6 branching) has been implicated in melanoma progression as demonstrated by cell adhesion, motility and invasion assays^{110,111,118,119,121,159}.

Proteomic, genomic and surface antigen expression profiling of tissue from stage III patients has started to yield strategies for categorising patients into prognostic subgroups^{154,156,158,160,161} but as yet there has been no comprehensive structural glycan analysis of the global glycoproteome of either melanoma cell lines or secondary metastatic tumour tissue.

Here we describe the first glycomic analysis of lymph node tumours from patients with stage III and stage IV melanoma. In this study we have characterised the membrane protein glycosylation of lymph node tissue from individuals with metastatic melanoma to assess the degree of diversity amongst individuals, to compare differences in the cell surface glycosylation pattern of stage III and stage IV individuals, and to identify potential prognostic markers within a stage III/IV patient cohort.

7.2 Materials and Methods

Stage III/IV melanoma tumour tissue

Fresh-frozen Melanoma lymph node tumour tissue samples (n=10, Table 1) were provided by the Melanoma Institute Australia Biospecimen Bank in collaboration with the Royal Prince Alfred Hospital, Sydney. Macquarie University Human Research Ethics committee and NSW Health Sydney Local Health Network granted ethics approval for the analysis of melanoma tissue samples. (Appendix 2). Tissue samples (~30 mg) were washed three times with PBS prior to the addition of lysis buffer for membrane protein enrichment.

Methods for membrane enrichment, PVDF *N*-glycan release, exoglycosidase digestion and analysis by PGC-LC-MS were as described in Chapter 5.2. *N*-glycans were released and analysed in duplicate from membrane protein preparations of each patient sample.

Table 1. Patient sample information

Patient ID	Stage	Primary subtype	Sex	Survival (Months)	Prognostic Group
196	III	SSM	Male	23.5	Poor
259	III	SSM	Female	67.4	Good
53	III	SSM	Male	86	Good
179	III	ALM	Male	25.5	Good
61	III	Unknown	Female	6.3	Poor
88	III	NM	Female	130.4	Good
322	III	SSM	Male	6.7	Poor
148	IV	SSM	Male	15.4	Poor
175	IV	SSM	Male	13.7	Poor
313	IV	NM	Female	7.7	Poor

For all associated clinical data refer to Appendix 1

7.3 Results

Characterisation of N-glycans of lymph node melanoma tumour tissue

To determine the overall *N*-linked glycan profile of lymph node tissue derived from melanoma metastasis, the total membrane protein global *N*-glycosylation profiles of ten pooled lymph node tumour tissue samples from patients with stage III/IV metastatic melanoma (Table 1) were characterised by capillary PGC-LC-MS (Figure 1). The ultracentrifugation enriched membrane protein fractions were dot blotted onto PVDF membrane, and the *N*-glycans released enzymatically with PNGase F. Released and reduced *N*-glycans from individual tumours were pooled and analysed by LC-ESI-MS in the negative mode before and after treatment with an array of exoglycosidase enzymes to confirm monosaccharide linkages. Glycan structures were assigned based on manual interpretation of MS² fragmentation spectra and diagnostic ions (as summarised in Chapter 3), combined with information generated from treatment with exoglycosidase enzyme combinations and PGC elution orders (refer to Chapter 4). A total of 66 compositions of *N*-glycans on the membrane proteins of lymph node tumour tissue were identified by MS and 97 *N*-glycan structures were completely assigned, including pauci mannose, high mannose, hybrid and complex type structures (Table 2).

Determination of N-glycan structural features

The global *N*-glycan profile of total membrane proteins was confirmed by treating the released *N*-glycan pool with different exoglycosidase enzyme combinations in order to confirm structural features, including the degree of branching (α 2-3,6,8,9 -Sialidase, ABS; β 1-3,4-Galactosidase, BTG), core fucosylation (α 1-2,3,4,6 -Fucosidase, BKF), sialic acid linkage (α 2-3,6,8,9 -Sialidase, ABS; α 2-3 -Sialidase, NAN1) and terminal epitopes (using a combination of all previous exoglycosidases in addition to β -N-Acetylhexosaminidase, GUH; and (α 1-3,4-Fucosidase, AMF). This analysis involved monitoring retention time of undigested *N*-glycan masses after each digestion step along with the appearance of expected digestion product masses. Figure 2 shows the extracted ion chromatograms for all glycan masses reported in Table 2. The collapse of peaks after exoglycosidase treatment is indicative of terminal monosaccharides cleaved by the enzymes; therefore, the corresponding abundance of each epitope/feature can be (relatively) quantitated.

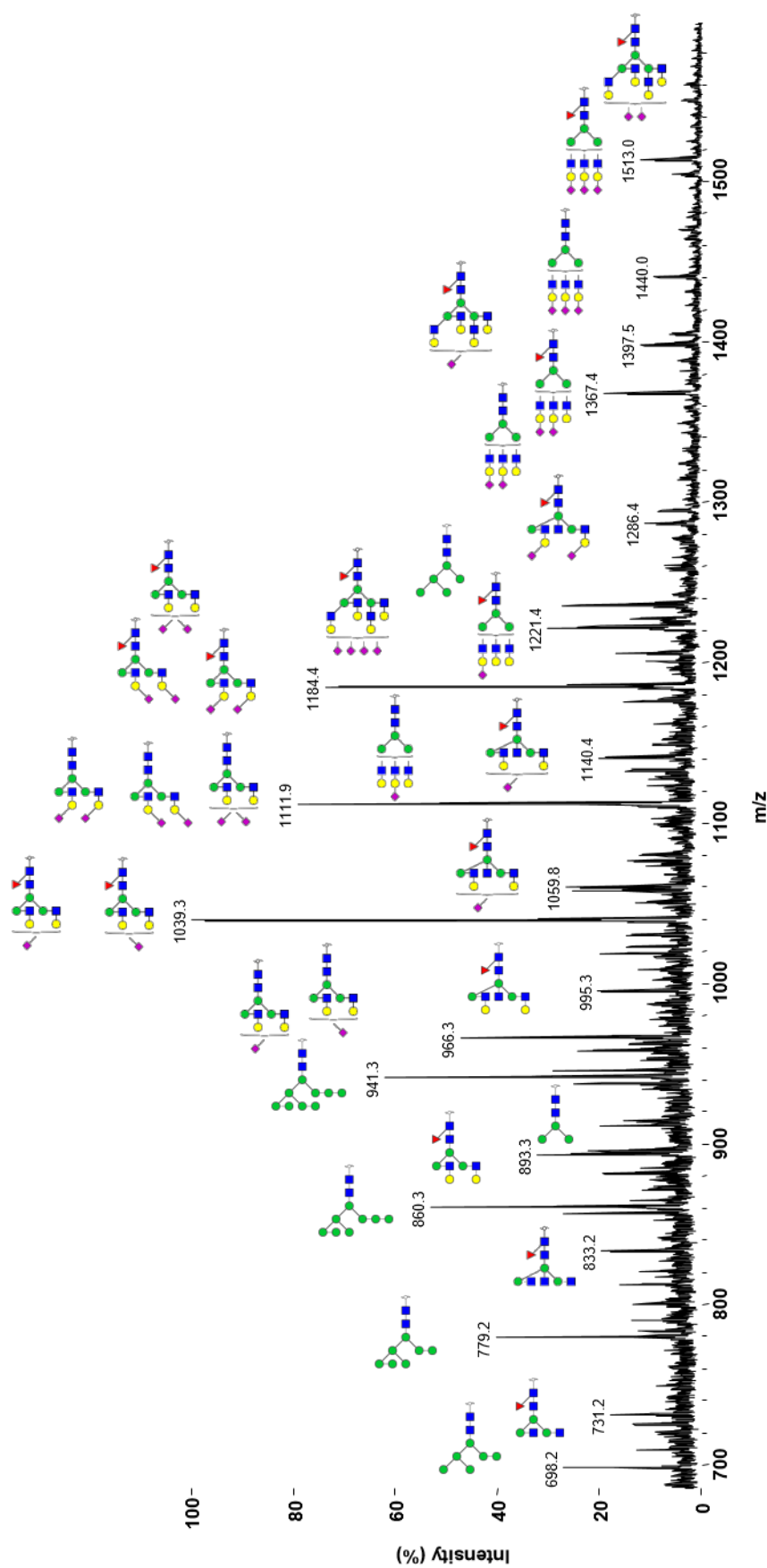


Figure 1. Summed negative mode MS spectrum of N-glycans released from pooled lymph node melanoma tumour tissue (n=10). Structures shown are deduced from interpretation of data on parent ion mass, LC isomer separation, MS/MS fragmentation diagnostic ions and exoglycosidase treatments. Structures and relative quantitation are summarised in Table 2.

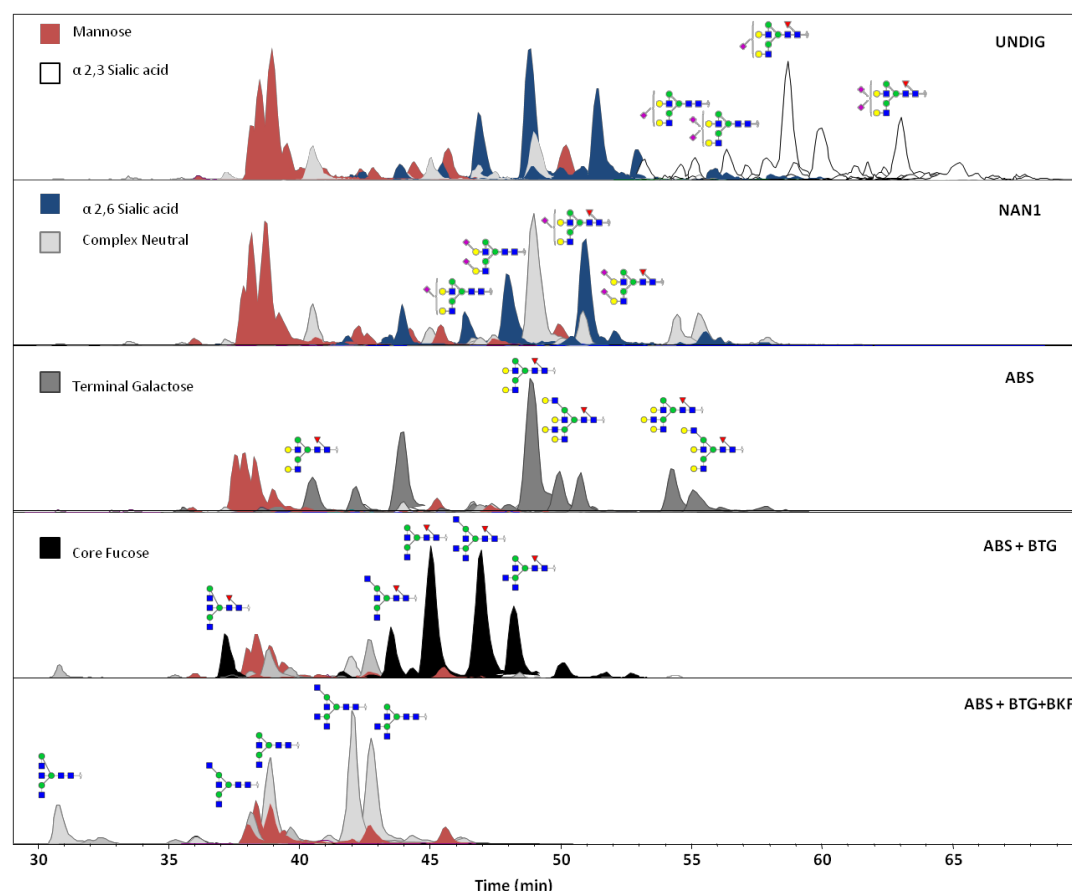


Figure 2. Structural features analysis of pooled lymph node melanoma tumour tissue (n=10) using exoglycosidase enzymes. Extracted ion chromatograms of (a) the total glycan masses (Figure 1); and digestion product masses after exoglycosidase treatment(s) as follows: (b) NAN1 removal of α 2-3 linked sialic acid, (c) Galactosylated (G1-4) structures after ABS removal of all terminal sialic acid residues, (d) ABS+BTG removal of terminal sialic acid and galactose, (e) ABS+BTG+BKF removal of core fucose, terminal sialic acid and galactose. Structures in panel (e) are summarised in Table 3.

Sialylated structures were confirmed by the presence of prominent B-cleavage ions at m/z 290 and m/z 655 and by comparing the total glycan masses with the profile after treatment with sialidases ABS and NAN1, which are specific for α 2-3,6 and α 2-6 linkages respectively. The resulting sialidase-treated profile was used to determine the degree of galactosylation (Figure 2, panel c) and to investigate whether there were structures present with outer arm fucosylation. As demonstrated in Chapter 4, bi-antennary structures with multiple fucose residues co-elute or appear as shoulder peaks with sialylated species of similar mass and are difficult to quantitate. Analysis of the sialidase treated glycan pool confirmed that outer arm fucosylation of bi-antennary species was not present.

A combination of sialidase and beta-galactosidase (BTG) was used to further investigate the presence of terminal epitopes and to confidently assign lactosamine extensions, tri-antennary isomers, LacdiNAc and structures with bisecting GlcNAc using a combination of PGC retention order and MS² fragmentation (Figure S2). The addition of BKF was then used to assess the degree of core fucosylation (Figure 2, panel d). A total of 26 digestion products were identified, assigned and quantitated in individual samples after digestion with ABS, BTG and BKF as summarised in Figure 5 and Table 3.

Sialic acid linkage

Sialic acid linkage types were differentiated (where possible) based on PGC retention order and the use of the sialidases with different specificities. EIC peaks of sialylated structures were monitored before and after NAN1 digestion. Loss of peaks after NAN1 treatment (Figure 2, panel b) indicated the presence of at least one α 2-3 linked sialic acid residue, while the stability of a peak following NAN1 treatment but peak loss following ABS (broad spectrum sialidase) treatment indicated that all sialic acid residues on that structure were α 2-6 linked. Mono- and di-sialylated linkage isomers are well separated by PGC for hybrid, mono and bi-antennary classes but are not so well resolved for tri- and tetra- antennary structures, so structures with more than two sialic acids and a mixture of linkages could not have the sialic acid linkage assigned.

Mannose and hybrid glycans

Glycan masses corresponding to the pauci mannose structures M2, M3 and M4 were identified consistently in the glycan profile before and after exoglycosidase treatment. Only single peaks were observed upon generation of extracted ion chromatograms for the masses of M2 and M3 with three structural isomers separated for M4. Based on PGC retention times and comparison to known glycan standards the M2 structure was assigned as the six-arm

isomer (M[6]2). In addition, fucosylated pauci mannosidic structures were confirmed by comparison of glycan profiles before and after the addition of BKF (α -1,2,3,4,6) fucosidase and the observation of the diagnostic ions m/z 350 and 368 derived from core fucose attachment. High-mannose glycans from M5 to M9 were identified and confirmed by MS² fragmentation. A glycan with ten hexoses was also observed and assigned as M9Glc1 based on the biosynthetic pathway. Furthermore, isomers of M6 and M7 were resolved by PGC and have been tentatively assigned based on high mannose PGC elution behaviour reported in Chapter 4 and previous studies⁷⁹.

Two masses corresponding to M4A1 (M4 with one antennary GlcNAc) and M5A1 (M5 with one antennary GlcNAc) were detected after digestion with exoglycosidases ABS, BTG and BKF confirming the presence of hybrid structures that were seen as galactosylated and sialylated in the total glycan profile. The presence of both α 2-6 and α 2-3 sialic acid linkages were confirmed by PGC retention order after NAN1 treatment as detailed above.

Complex Type glycans

Profiling of the *N*-glycan masses released from the tumour tissue membrane proteins indicated the presence of highly complex structures (Figure 1). To assess the degree of branching in the profile a combination of sialidase, galactosidase and fucosidase enzymes was used to trim structures back to the antennary GlcNAc. Mono-, bi-, tri- and tetra-antennary structures were verified by interpretation of MS² spectra acquired for the digestion products using the diagnostic ions as described in Chapter 3. The presence of both tri-antennary isomers (position of third antennary GlcNAc residue on the 3- or 6-arm mannose) was confirmed by PGC separation and MS² fragmentation (Supplementary Figure S2).

Additionally, bisecting GlcNAc was confirmed to be expressed on bi-, tri- and tetra-antennary classes. Bi-antennary structures containing bisecting GlcNAc were distinguished from tri-antennary structures of the same mass based on known PGC elution behaviour (refer to Chapter 4) and the presence of the diagnostic D-221 ion¹⁰⁰ (Supplementary Figure S3).

LacdiNAc terminal epitope

Sialylated bi-antennary structures carrying the LacdiNAc (GalNAc- GlcNAc) epitope on one or both arms were confirmed by the fragment ion at m/z 696 (b3 ion) that corresponds to Sia-GalNAc-GlcNAc (Figure 3, panels a, b and e). Structures with a LacdiNAc on one arm and LacNAc (Gal-GlcNAc) on the other could also be assigned. These structural assignments were further validated by the appearance of the diagnostic F ion, m/z 465 (two HexNAc residues) after digestion with ABS (Figure 3, panels c and d). These glycans were also separated from

their tri- and tetra- antennary mass isomers by PGC retention differences. GalNAc residues were differentiated from GlcNAc, where in doubt, by enzyme digestion with GUH, a hexaminidase specific for terminal GlcNAc but not GalNAc. The digestion products F(6)A1GalNAc1 (m/z 731.3) and F(6)A2GalNAc2 (m/z 934.4) were detected after treatment with a combination of ABS, BTG and GUH confirming the presence of terminal GalNAc residues belonging to LacdiNAc motif.

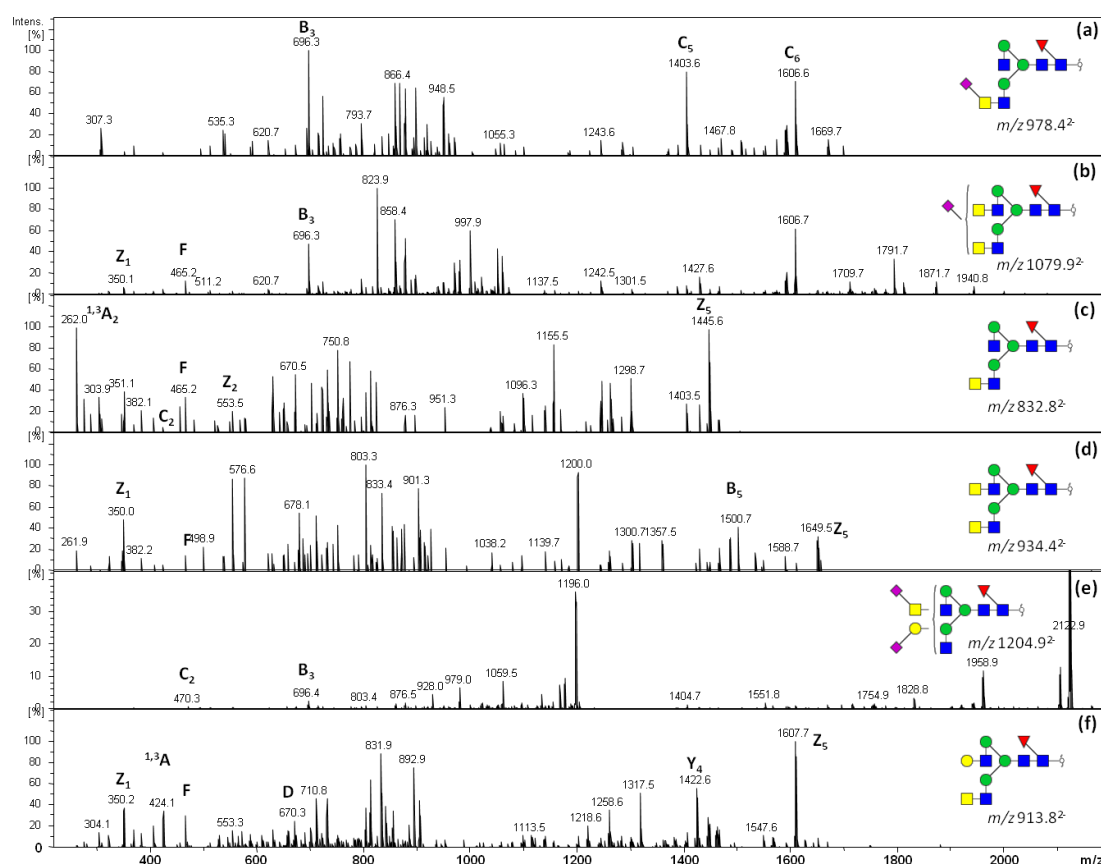


Figure 3. MS² fragmentation spectra of bi-antennary glycans with the LacdiNAc epitope identified from melanoma lymph node tissue. Diagnostic ions for identification of sialylated LacdiNAc m/z 696 (a, b and e) and the HexNAc-HexNAc disaccharide m/z 465 (b, c, d and f).

Lactosamine extensions

The masses of sialylated tetra-antennary structures (m/z 1348.5³⁻, m/z 1470.2³⁻) with lactosamine extension(s) were observed as low intensity peaks in the total *N*-glycan profile, but could not be quantitated due to poor quality EICs. Also bi- and tri-antennary classes with one lactosamine unit could not be distinguished from isomers by MS² fragmentation alone. However, confident assignment of the lactosamine extension units was possible after treatment with ABS and BTG, whereby galactose residues remain intact if they are extended with the β 1-3 linked GlcNAc on lactosamine extensions, as the enzyme is not able to access

the galactose residue. The BTG digestion products of structures with lactosamine extension(s) were confirmed as bi-, tri-, and tetra-antennary with one lactosamine repeat and tetra-antennary with two lactosamine repeats on a single arm of the chitobiose core. Evidence for isomers in the PGC chromatogram suggested that these were arm isomers of the structures but this could not be fully assigned by MS² fragmentation. The fragment masses m/z 627 (GlcNAc-Gal-GlcNAc on 6-antenna) and m/z 585 (GlcNAc-Gal-GlcNAc, C-type ion) were common in all fragmentation profiles of the lactosamine digestion products and were used as diagnostic ions (Figure 4).

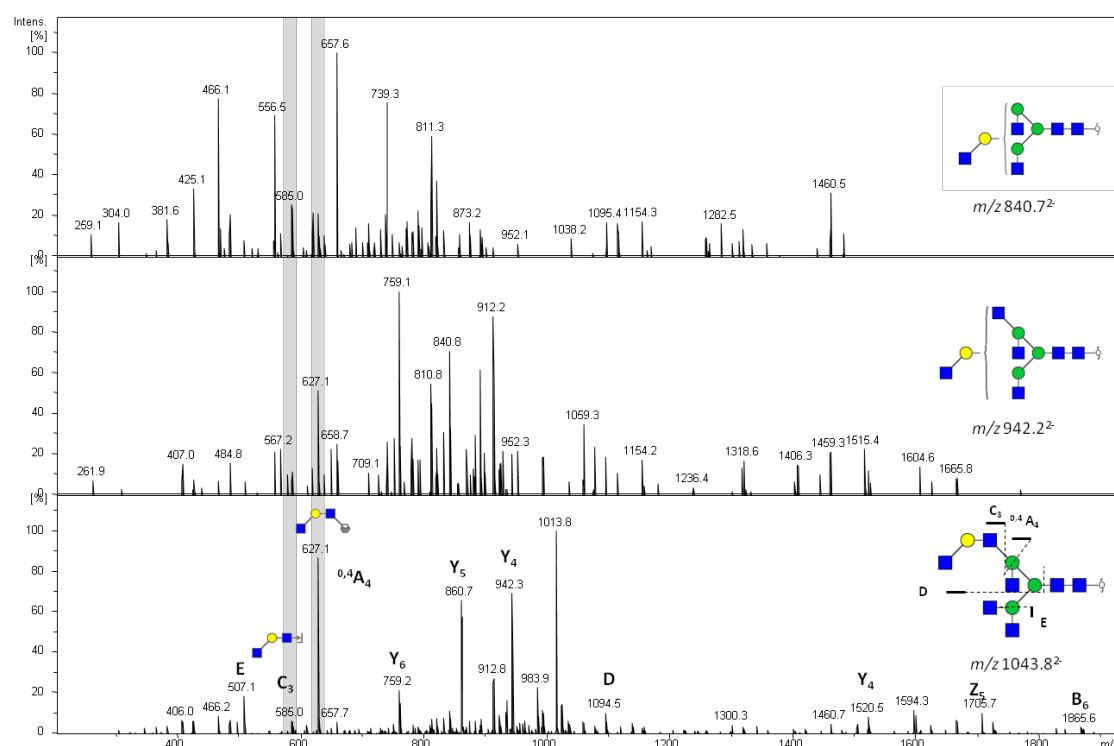


Figure 4. MS² fragmentation spectra of the digestion products of bi-, tri- and tetra-antennary structures with one lactosamine extension after treatment with ABS, BTG and BKF (Table 2). Diagnostic ions used for the identification of polylactosamine m/z 585 and m/z 627 are highlighted.
















Relative quantitation of N-glycan structures in lymph node melanoma tumour tissue from individual patients

Having determined in detail the *N*-glycan structures displayed on the cell membrane proteins of released glycans pooled from different lymph node melanoma tumour tissue samples, the relative abundance of the 97 fully characterised *N*-glycan structures were calculated from the EICs of each mass in the glycoprofile (Table 2). These structures were grouped into different glycan classes based on the structural determinants, and were used as the basis to compare the similarities and differences between 10 individuals and patient sub groups as classified by disease stage, prognosis and primary tumour subtype.

The overall glycosylation profiles of 10 individuals' lymph node melanoma tissue samples were compared (Supplementary Figure S1). There was a high variance between individuals in abundance of both the major components of bi-antennary glycans (19.2-59.1%) and high-mannose (18.3-40.9%) structures (Figure 6) with M8 and M9 the most abundant structures within the high-mannose group. Complex type glycans with core fucosylation made up between 27 and 55% of the glycan population. Between 40 and 63% of glycans were sialylated.

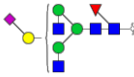


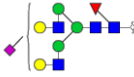
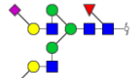
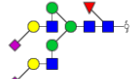
Quantitation of glycan classes after exoglycosidase digestion (Figure 7) allowed us to accurately compare the apparently lower abundance higher antennary classes, as well as allowing quantitation of individual tri-antennary isomeric structures and the amount of lactosamine extension(s) (as discussed in chapter 6).

Table 2. *N*-glycans released from lymph node melanoma tumour tissue of Stage III/IV individual patients (n=7, n=3 respectively). Relative % abundance was calculated by integration of the EICs of each mass and expressed as a percentage of the total glycan abundance. The mean relative abundance and standard deviation for Stage III and Stage IV samples are shown here.

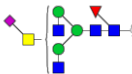
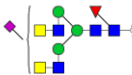
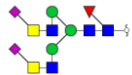
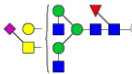
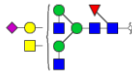
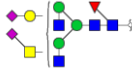



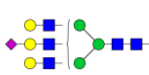
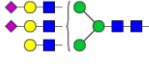





Glycan Class	Structure	Mass		Relative % Abundance (mean \pm s.d.)		
		[M-H] ⁻	[M-2H] ²⁻	Stage III (n=7)		Stage IV (n=3)
Pauci Mannose	M2 	749.3		0.51 \pm 0.32	0.52 \pm 0.25	
	M3 	911.3		1.85 \pm 1.04	1.53 \pm 1.58	
	M4 	1073.3		0.84 \pm 0.27	0.74 \pm 0.09	
	F(6)M2 	895.3		2.23 \pm 1.93	2.17 \pm 1.86	
	F(6)M3 	1057.4		2.23 \pm 0.94	2.89 \pm 1.70	
	F(6)M4 	1219.4		0.13 \pm 0.10	0.13 \pm 0.13	
High Mannose	F(6)M5 	1381.5		0.06 \pm 0.06	0.13 \pm 0.14	
	M5 	1235.4	617.2	3.91 \pm 2.21	1.77 \pm 0.66	
	M6 	1397.5	698.3	2.82 \pm 0.94	3.38 \pm 0.80	
	M7 	1559.5	779.3	5.46 \pm 2.27	6.84 \pm 2.45	
	M8 		860.3	9.22 \pm 3.65	11.08 \pm 3.97	
	M9 		941.3	9.44 \pm 3.40	9.61 \pm 3.10	
	M9Glc1 		1022.3	0.53 \pm 0.17	0.55 \pm 0.15	
Hybrid	M5A1G1 		799.8	0.69 \pm 0.25	0.44 \pm 0.11	
	M4A1G1S(6)1 		864.3	1.16 \pm 0.49	0.87 \pm 0.54	

Glycan Class	Structure	Mass		Relative % Abundance (mean ± s.d.)						
		[M-H] ⁻	[M-2H] ²⁻	Stage III (n=7)			Stage IV (n=3)			
Hybrid	M4A1G1S(3)1		864.3	0.56	±	0.27	0.77	±	0.43	
	M5A1G1S(6)1		945.3	1.38	±	0.65	0.80	±	0.26	
	M5A1G1S(3)1		945.3	0.67	±	0.38	0.81	±	0.57	
	F(6)M4A1G1S(6)1		937.3	0.78	±	0.81	0.47	±	0.14	
	F(6)M4A1G1S(3)1		937.3	0.62	±	0.41	0.43	±	0.24	
	F(6)M5A1G1(6)1		1018.4	0.27	±	0.23	0.39	±	0.50	
	F(6)M5A1G1(3)1		1018.4	0.26	±	0.32	0.21	±	0.29	
Mon-antennary	F(6)A1[3]		1260.5	0.15	±	0.09	0.34	±	0.33	
	F(6)A1[6]		1260.5	0.20	±	0.12	0.21	±	0.11	
	F(6)A1[3]G1		1422.5	710.8	0.08	±	0.07	0.03	±	0.01
	F(6)A1[6]G1		1422.5	710.8	0.07	±	0.02	0.06	±	0.02
	A1[3]G1S(6)1		783.3	0.92	±	0.40	0.50	±	0.31	
	A1[6]G1S(6)1		783.3	0.25	±	0.11	0.40	±	0.20	
	A1G1S(3)1		783.3	0.10	±	0.12	0.02	±	0.04	
	F(6)A1[3]G1S(6)1		856.3	1.75	±	1.07	2.34	±	0.53	
	F(6)A1[6]G1S(6)1		856.3	0.71	±	0.40	0.59	±	0.17	
	F(6)A1G1S(3)1		856.3	0.12	±	0.17	0.00	±	0.00	

Glycan Class	Structure	Mass		Relative % Abundance (mean \pm s.d.)			
		[M-H] ⁻	[M-2H] ²⁻	Stage III (n=7)		Stage IV (n=3)	
	F(6)A1G1S(3)1	856.3		0.91	\pm 0.55	0.66	\pm 0.46
Bi-antennary	A2[6]G1	739.3		0.07	\pm 0.02	0.14	\pm 0.15
	A2[3]G1	739.3		0.09	\pm 0.04	0.12	\pm 0.05
	A2G2	820.3		0.95	\pm 0.84	0.55	\pm 0.13
	A2G1S(6)1	884.8		0.39	\pm 0.29	0.25	\pm 0.06
	A2G2S(6)1	965.8		2.91	\pm 1.49	2.81	\pm 1.17
	A2G1S(3)1	884.8		0.02	\pm 0.03	0.10	\pm 0.09
	A2G2S(3)1	965.8		0.78	\pm 0.49	1.00	\pm 0.64
	A2G2S(6)2	1111.4		4.77	\pm 2.86	4.70	\pm 2.45
	A2G2S(3,6)2	1111.4		1.12	\pm 0.61	1.00	\pm 0.09
	A2G2S(3,3)2	1111.4		0.64	\pm 0.38	0.44	\pm 0.60
	F(6)A2	1463.5	731.3	1.38	\pm 1.66	0.88	\pm 0.59
	F(6)A2[6]G1	812.3		0.59	\pm 0.41	0.45	\pm 0.21
	F(6)A2[3]G1	812.3		0.50	\pm 0.43	0.36	\pm 0.23
	F(6)A2G2	893.3		2.88	\pm 2.17	3.29	\pm 3.05

Glycan Class	Structure	Mass		Relative % Abundance (mean \pm s.d.)			
		[M-H] ⁻	[M-2H] ²⁻	Stage III (n=7)		Stage IV (n=3)	
Bi-antennary	F(6)A2G1S(6)1		957.8	0.85	\pm 0.73	0.82	\pm 0.58
			957.8	0.18	\pm 0.10	0.17	\pm 0.02
	F(6)A2G2S(6)1		1038.9	4.26	\pm 1.68	6.41	\pm 2.09
			957.8	0.28	\pm 0.17	0.16	\pm 0.09
	F(6)A2G1S(3)1		957.8	0.36	\pm 0.24	0.44	\pm 0.14
			1038.9	4.81	\pm 4.16	5.76	\pm 4.77
	F(6)A2G2S(3)1		1038.9	0.88	\pm 1.76	0.31	\pm 0.48
			1184.4	1.32	\pm 0.56	1.26	\pm 0.22
	F(6)A2G2S(6)2		1184.4	3.03	\pm 1.89	2.30	\pm 1.25
			1184.4	3.72	\pm 2.31	3.05	\pm 2.64
	F(6)A2G2S(3,6)2		1184.4	0.17	\pm 0.12	0.22	\pm 0.09
							
	F(6)A2G2S(3)2		1184.4				

Glycan Class	Structure	Mass		Relative % Abundance (mean \pm s.d.)			
		[M-H] ⁻	[M-2H] ²⁻	Stage III (n=7)		Stage IV (n=3)	
Bisecting GlcNAc	A2B		759.8	0.07	\pm 0.05	0.09	\pm 0.06
	A2B[3]G1		840.8	0.04	\pm 0.04	0.02	\pm 0.03
	A2B[6]G1		840.8	0.13	\pm 0.09	0.17	\pm 0.21
	A2BG2		921.8	0.12	\pm 0.12	0.10	\pm 0.11
	A2BG1S(6)1		986.4	0.04	\pm 0.04	0.06	\pm 0.05
	A2BG2S(6)1		1067.4	0.09	\pm 0.04	0.10	\pm 0.11
	A2BG2S(6)2		1212.9	0.02	\pm 0.02	0.01	\pm 0.03
	F(6)A2B		832.8	0.40	\pm 0.33	0.35	\pm 0.21
	F(6)A2[3]BG1		913.8	0.11	\pm 0.04	0.25	\pm 0.28
	F(6)A2[6]BG1		913.8	0.54	\pm 0.46	1.04	\pm 0.79
	F(6)A2BG2		994.9	0.85	\pm 0.87	0.12	\pm 0.07
	F(6)A2BG1S(6)1		1059.4	0.28	\pm 0.20	0.30	\pm 0.35
	F(6)A2BG2S(6)1		1140.4	0.65	\pm 0.46	0.49	\pm 0.53
	F(6)A2BG2S(6)2		1285.9	0.20	\pm 0.15	0.25	\pm 0.18

Glycan Class	Structure	Mass		Relative % Abundance (mean \pm s.d.)			
		[M-H] ⁻	[M-2H] ²⁻	Stage III (n=7)		Stage IV (n=3)	
LacdiNAc	F(6)A2GalNAc1S(6)1 	978.4		0.25	\pm 0.34	0.08	\pm 0.08
	F(6)A2GalNAc2S(6)1 	1079.9		0.24	\pm 0.37	0.14	\pm 0.15
	F(6)A2GalNAc2S(6)2 	1225.4		0.06	\pm 0.12	0.00	\pm 0.00
	F(6)A2G1GalNAc1S(6)1 	1059.4		0.23	\pm 0.50	0.00	\pm 0.00
	F(6)A2G1GalNAc1S1 	1059.4		0.13	\pm 0.26	0.04	\pm 0.07
	F(6)A2G1GalNAc1S2 	1204.9		0.09	\pm 0.19	0.00	\pm 0.00
	F(6)A2G1GalNAc1S(3,6)2 	1204.9		0.43	\pm 0.57	0.28	\pm 0.12
Tri-antennary	A3[6,6,3]G3 	1002.9		0.09	\pm 0.06	0.05	\pm 0.05
	A[6,3,3]3G3 	1002.9		0.08	\pm 0.09	0.17	\pm 0.08
	A3G3S1 	1148.4		0.26	\pm 0.14	0.42	\pm 0.02
	A3G3S2 	1293.9		0.21	\pm 0.09	0.22	\pm 0.05
	A3G3S3 	1439.5		0.34	\pm 0.18	0.17	\pm 0.09
	F(6)A3[6,6,3]G3 	1075.9		0.18	\pm 0.13	0.29	\pm 0.23
	F(6)A3[6,3,3]G3 	1075.9		0.12	\pm 0.09	0.16	\pm 0.10
	F(6)A2G2Lac 	1075.9		0.12	\pm 0.11	0.02	\pm 0.04
	FA3G3S1 	1221.4		1.29	\pm 0.90	1.27	\pm 0.13

Glycan Class	Structure	Mass		Relative % Abundance (mean \pm s.d.)		
		[M-H] ⁻	[M-2H] ²⁻	Stage III (n=7)	Stage IV (n=3)	
	FA3G3S2	1366.9		1.10 \pm 0.43	1.01 \pm 0.06	
	FA3G3S3	1512.5		1.09 \pm 0.35	1.37 \pm 0.34	
Tetra-antennary	A4G4S1	1331		0.03 \pm 0.03	0.05 \pm 0.01	
	A4G4S4	1767.6		0.01 \pm 0.04	0.00 \pm 0.00	
	F(6)A4	934.4		0.40 \pm 0.85	0.13 \pm 0.08	
	F(6)A4G4	1258.5		0.09 \pm 0.06	0.08 \pm 0.01	
	F(6)A4G4S(6)1	1404		0.18 \pm 0.15	0.22 \pm 0.06	
	F(6)A4G4S2	1549.6		0.14 \pm 0.18	0.18 \pm 0.18	
	F(6)A4G4S3	1695.1		0.03 \pm 0.05	0.04 \pm 0.03	
	F(6)A4G4S4	1840.6		1.22 \pm 1.56	1.31 \pm 0.62	

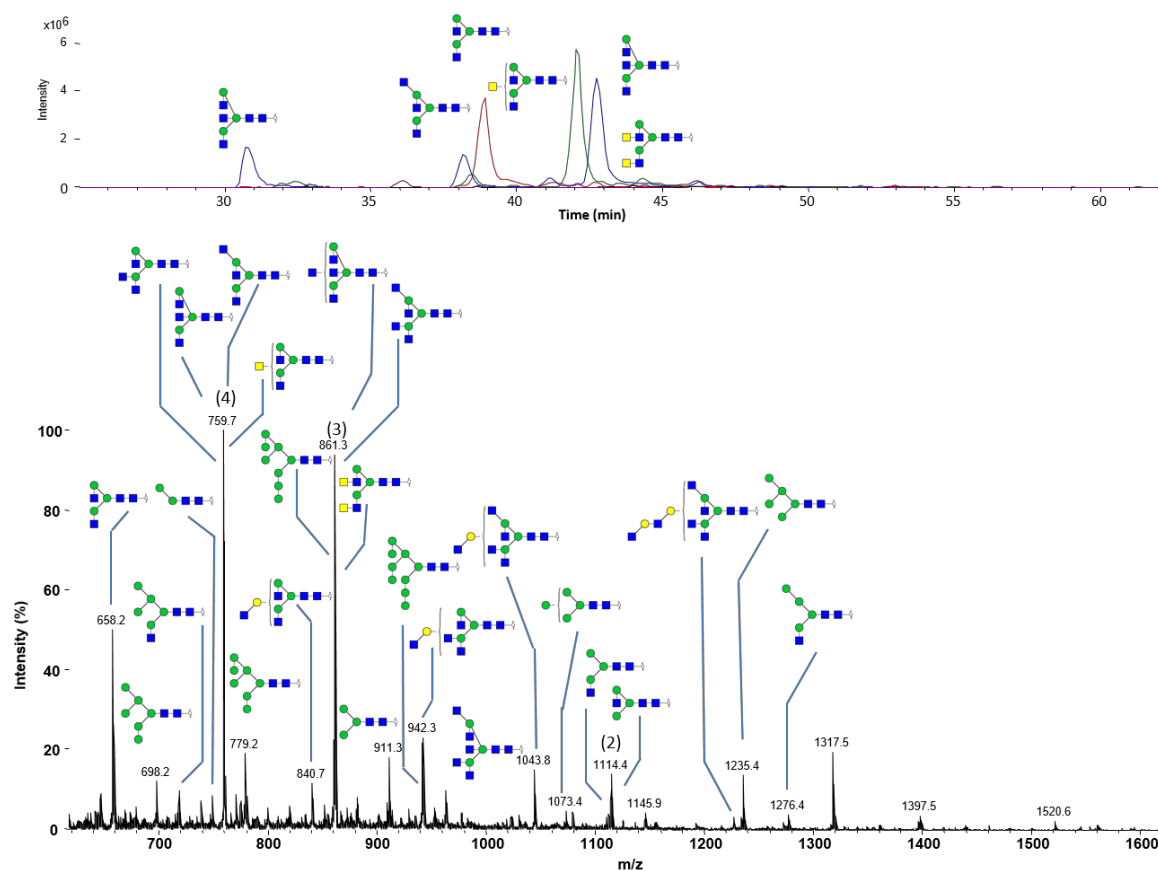


Figure 5. PGC-LC chromatogram and summed MS spectrum of *N*-glycans released from pooled lymph node melanoma tumour tissue after exoglycosidase treatment with ABS, BTG and BKF. Structures shown are deduced from interpretation of data on parent ion mass, LC isomer separation, MS² fragmentation diagnostic ions and exoglycosidase specificities. Structures and relative quantitation are summarised in Table 3.

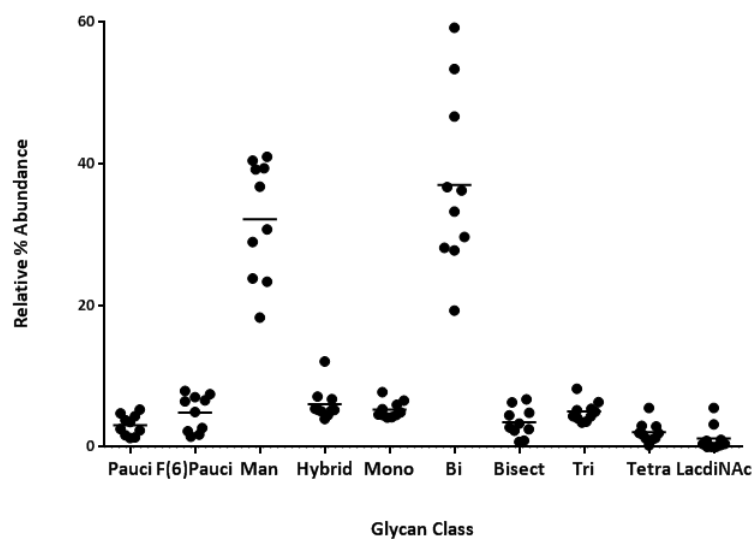


Figure 6. Relative percentage abundance of glycan classes for 10 individual lymph node tissue samples quantitated from the total glycan profile of individual patients.

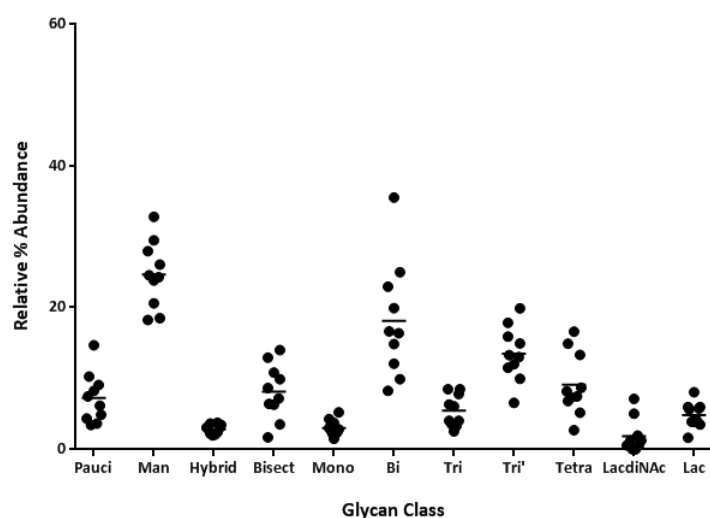



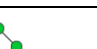




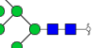

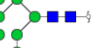


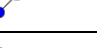


Figure 7. Relative percentage abundance of glycan classes for 10 individual lymph node tissue samples quantitated after ABS, BTG and BKF digestion. Including Tetra-antennary, Tri-antennary isomers (Tri β 1-4 branch and Tri' β 1-6 branch) and structures with lactosamine extension (s) (Lac) which could not be accurately quantitated in the total glycan profile.

Table 3. Structures resulting from exoglycosidase (ABS, BTG + BKF) treatment of *N*-glycans released from lymph node melanoma tumour tissue of Stage III/IV individual patients (n=7, n=3 respectively). Relative % abundance was calculated by integration of the EICs of each mass and expressed as a percentage of the total glycan abundance after exoglycosidase digestion with ABS, BTG and BKF.

Glycan Class	Structure	Mass		Stage III (n=7)			Stage IV (n=4)			MS ²
		[M-H] ¹⁻	[M-2H] ²⁻							
Pauci Mannose	M2 	749.3		2.21 ± 1.62			1.99 ± 0.60			Y
	M3 	911.3		4.06 ± 2.76			4.85 ± 2.67			Y
	M4 	1073.3		1.18 ± 0.65			1.14 ± 0.38			Y
High Mannose	M5 	1235.4	617.2	2.24 ± 0.95			2.36 ± 0.56			Y
	M6 	1397.5	698.3	4.66 ± 1.25			5.51 ± 1.47			Y
	M7 	1559.5	779.3	6.51 ± 1.64			6.85 ± 2.04			Y
	M8 	1721.6	860.3	6.68 ± 2.25			6.37 ± 1.31			Y
	M9 	1883.7	941.3	4.57 ± 1.14			3.60 ± 1.14			Y
	M9Glc1 	2045.7	1022.3	0.35 ± 0.11			0.25 ± 0.20			Y
Hybrid	M4A1 	1276.5	637.7	0.73 ± 0.26			0.54 ± 0.24			Y
	M5A1 	1438.5	718.8	2.28 ± 0.46			2.15 ± 0.51			Y
Bisecting GlcNAc	A2B 	1520.6	759.8	8.35 ± 3.66			6.46 ± 4.54			Y
	A3B 		861.3	0.71 ± 0.38			0.98 ± 0.49			Y
	A4B 		962.8	0.13 ± 0.15			0.26 ± 0.17			Y

Glycan Class	Structure	Mass	Stage III	Stage IV	MS ²
Mono-antennary	A1[3]	1114.4	1.91 ± 0.79	1.83 ± 0.56	Y
	A1[6]	1114.4	1.02 ± 0.53	1.27 ± 0.60	Y
Bi-antennary	A2	1317.5 658.2	18.81 ± 7.97	16.90 ± 6.86	Y
Tri-antennary	A3[6,6,3]	1520.6 759.8	5.01 ± 1.65	6.31 ± 2.83	Y
	A3[6,3,3]	1520.6 759.8	12.66 ± 3.60	14.31 ± 3.82	Y
Tetra-antennary	A4	861.3	8.49 ± 4.06	10.69 ± 4.34	Y
LacdiNac	A2GalNac1	759.8	1.67 ± 1.87	0.45 ± 0.60	Y
	A2GalNac2	861.3	0.67 ± 0.95	0.00 ± 0.00	Y
Lactosamine	A2Lac1	840.8	1.71 ± 0.93	1.03 ± 0.73	Y
	A3Lac1	942.3	1.24 ± 0.36	1.61 ± 0.47	Y
	A4Lac1	1043.8	1.35 ± 0.76	1.56 ± 1.15	Y
	A4Lac2	1226.4	0.40 ± 0.15	0.47 ± 0.47	Y
	nd	759.8	0.15 ± 0.37	0.18 ± 0.37	Y
	nd	1145.4	0.24 ± 0.33	0.08 ± 0.15	Y

nd = not determined

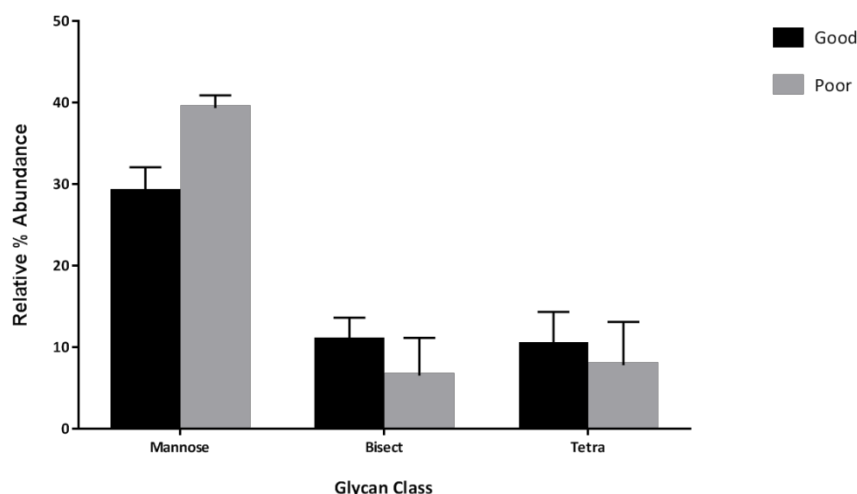


Figure 8. Comparison of the relative abundance of mannose, bisecting GlcNAc and tetra antennary glycan classes between good (n=3) and poor (n=3) prognostic stage III patient groups after enzyme digestion of the released glycans from lymph node melanoma tissue with ABS, BTG and BKF.

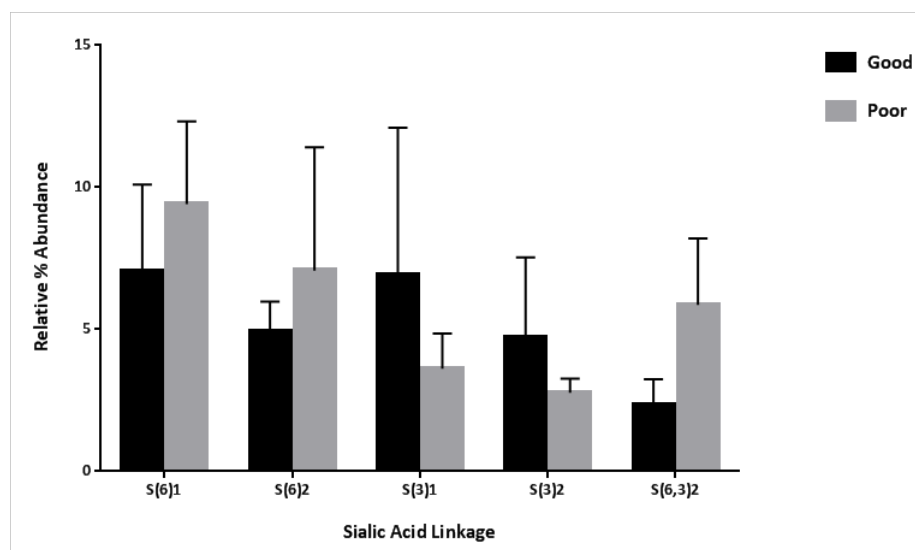


Figure 9. Comparison of the relative abundance of sialic acid linkages between good (n=3) and poor (n=3) prognostic stage III patient groups calculated for mono- (S1) and di-sialylated (S2) glycan structures released from individual tumour tissues. S(6) = α 2-6 and S(3)= α 2-3 linked sialic acid.

Comparison of individual patient variation in membrane protein glycoprofile

Detailed structural glycan features were quantitated relative to each other for each of the 10 patient samples. Overall, the most abundant structure was not consistent for all patients and the data shows variation between M8 (n=3), M9 (n=3), bi-antennary fully sialylated (n=1) and mono-sialylated core fucosylated bi-antennary (n=3) as the predominant structure ranging from 10.2-14% of the total glycan profile (highlighted peaks Supplementary Figure S1). The classification of glycan abundances into the main structural classes allows for the comparison of relative changes between patients. Here, we observed that the highest degree of variation between individuals was within the high mannose and bi-antennary classes (Figure 6); this range was so high that no statistically significant trends related prognosis could be determined. Additionally the percentage abundance of sialylated structures also showed variation.

No significant differences in the glycosylation profile of stage III compared to stage IV

The two sample sets of lymph node melanoma tumour tissue were from stage III (n=7) and stage IV (n=3) patients. These two sample populations were compared to identify any stage specific glycan characteristics. The mean abundances for individual glycans and standard deviation are displayed in Table 2 and Table 3 (after digestion) for the two patient subgroups. Overall it was found that it was not possible to significantly differentiate between the two stages based on their expressed glycan structural classes.

Stage III glycosylation profile and prognosis

An aim of this study was to investigate whether the prognosis of stage III patients could be predicted by the glycosylation profile of the removed lymph node metastasis tissue. Stage III samples were divided retrospectively into a good prognostic group (n=3) who had a survival of greater than 24 months and poor prognosis group (n=3) who had a survival of less than 24 months. No statistically significant differences were observed but there were clear trends in some glycan class abundances between the two groups. The good prognostic group showed an overall lower abundance of high mannose glycans compared to the poor prognostic group. The good prognostic group also had a high average abundance of bisecting GlcNAc bi-antennary glycans (Figure 8). The two groups had a difference in sialic acid linkages within the bi-antennary class with the poor prognostic group having a higher amount of α 2-6 linked mono- and di-sialylated residues compared to the good prognostic group which had an overall higher abundance of α 2-3 linked sialic acid residues (Figure 9).

Comparison of primary tumour subtypes of lymph node melanoma tumour tissue

Within the stage III sample set there were samples classified as from three different primary subtypes of melanoma: superficial spreading (SSM; n=4), nodular (NM; n=1) and acral lentiginous (ALM; n=1). The glycosylation profiles of the three subtypes were compared to investigate any differences in glycan classes. In this preliminary comparison, the SSM and NM samples showed similar profiles but the ALM was very different (Supplementary Figure S1). The ALM patient tissue had an overall higher percentage of complex type glycans compared to high mannose and core fucosylation. Differences were also observed in the levels of sialylated structures and also the amount of α 2-3 linked sialic acid.

7.4 Discussion

This is the first report of the detailed glycan characterisation of metastatic melanoma lymph node tumour tissue.

Previous studies using melanoma cell lines demonstrated the importance of cell surface glycosylation in the progression of disease. More specifically a correlation has been made between the abundance of *N*-glycans with β 1-6 branching and lactosamine extension(s) with disease progression^{118,121,159}.

In the previous chapter, analysis parameters for the ratio of tri- and tetra-antennary glycans compared to high mannose and bi-antennary glycans were investigated. Following the observation that tetra-antennary glycans are underrepresented and the difficulty in distinguishing tri-antennary branching isomers in a glycoprofile obtained by ESI-MS in negative ion mode, the work described in this chapter analyses glycans released from tumour tissue samples before and after exoglycosidase treatment. Using this approach the relative abundance of all structures containing the β 1-6 branch could be determined (Table 3), whereas comparison of the abundances of the tri- and tetra-antennary structural classes was previously limited due to their underrepresentation before exoglycosidase treatment. Although β 1-6 branched structures were a dominant feature of the global glycosylation profile ($14.5 \pm 3.5\%$) of this sample set, there was no statistically significant difference in the percentage abundance between patient sub groups. (Table 3, Figure 8). Therefore this glycosylation feature may be characteristic of the progression from primary to metastatic disease but the levels may not change at the later disease stages (III/IV) at the global level. A characteristic of melanoma is an increased expression of galectin-3 which binds to galactose residues of poly LacNAc repeats^{23,162}. The increase in abundance of the β 1-6 branch may play a role in tumour cell adhesion and metastasis by facilitating the interaction of tumour cells with

galectin-3 expressed on the surface of endothelial cells¹⁶³. Further investigation into the branching on individual proteins isolated from tumour tissue of different disease stages from the same individual is needed.

The LacdiNAc epitope was detected at low levels in both stage III and IV patient tumours but was not present in all samples. GalNAc is added to GlcNAc residues by the action of a β 1-4 N-acetylgalactosaminyltransferase (β 4GalNAcT3/4) to form the LacdiNAc group that can be modified by sulfation¹⁶⁴, sialylation¹⁵¹ and/or fucosylation¹⁶⁵⁻¹⁶⁷. This epitope has been identified on a number of mammalian proteins commonly as part of bi-antennary *N*-glycan structures produced by a variety of different cell types including lysosome-associated membrane glycoproteins LAMPs-1 and -2 from 293 cells¹⁶⁸, glycodelin from amniotic fluid¹⁶⁶, erythropoietin and other proteins synthesised in a human ovarian cancer cell line, SKOV3¹⁶⁹ and tissue plasminogen activator isolated from a Bowes melanoma cell line¹⁵¹. Expression of LacdiNAc and the *B4GALNT3/4* genes have been associated with disease progression and prognosis in a number of cancers¹⁶⁵. In colon¹⁷⁰, ovarian^{167,169}, pancreatic¹⁷¹ and prostate¹⁷² cancers the increased abundance of the LacdiNAc epitope and/or expression of *B4GALNT3/4* genes correlates with poor prognosis. An opposite observation was made in breast cancer¹⁷³ and neuroblastoma¹⁷⁴ where the increased presence was correlated with a good prognosis and a suppression of cell migration and invasion of neuroblastoma cells. We did not find a significant difference in abundance of LacdiNAc between the stage III poor and good classified prognostic groups of patients in this study but the variation in abundance between individuals should be explored in relation to other clinical features including mutation status.

Due to the small number of patients included in this study and very high degree of individual variation in individual glycan structures, no significant differences were observed between the patient subgroups compared. Nevertheless trends in the abundance of bi-antennary, high mannose and sialic acid linkages were noticeable in this preliminary study of 10 patients. In particular, an overall higher abundance of α 2-3 linked sialic acid in patients with poor prognosis. Previous studies have also reported a change in the abundance of α 2-3 linked sialic acid in variants of the B16 mouse model. A higher proportion of α 2-3linked sialic acid was observed in a highly metastatic variant compared to α 2-6 in the low metastasising variant¹²⁰.

The high degree of individual variation in the relative abundance of glycan classes is not surprising given the diversity amongst the sample set (clinical table appendix 1). Although samples are classified as either stage III or stage IV they are from individuals of different ages, gender, primary subtypes, mutation status and excised from different lymph node locations

within the body. It has been shown that the gene and protein expression profiles for individuals classified with the same histological and clinical disease also exhibit a large degree of heterogeneity¹⁵⁵. Studies using cell surface labeling have also shown that cell lines derived from three different metastatic melanoma lesions isolated from the same individual, express varying abundances of glycoproteins. These glycoproteins not only varied in abundance but also in molecular weight distribution¹⁷⁵. That study highlights the high level of variability of the cell surface proteins that occur in different metastatic lesions from a single person. This observation could imply that glycosylation changes on these membrane proteins that are specific to diverse groups of individuals may not exist. Alternatively, it may be that the glycosylation changes that obviously do occur may be specific to only one or more glycoproteins that are also correlated with cancer metastasis and were in too low abundance to be observed in the global glycosylation profile.

Such questions require further investigation and larger sample sets in order to characterise the glycosylation profile of specific cell surface glycoproteins that have been identified by immunohistochemistry as potential prognostic indicators. Altered expression could be accompanied by altered glycosylation, which could prove to be a more specific, or complementary, marker of clinical stage or treatment prognosis.

7.5 Supplementary Material

Figure S1. Summed MS spectra of *N*-glycans released from 10 individual stage III (n=7) and stage IV (n=3) lymph node melanoma tumour tissue samples. Primary subtypes SSM (n=6), NM (n=2), ALM (n=1) and unknown (n=1) are indicated.

*= Good prognostic patients. Highlighted peaks represent the most abundant structures; Red=High mannose M8 (m/z 860.3²⁻) and M9 (m/z 941.3²⁻) structures, blue= sialylated bi-antennary F(6)A2G2S1 (m/z 860.3²⁻) and A2G2S2 (m/z 1111.4²⁻).

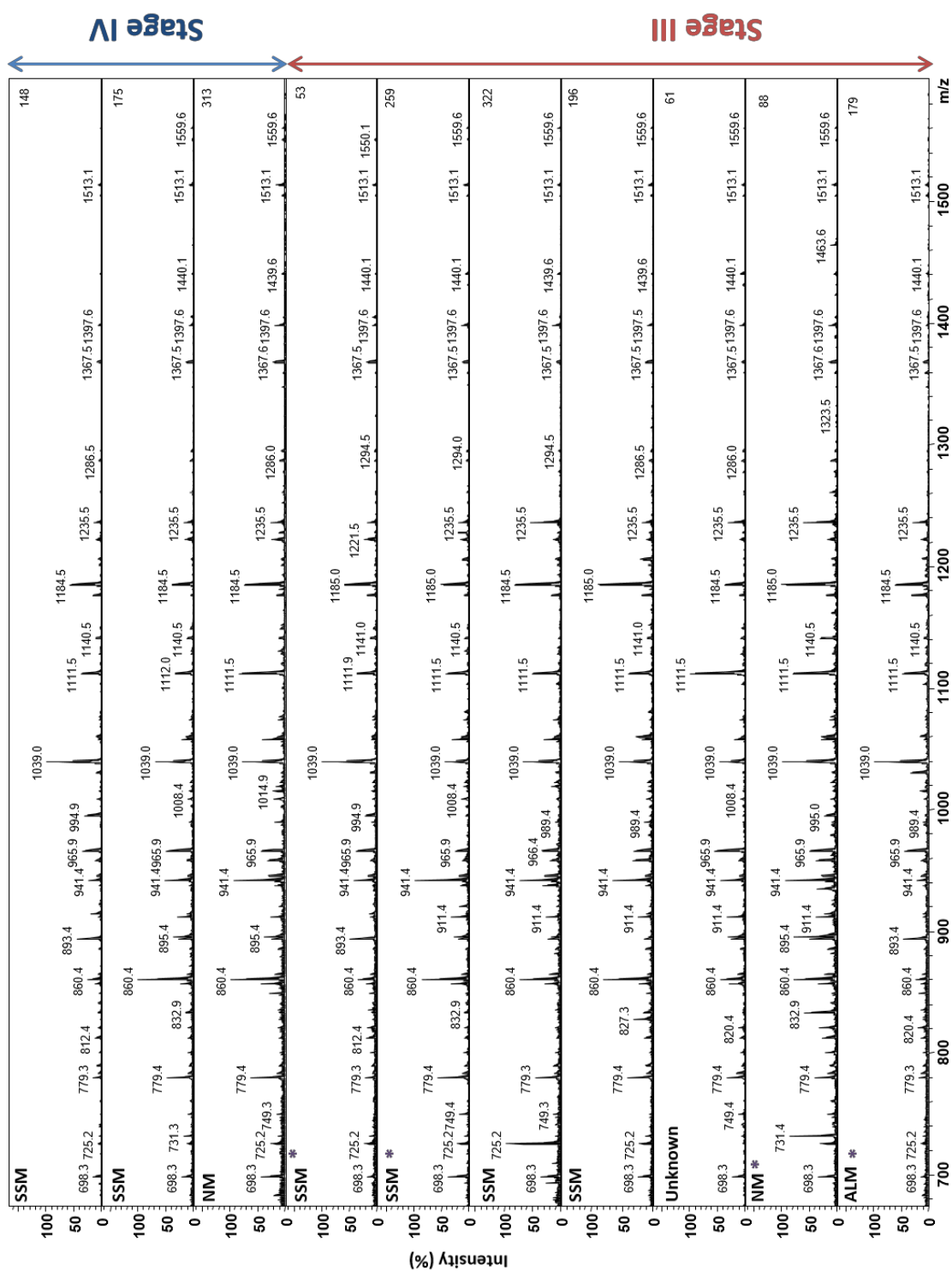


Figure S2. (a) Extracted ion chromatogram and (b) MS² negative-ion fragmentation spectra of the structural isomers of (HexNAc)₃ +(Man)₃(GlcNAc)₂ *m/z* 759.8². Four isomers of (HexNAc)₃+(Man)₃(GlcNAc)₂ were confirmed using PGC elution order and MS² fragmentation.

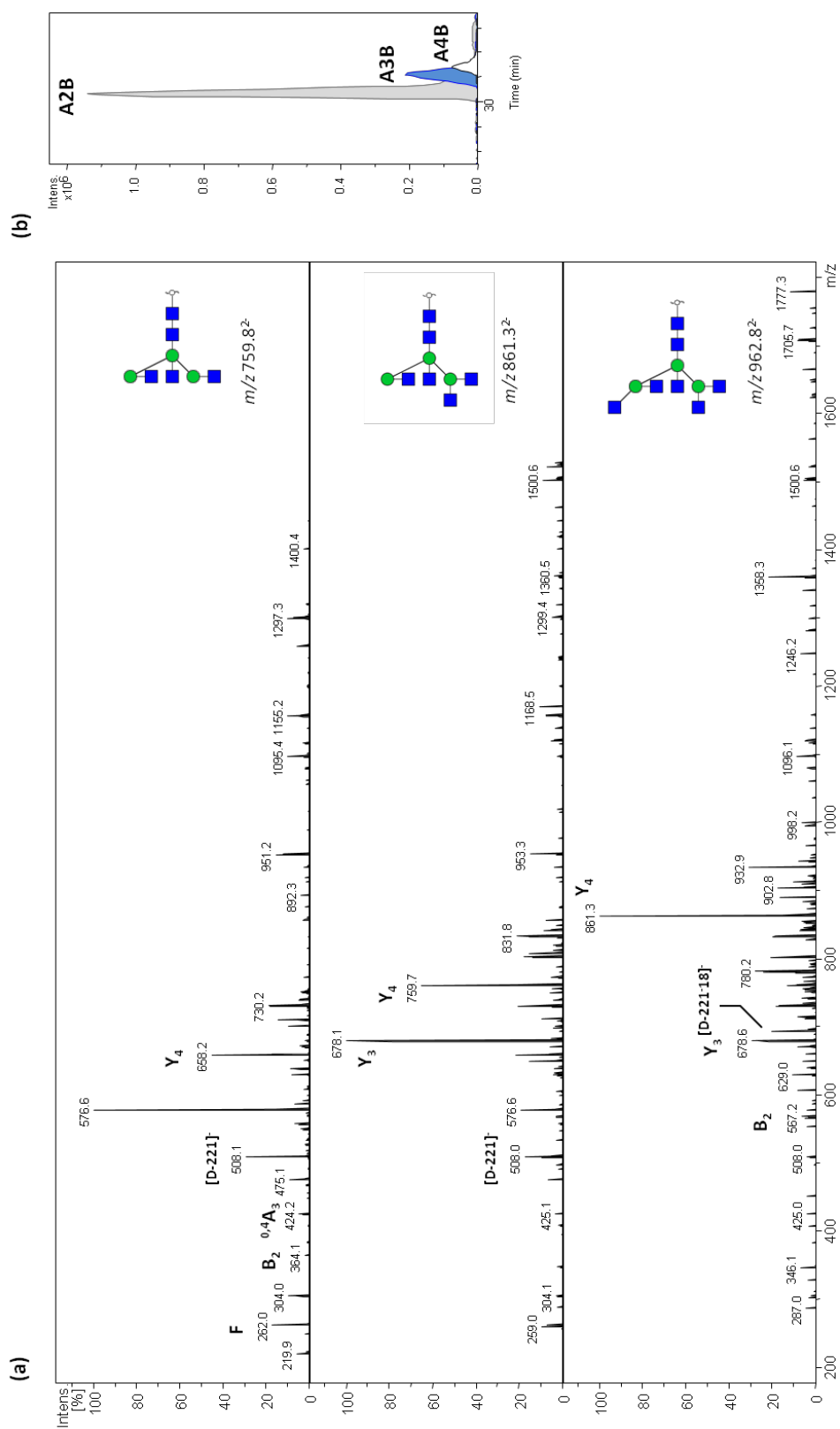
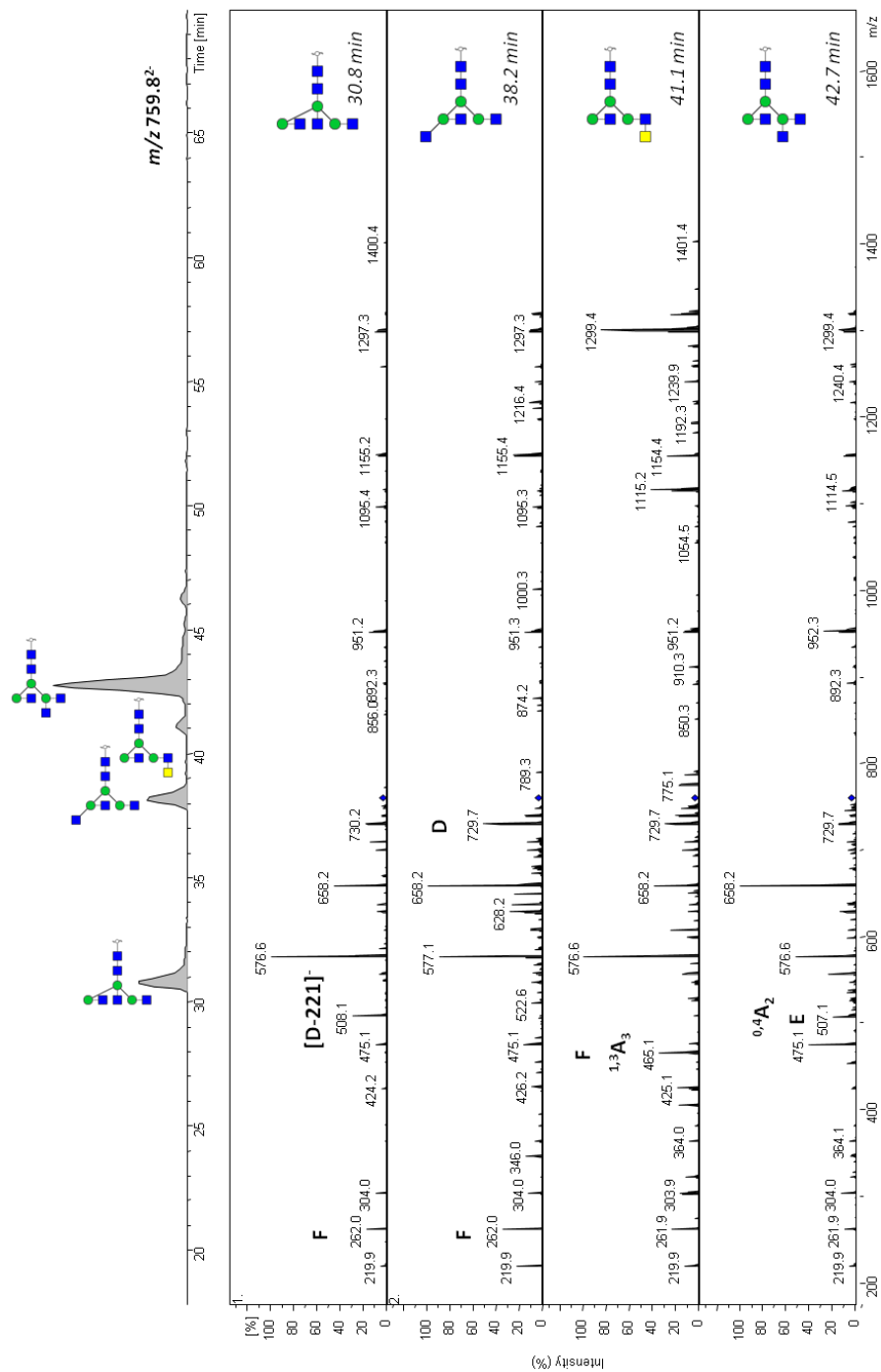


Figure S3. (a) MS² negative-ion fragmentation spectra and (b) Extracted ion chromatograms of the masses corresponding to bi- (A2B), tri- (A3B) and tetra- (A4B) antennary species with bisecting GlcNAc.



Chapter 8

Summary and Future Directions

8.1 Summary

In this study the *N*-glycosylation profile of metastatic melanoma was investigated using a combination of PGC-LC-MS/MS and exoglycosidase enzymes. The identification of prognostic markers of stage III melanoma is of great importance in melanoma research as currently the mortality rate for patients at this stage of disease is highly variable. As summarised in the literature review (Publication 1) most studies to date have focused on cell line models and the use of lectin based methods to investigate the role of glycosylation in melanoma progression. A review of the literature highlights the lack of studies on the detailed characterisation of the global cell surface glycosylation of melanoma tissue (summarised in Chapter 1 Figure 12).

In this work an orthogonal analytical workflow was optimised to accurately characterise cell-surface oligosaccharides released from the proteins in melanoma tumour samples and cell line models. The strategy-maximised information obtained from LC and MS/MS outputs combined with exoglycosidases determined over 100 glycan structures, including isomers, on tissue and cell line proteins.

Before analysing melanoma samples the benefits and limitations of existing methodologies (LC retention, MS, MS/MS and exoglycosidase specificities) were optimised by analysis of well-characterised *N*-glycans released from glycoprotein standards and application to the characterisation of human saliva *N*-glycosylation. From these studies new experimental tools and informatics resources were developed to aid data interpretation and the accurate characterisation of complex *N*-glycan mixtures as analysed by capillary PGC-LC-ESI-MS/MS (Chapters 2 to 4).

Specifically, the use of PGC LC separation and MS/MS diagnostic fragment ions were optimised for the assignment of structural isomers of over 200 glycans released from human saliva and as a result an annotated MS/MS spectral library (publication 2) was developed. In addition, the PGC elution time behaviour of known *N*-glycan structures ranging from small pauci mannose to branched multi-antennary complex type released from seven glycoprotein standards were mapped and a retention time database of over 100 *N*-glycan structures with corresponding MS/MS spectral data was compiled (publication 3) and deposited into Unicarb-DB. Together, these studies emphasise how valuable the addition of PGC retention order is for the assignment of *N*-glycan structures, as even though absolute retention times may vary, the elution order based on glycan structural features is consistent.

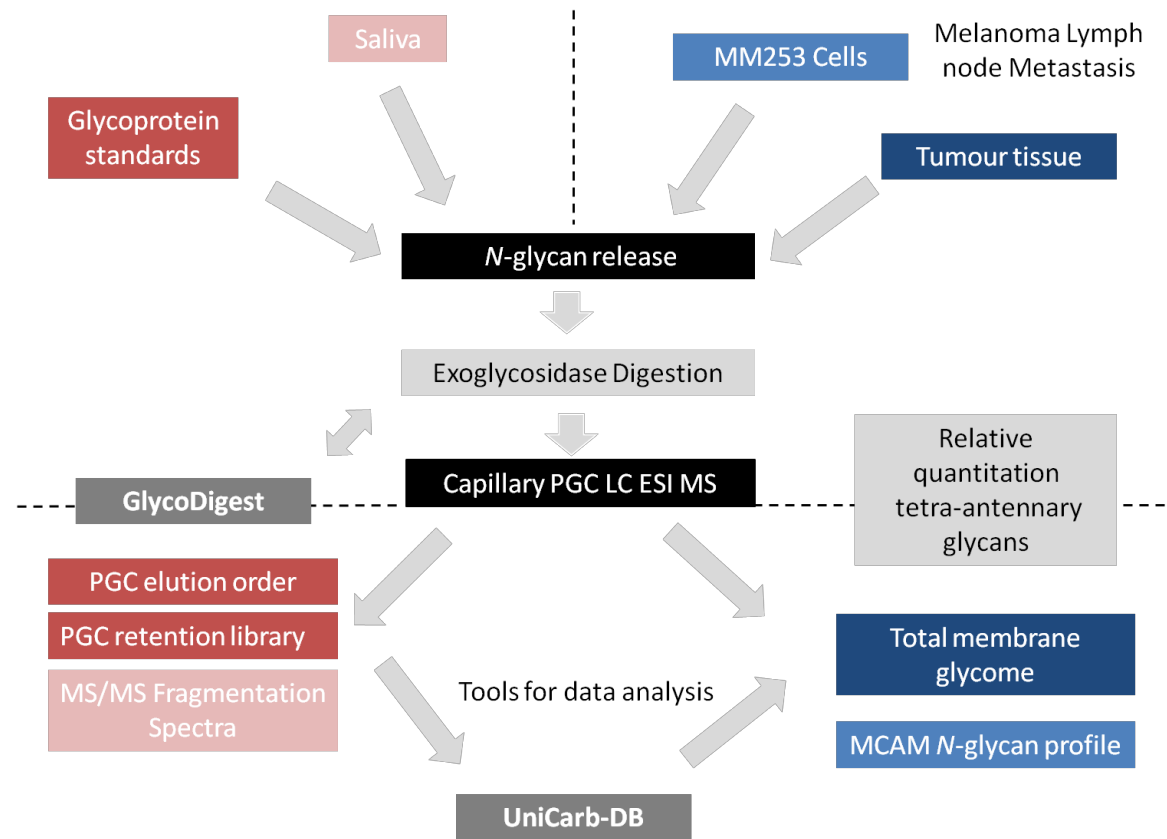


Figure 1. Thesis overview.

In both these optimisation studies, panels of exoglycosidase enzymes were used to confirm specific residues linkages and to validate the structure assignments. In addition, these enzymes were also used to simplify complex samples, for example to remove terminal epitopes and to increase the range of determined structures and for the inclusion of digestion products in the spectral database. Furthermore, to aid the data interpretation when using exoglycosidase enzymes alone and in array format, a bioinformatics resource, GlycoDigest, was developed based on literature and experimental evidence (publication 4).

The availability then of annotated MS² spectra derived from human saliva and glycoprotein standards was also an important resource for the interpretation of the structures of glycans released from previously uncharacterised samples including melanoma tissue and cell lines. By combining information generated from LC and mass spectrometry, structures could be more accurately assigned, especially by the capacity to distinguish isomeric and isobaric structures. This work now forms a central resource including a knowledgebase of PGC elution behaviour (Chapter 3), annotated MS/MS spectra (Chapter 2) and a tool for exoglycosidase specificity (Chapter 4) in the UniCarbKB glycan knowledgebase being developed by our research group.

8.2 Melanoma glycosylation

The developed workflow was then applied to investigate glycosylation changes occurring in metastatic melanoma. Initial experiments were conducted on a cell line model where analysis of the global glycosylation of the membrane proteins of a metastatic melanoma cell line derived from the lymph node (MM253) and the prognostic biomarker glycoprotein MCAM from the same cell line confirmed the glycosylation characteristics documented in the literature, and added specific glycan features, including structures containing the unusual LacdiNAc motif that could be potential additional prognostic markers (Chapter 5).

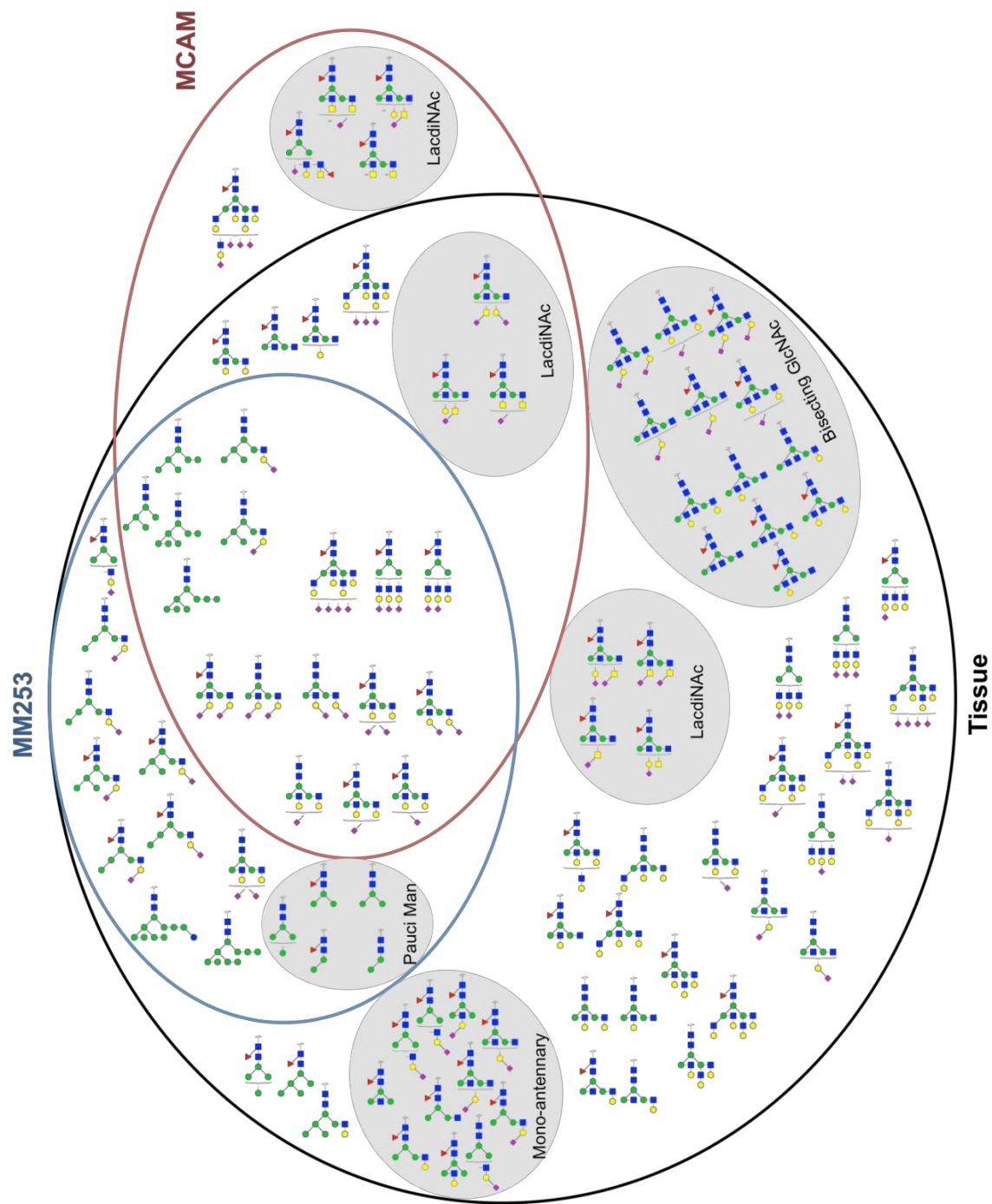
The initial analysis of patient melanoma metastatic lymph node tissue samples (Chapter 7) revealed that the previously reported class of glycans containing β 1-6 linked GlcNAc, that have been associated with metastasis, were detected at very low levels. More in-depth characterisation of the glycan structures carrying this motif using exoglycosidase digestion led to the observation that glycans with multiple antennae (> bi-antennary) and with poly LacNAc extensions were under-represented in the total glycan profile when detected in the base peak chromatogram as their undigested galactosylated and sialylated forms prior to exoglycosidase

treatment. Due to the potential importance of these structural classes in melanoma, improved analysis parameters including increasing the target mass window and the use of exoglycosidase enzymes for detection and quantitation of these multi-antennary structures relative to the bi-antennary and high mannose glycans, were investigated using the known tetra-antennary structures released from a standard glycoprotein (α 1-acid glycoprotein). This approach was then applied to the analysis of the glycans released from the membrane proteins of the MM253 cell line (publication 5).

Comparison of the glycosylation profile of the isolated cell surface protein MCAM and the enriched membrane fraction of the metastatic melanoma cell line MM253 (Figure 2) revealed that glycan classes including structures with LacdiNAc and polylactosamine units carried by a minority of cell surface proteins may be too low in abundance to be detected when analysing the total membrane glycome. The high abundance of mannose type glycans in the profile of total membranes and not on MCAM indicated that the total membrane enrichment method has enriched both the inner (less-processed glycans) and outer (more processed glycans) membrane proteins.

From this study it was decided to also use this approach to quantitate the glycans released from melanoma lymph node metastatic tissue proteins both before and after exoglycosidase digestion with sialidase, beta-galactosidase and alpha fucosidase. The abundances of structures present in the total profile and the abundance of each branched class (after removing these terminal epitopes) was compared in individual and subtype patient lymph node tumour tissue samples. Mannose type glycans were also a dominant feature of the tissue glycan profile, but were lower in abundance compared to the cell line model, suggesting the higher abundance of mannose structures may be associated with cell culture conditions. Comparison of the cell line and the pooled tissue profile after exoglycosidase treatment revealed that the scaffold bi-, tri- and tetra-antennary structures were present in both sample types, although the number of identified structures and relative abundance of complex type glycans were significantly greater in the tissue samples. In the tissue samples there was also a presence of bisecting GlcNAc and mono-antennary structures that were absent from the cell line profiles (Figure 2).

Figure 2. Venn diagram of common and unique *N*-glycan structures identified on membrane proteins from the metastatic melanoma cell line MM253, stage III/IV lymph node tumour tissue and MCAM. Shaded regions indicate glycan structural features that differ between the three samples.



A feature of the glycosylation profile of the melanoma prognostic marker MCAM isolated from MM253 cells was the presence of the LacdiNAc epitope. Although this low abundance epitope was not observed in the total cultured cell membrane profile it was detected in patient tissue samples in varying abundance. This may be explained by a variable amount of MCAM present on the surface of the metastatic lymph node melanoma cells in different people at various disease stages.

The glycosylation profile of the lymph node metastatic tissue from the different patient subgroups including prognosis, primary histology type and disease stage were investigated with an aim to identify any subtype-associated glycan features. Although trends in the abundance of (2,3/2,6) sialic acid linkage types, high mannose, bisecting GlcNAc and tetra-antennary classes between good and poor prognostic groups were observed, unfortunately no unique structures or statistically significant changes in abundance were identified. Due to the small sample population and individual variation observed, a larger study should be conducted before any conclusions are drawn as to whether the glycosylation profile can be used as a parameter to predict patient prognosis or not.

This in-depth *N*-glycan characterisation of tumour tissue complements existing studies using lectin-based approaches^{110,119,176} by confirming that glycan motifs previously identified in cell models correlated with metastatic potential are present in patient samples. It also advances our knowledge by identifying the individual structures that carry these motifs as well as potential new MCAM specific glycan biomarkers.

Overall, this study highlights the benefits of orthogonal (LC retention, MS and MS/MS, exoglycosidase) methods for analysis of the protein glycosylation of complex cancer tissue samples, and has provided the first detailed characterisation of the *N*-glycan structures present in metastatic melanoma lymph node cell and tissue samples as well as of the prognostic marker MCAM, using mass spectrometry based methods. The data generated in this thesis has been deposited into a cancer and tissue specific domain within UniCarb-DB (www.unicarbk.org) and will be available to aid future analysis of larger patient datasets. The study contributes to our understanding of glycosylation alterations in melanoma metastasis and points towards using specific glycosylation changes as prognostic markers of lymph node metastasis and potentially as specific targets for therapeutic intervention.

8.3 Future Directions

This study of stage III/IV melanoma tissue samples has provided a detailed representation of the cell surface *N*-glycome and demonstrated the need to investigate larger sample populations from individuals with less diverse clinical pathologies in order to better understand normal individual variation compared to disease associated variations. Patient matched normal lymph node tissue and tumour tissue should also be compared as the lymph node samples contain both tumour and lymphatic cells. Unfortunately for this study we were unable to obtain these samples but they are now being collected and stored to aid future projects. It would also be useful to monitor glycosylation changes between primary, secondary and distant metastasis from the same individual but primary melanoma tumour tissue is often limited due to the small size of tumours.

Application of MALDI imaging technology for the analysis of surface glycan localisation in combination with histopathology mapping could also be a useful approach to distinguish areas of tumour from necrotic and lymph cells and to eliminate bias introduced from enrichment methods. More detailed site-specific glycan analysis of targeted glycoproteins including that of MCAM isolated from MM253 cell line model, tumour tissue and healthy tissue is also an area of interest to gain a better understanding of individual protein glycosylation changes and the functions of specific glycan signatures. The isolation and analysis of MCAM from patient tissue samples was outside of the scope of this thesis as only limited amounts of tissue could be obtained. It would be interesting to first identify whether all stage III and IV patient tumours express MCAM and then to isolate and analyse MCAM from different prognostic groups. Alternative approaches and technologies should also be explored for the detection and analysis of *N*-glycan structures with multiple extended polylactosamine antennae including the use of enzymes specific for lactosamine repeating units (for example endo-beta-galactosidase) and MALDI-MS analysis which is useful for detecting glycans in the higher mass range.

Further investigation into whether the LacdiNAc epitope is MCAM specific in the cell lines and tissue or is carried by other melanoma associated cell surface proteins could increase the diagnostic potential of MCAM as a biomarker. It would also be interesting to analyse the glycosylation profile of enriched membrane proteins from the MM253 cell line after culturing in 3D to better represent a tumour and compare to 2D cultured cell profile.

References

1. Ceroni, A. *et al.* GlycoWorkbench: a tool for the computer-assisted annotation of mass spectra of glycans. *Journal of proteome research* **7**, 1650-1659 (2008).
2. Tsao, H., Chin, L., Garraway, L. A. & Fisher, D. E. Melanoma: from mutations to medicine. *Genes & development* **26**, 1131-1155 (2012).
3. Greenwald, H. S., Friedman, E. B. & Osman, I. Superficial spreading and nodular melanoma are distinct biological entities: a challenge to the linear progression model. *Melanoma research* **22**, 1-8 (2012).
4. Mar, V., Roberts, H., Wolfe, R., English, D. R. & Kelly, J. W. Nodular melanoma: a distinct clinical entity and the largest contributor to melanoma deaths in Victoria, Australia. *Journal of the American Academy of Dermatology* **68**, 568-575 (2013).
5. Egger, M. E. *et al.* Outcomes and prognostic factors in superficial spreading melanoma. *American journal of surgery* **206**, 861-867; discussion 867-868 (2013).
6. Reed, J. A. & Shea, C. R. Lentigo maligna: melanoma in situ on chronically sun-damaged skin. *Archives of pathology & laboratory medicine* **135**, 838-841 (2011).
7. Piliang, M. P. Acral lentiginous melanoma. *Clinics in laboratory medicine* **31**, 281-288 (2011).
8. Balch, C. M. *et al.* Final version of 2009 AJCC melanoma staging and classification. *Journal of clinical oncology : official journal of the American Society of Clinical Oncology* **27**, 6199-6206 (2009).
9. Braeuer, R. R. *et al.* Why is melanoma so metastatic? *Pigment cell & melanoma research* **27**, 19-36 (2014).
10. Mohr, P., Eggermont, A. M., Hauschild, A. & Buzaid, A. Staging of cutaneous melanoma. *Annals of oncology : official journal of the European Society for Medical Oncology / ESMO* **20 Suppl 6**, vi14-21 (2009).
11. Bognoux, A. C. & Solassol, J. The contribution of proteomics to the identification of biomarkers for cutaneous malignant melanoma. *Clinical biochemistry* **46**, 518-523 (2013).
12. <http://www.hlifestyle.net/melanoma-early-diagnosis-is-important/>.
13. Vidwans, S. J. *et al.* A melanoma molecular disease model. *PloS one* **6**, e18257 (2011).
14. Bittner, M. *et al.* Molecular classification of cutaneous malignant melanoma by gene expression profiling. *Nature* **406**, 536-540 (2000).
15. Scolyer, R. A., Long, G. V. & Thompson, J. F. Evolving concepts in melanoma classification and their relevance to multidisciplinary melanoma patient care. *Molecular oncology* **5**, 124-136 (2011).
16. Banfalvi, T. *et al.* Comparison of prognostic significance of serum 5-S-Cysteinyl-dopa, LDH and S-100B protein in Stage III-IV malignant melanoma. *Pathol Oncol Res* **8**, 183-187 (2002).
17. Finck, S. J., Giuliano, A. E. & Morton, D. L. LDH and melanoma. *Cancer* **51**, 840-843 (1983).
18. Gogas, H. *et al.* Biomarkers in melanoma. *Annals of oncology : official journal of the European Society for Medical Oncology / ESMO* **20 Suppl 6**, vi8-13 (2009).
19. Buer, J. *et al.* Elevated serum levels of S100 and survival in metastatic malignant melanoma. *British journal of cancer* **75**, 1373-1376 (1997).
20. Link-Lenczowski, P. & Litynska, A. Glycans in melanoma screening. Part 2. Towards the understanding of integrin N-glycosylation in melanoma. *Biochemical Society transactions* **39**, 374-377 (2011).
21. Wai Wong, C., Dye, D. E. & Coombe, D. R. The role of immunoglobulin superfamily cell adhesion molecules in cancer metastasis. *International journal of cell biology* **2012**, 340296 (2012).

22. Haass, N. K., Smalley, K. S., Li, L. & Herlyn, M. Adhesion, migration and communication in melanocytes and melanoma. *Pigment cell research / sponsored by the European Society for Pigment Cell Research and the International Pigment Cell Society* **18**, 150-159 (2005).
23. Dye, D. E., Medic, S., Ziman, M. & Coombe, D. R. Melanoma biomolecules: independently identified but functionally intertwined. *Frontiers in oncology* **3**, 252 (2013).
24. Shih, I. M., Elder, D. E., Hsu, M. Y. & Herlyn, M. Regulation of Mel-CAM/MUC18 expression on melanocytes of different stages of tumor progression by normal keratinocytes. *The American journal of pathology* **145**, 837-845 (1994).
25. Lehmann, J. M. *et al.* Discrimination between benign and malignant cells of melanocytic lineage by two novel antigens, a glycoprotein with a molecular weight of 113,000 and a protein with a molecular weight of 76,000. *Cancer research* **47**, 841-845 (1987).
26. Lei, X., Guan, C. W., Song, Y. & Wang, H. The multifaceted role of CD146/MCAM in the promotion of melanoma progression. *Cancer cell international* **15**, 3 (2015).
27. Adamczyk, B., Tharmalingam, T. & Rudd, P. M. Glycans as cancer biomarkers. *Biochimica et biophysica acta* **1820**, 1347-1353 (2012).
28. Dube, D. H. & Bertozzi, C. R. Glycans in cancer and inflammation--potential for therapeutics and diagnostics. *Nat Rev Drug Discov* **4**, 477-488 (2005).
29. Christiansen, M. N. *et al.* Cell surface protein glycosylation in cancer. *Proteomics* **14**, 525-546 (2014).
30. Johnson, J. P. Cell adhesion molecules in the development and progression of malignant melanoma. *Cancer metastasis reviews* **18**, 345-357 (1999).
31. McGary, E. C., Lev, D. C. & Bar-Eli, M. Cellular adhesion pathways and metastatic potential of human melanoma. *Cancer biology & therapy* **1**, 459-465 (2002).
32. Opdenakker, G., Rudd, P. M., Ponting, C. P. & Dwek, R. A. Concepts and principles of glycobiology. *Faseb J* **7**, 1330-1337 (1993).
33. Moremen, K. W., Tiemeyer, M. & Nairn, A. V. Vertebrate protein glycosylation: diversity, synthesis and function. *Nature reviews. Molecular cell biology* **13**, 448-462 (2012).
34. Varki, A. Factors controlling the glycosylation potential of the Golgi apparatus. *Trends Cell Biol* **8**, 34-40 (1998).
35. Varki, A. & Sharon, N. in *Essentials of Glycobiology* (eds A. Varki *et al.*) (2009).
36. Van den Steen, P., Rudd, P. M., Dwek, R. A. & Opdenakker, G. Concepts and principles of O-linked glycosylation. *Critical reviews in biochemistry and molecular biology* **33**, 151-208 (1998).
37. Weerapana, E. & Imperiali, B. Asparagine-linked protein glycosylation: from eukaryotic to prokaryotic systems. *Glycobiology* **16**, 91R-101R (2006).
38. Stanley, P., Schachter, H. & Taniguchi, N. in *Essentials of Glycobiology* (eds A. Varki *et al.*) (2009).
39. Aebi, M. N-linked protein glycosylation in the ER. *Biochimica et biophysica acta* **1833**, 2430-2437 (2013).
40. Breitling, J. & Aebi, M. N-linked protein glycosylation in the endoplasmic reticulum. *Cold Spring Harb Perspect Biol* **5**, a013359 (2013).
41. Stanley, P. Golgi glycosylation. *Cold Spring Harb Perspect Biol* **3** (2011).
42. Hammond, C., Braakman, I. & Helenius, A. Role of N-linked oligosaccharide recognition, glucose trimming, and calnexin in glycoprotein folding and quality control. *Proceedings of the National Academy of Sciences of the United States of America* **91**, 913-917 (1994).
43. Taniguchi, N. & Korekane, H. Branched N-glycans and their implications for cell adhesion, signaling and clinical applications for cancer biomarkers and in therapeutics. *BMB reports* **44**, 772-781 (2011).
44. Taniguchi, N. a. K., Y. in *Glycoscience: Biology and Medicine* (Springer Japan, 2014).

45. Ihara, H., Ikeda, Y. & Taniguchi, N. Reaction mechanism and substrate specificity for nucleotide sugar of mammalian α 1,6-fucosyltransferase--a large-scale preparation and characterization of recombinant human FUT8. *Glycobiology* **16**, 333-342 (2006).
46. Stanley, P. & Cummings, R. D. in *Essentials of Glycobiology* (eds A. Varki *et al.*) (2009).
47. Varki, A. & Schauer, R. in *Essentials of Glycobiology* (eds A. Varki *et al.*) (2009).
48. Pabst, M. & Altmann, F. Glycan analysis by modern instrumental methods. *Proteomics* **11**, 631-643 (2011).
49. Marino, K., Bones, J., Kattla, J. J. & Rudd, P. M. A systematic approach to protein glycosylation analysis: a path through the maze. *Nature chemical biology* **6**, 713-723 (2010).
50. Thaysen-Andersen, M. & Packer, N. H. Advances in LC-MS/MS-based glycoproteomics: getting closer to system-wide site-specific mapping of the N- and O-glycoproteome. *Biochimica et biophysica acta* **1844**, 1437-1452 (2014).
51. Hua, S. *et al.* Site-specific protein glycosylation analysis with glycan isomer differentiation. *Analytical and bioanalytical chemistry* **403**, 1291-1302 (2012).
52. Moh, E. S., Thaysen-Andersen, M. & Packer, N. H. Relative versus absolute quantitation in disease glycomics. *Proteomics. Clinical applications* **9**, 368-382 (2015).
53. Alley, W. R., Jr. & Novotny, M. V. Structural glycomic analyses at high sensitivity: a decade of progress. *Annual review of analytical chemistry* **6**, 237-265 (2013).
54. Harvey, D. J. Proteomic analysis of glycosylation: structural determination of N- and O-linked glycans by mass spectrometry. *Expert review of proteomics* **2**, 87-101 (2005).
55. Bhavanandan, V. P., Umemoto, J. & Davidson, E. A. Characterization of an endo- α -N-acetyl galactosaminidase from *Diplococcus pneumoniae*. *Biochemical and biophysical research communications* **70**, 738-745 (1976).
56. Merry, A. H. *et al.* Recovery of intact 2-aminobenzamide-labeled O-glycans released from glycoproteins by hydrazinolysis. *Analytical biochemistry* **304**, 91-99 (2002).
57. Royle, L. *et al.* An analytical and structural database provides a strategy for sequencing O-glycans from microgram quantities of glycoproteins. *Analytical biochemistry* **304**, 70-90 (2002).
58. Kozak, R. P., Royle, L., Gardner, R. A., Fernandes, D. L. & Wuhrer, M. Suppression of peeling during the release of O-glycans by hydrazinolysis. *Analytical biochemistry* **423**, 119-128 (2012).
59. Anumula, K. R. Advances in fluorescence derivatization methods for high-performance liquid chromatographic analysis of glycoprotein carbohydrates. *Analytical biochemistry* **350**, 1-23 (2006).
60. Wilson, N. L., Schulz, B. L., Karlsson, N. G. & Packer, N. H. Sequential analysis of N- and O-linked glycosylation of 2D-PAGE separated glycoproteins. *Journal of proteome research* **1**, 521-529 (2002).
61. Abd Hamid, U. M. *et al.* A strategy to reveal potential glycan markers from serum glycoproteins associated with breast cancer progression. *Glycobiology* **18**, 1105-1118 (2008).
62. Royle, L., Radcliffe, C. M., Dwek, R. A. & Rudd, P. M. Detailed structural analysis of N-glycans released from glycoproteins in SDS-PAGE gel bands using HPLC combined with exoglycosidase array digestions. *Methods in molecular biology* **347**, 125-143 (2006).
63. Royle, L. *et al.* HPLC-based analysis of serum N-glycans on a 96-well plate platform with dedicated database software. *Analytical biochemistry* **376**, 1-12 (2008).
64. Jensen, P. H., Karlsson, N. G., Kolarich, D. & Packer, N. H. Structural analysis of N- and O-glycans released from glycoproteins. *Nature protocols* **7**, 1299-1310 (2012).
65. Han, L. & Costello, C. E. Mass spectrometry of glycans. *Biochemistry. Biokhimiia* **78**, 710-720 (2013).

66. Kailemia, M. J., Ruhaak, L. R., Lebrilla, C. B. & Amster, I. J. Oligosaccharide analysis by mass spectrometry: a review of recent developments. *Analytical chemistry* **86**, 196-212 (2014).
67. Ahn, J., Bones, J., Yu, Y. Q., Rudd, P. M. & Gilar, M. Separation of 2-aminobenzamide labeled glycans using hydrophilic interaction chromatography columns packed with 1.7 microm sorbent. *Journal of chromatography. B, Analytical technologies in the biomedical and life sciences* **878**, 403-408 (2010).
68. Bones, J. *et al.* 2D-LC analysis of BRP 3 erythropoietin N-glycosylation using anion exchange fractionation and hydrophilic interaction UPLC reveals long poly-N-acetyl lactosamine extensions. *Analytical chemistry* **83**, 4154-4162 (2011).
69. Campbell, M. P., Royle, L., Radcliffe, C. M., Dwek, R. A. & Rudd, P. M. GlycoBase and autoGU: tools for HPLC-based glycan analysis. *Bioinformatics* **24**, 1214-1216 (2008).
70. Stockmann, H., O'Flaherty, R., Adamczyk, B., Saldova, R. & Rudd, P. M. Automated, high-throughput serum glycoprofiling platform. *Integr Biol (Camb)* **7**, 1026-1032 (2015).
71. Knezevic, A. *et al.* High throughput plasma N-glycome profiling using multiplexed labelling and UPLC with fluorescence detection. *The Analyst* **136**, 4670-4673 (2011).
72. Knezevic, A. *et al.* Variability, heritability and environmental determinants of human plasma N-glycome. *Journal of proteome research* **8**, 694-701 (2009).
73. Domann, P., Spencer, D. I. & Harvey, D. J. Production and fragmentation of negative ions from neutral N-linked carbohydrates ionized by matrix-assisted laser desorption/ionization. *Rapid communications in mass spectrometry : RCM* **26**, 469-479 (2012).
74. Shahrokh, Z. *et al.* Erythropoietin produced in a human cell line (Dynepo) has significant differences in glycosylation compared with erythropoietins produced in CHO cell lines. *Molecular pharmaceutics* **8**, 286-296 (2011).
75. Packer, N. H., Lawson, M. A., Jardine, D. R. & Redmond, J. W. A general approach to desalting oligosaccharides released from glycoproteins. *Glycoconjugate journal* **15**, 737-747 (1998).
76. Karlsson, N. G. *et al.* Negative ion graphitised carbon nano-liquid chromatography/mass spectrometry increases sensitivity for glycoprotein oligosaccharide analysis. *Rapid communications in mass spectrometry : RCM* **18**, 2282-2292 (2004).
77. Pabst, M. & Altmann, F. Influence of electrosorption, solvent, temperature, and ion polarity on the performance of LC-ESI-MS using graphitic carbon for acidic oligosaccharides. *Analytical chemistry* **80**, 7534-7542 (2008).
78. Stadlmann, J., Pabst, M., Kolarich, D., Kunert, R. & Altmann, F. Analysis of immunoglobulin glycosylation by LC-ESI-MS of glycopeptides and oligosaccharides. *Proteomics* **8**, 2858-2871 (2008).
79. Pabst, M. *et al.* Isomeric analysis of oligomannosidic N-glycans and their dolichol-linked precursors. *Glycobiology* **22**, 389-399 (2012).
80. Pabst, M., Bondili, J. S., Stadlmann, J., Mach, L. & Altmann, F. Mass + retention time = structure: a strategy for the analysis of N-glycans by carbon LC-ESI-MS and its application to fibrin N-glycans. *Analytical chemistry* **79**, 5051-5057 (2007).
81. Everest-Dass, A. V., Abrahams, J. L., Kolarich, D., Packer, N. H. & Campbell, M. P. Structural feature ions for distinguishing N- and O-linked glycan isomers by LC-ESI-IT MS/MS. *Journal of the American Society for Mass Spectrometry* **24**, 895-906 (2013).
82. Aich, U. *et al.* Evaluation of desialylation during 2-amino benzamide labeling of asparagine-linked oligosaccharides. *Analytical biochemistry* **458**, 27-36 (2014).
83. Yin, H. & Killeen, K. The fundamental aspects and applications of Agilent HPLC-Chip. *J Sep Sci* **30**, 1427-1434 (2007).
84. Novotny, M. V., Alley, W. R., Jr. & Mann, B. F. Analytical glycobiology at high sensitivity: current approaches and directions. *Glycoconjugate journal* **30**, 89-117 (2013).

85. Lin, S. L., Lin, T. Y. & Fuh, M. R. Microfluidic chip-based liquid chromatography coupled to mass spectrometry for determination of small molecules in bioanalytical applications: an update. *Electrophoresis* **35**, 1275-1284 (2014).
86. Ni, W., Bones, J. & Karger, B. L. In-depth characterization of N-linked oligosaccharides using fluoride-mediated negative ion microfluidic chip LC-MS. *Analytical chemistry* **85**, 3127-3135 (2013).
87. Alley, W. R., Jr., Madera, M., Mechref, Y. & Novotny, M. V. Chip-based reversed-phase liquid chromatography-mass spectrometry of permethylated N-linked glycans: a potential methodology for cancer-biomarker discovery. *Analytical chemistry* **82**, 5095-5106 (2010).
88. Staples, G. O. *et al.* A chip-based amide-HILIC LC/MS platform for glycosaminoglycan glycomics profiling. *Proteomics* **9**, 686-695 (2009).
89. Hua, S. *et al.* Differentiation of cancer cell origin and molecular subtype by plasma membrane N-glycan profiling. *Journal of proteome research* **13**, 961-968 (2014).
90. Song, T., Ozcan, S., Becker, A. & Lebrilla, C. B. In-depth method for the characterization of glycosylation in manufactured recombinant monoclonal antibody drugs. *Analytical chemistry* **86**, 5661-5666 (2014).
91. Hua, S. *et al.* Isomer-specific chromatographic profiling yields highly sensitive and specific potential N-glycan biomarkers for epithelial ovarian cancer. *Journal of chromatography. A* **1279**, 58-67 (2013).
92. Bynum, M. A. *et al.* Characterization of IgG N-glycans employing a microfluidic chip that integrates glycan cleavage, sample purification, LC separation, and MS detection. *Analytical chemistry* **81**, 8818-8825 (2009).
93. Zaia, J. Mass spectrometry and glycomics. *Omics : a journal of integrative biology* **14**, 401-418 (2010).
94. Wuhrer, M. Glycomics using mass spectrometry. *Glycoconjugate journal* **30**, 11-22 (2013).
95. Tharmalingam, T., Adamczyk, B., Doherty, M. A., Royle, L. & Rudd, P. M. Strategies for the profiling, characterisation and detailed structural analysis of N-linked oligosaccharides. *Glycoconjugate journal* **30**, 137-146 (2013).
96. Harvey, D. J. Analysis of carbohydrates and glycoconjugates by matrix-assisted laser desorption/ionization mass spectrometry: an update for 2007-2008. *Mass spectrometry reviews* **31**, 183-311 (2012).
97. Haslam, S. M., North, S. J. & Dell, A. Mass spectrometric analysis of N- and O-glycosylation of tissues and cells. *Current opinion in structural biology* **16**, 584-591 (2006).
98. Harvey, D. J. Collision-induced fragmentation of underivatized N-linked carbohydrates ionized by electrospray. *Journal of mass spectrometry : JMS* **35**, 1178-1190 (2000).
99. Domon, B., Costello, C.E. A systematic nomenclature for carbohydrate fragmentations in FAB-MS/MS spectra of glycoconjugates. *Glycoconjugate journal* **5**, 397-409 (1988).
100. Harvey, D. J., Royle, L., Radcliffe, C. M., Rudd, P. M. & Dwek, R. A. Structural and quantitative analysis of N-linked glycans by matrix-assisted laser desorption ionization and negative ion nanospray mass spectrometry. *Analytical biochemistry* **376**, 44-60 (2008).
101. Harvey, D. J. Fragmentation of negative ions from carbohydrates: part 3. Fragmentation of hybrid and complex N-linked glycans. *Journal of the American Society for Mass Spectrometry* **16**, 647-659 (2005).
102. Harvey, D. J. Fragmentation of negative ions from carbohydrates: part 2. Fragmentation of high-mannose N-linked glycans. *Journal of the American Society for Mass Spectrometry* **16**, 631-646 (2005).

103. Harvey, D. J. *et al.* Fragmentation of negative ions from N-linked carbohydrates: part 6. Glycans containing one N-acetylglucosamine in the core. *Rapid communications in mass spectrometry : RCM* **28**, 2008-2018 (2014).
104. Mechref, Y., Hu, Y., Desantos-Garcia, J. L., Hussein, A. & Tang, H. Quantitative glycomics strategies. *Molecular & cellular proteomics : MCP* **12**, 874-884 (2013).
105. Orlando, R. Quantitative glycomics. *Methods in molecular biology* **600**, 31-49 (2010).
106. Cooper, C. A., Gasteiger, E. & Packer, N. H. GlycoMod--a software tool for determining glycosylation compositions from mass spectrometric data. *Proteomics* **1**, 340-349 (2001).
107. Cooper, C. A., Harrison, M. J., Wilkins, M. R. & Packer, N. H. GlycoSuiteDB: a new curated relational database of glycoprotein glycan structures and their biological sources. *Nucleic acids research* **29**, 332-335 (2001).
108. Campbell, M. P. *et al.* UniCarbKB: building a knowledge platform for glycoproteomics. *Nucleic acids research* **42**, D215-221 (2014).
109. Hayes, C. A. *et al.* UniCarb-DB: a database resource for glycomic discovery. *Bioinformatics* **27**, 1343-1344 (2011).
110. Ochwat, D., Hoja-Lukowicz, D. & Litynska, A. N-glycoproteins bearing beta1-6 branched oligosaccharides from the A375 human melanoma cell line analysed by tandem mass spectrometry. *Melanoma research* **14**, 479-485 (2004).
111. Przybylo, M., Martuszezowska, D., Pochec, E., Hoja-Lukowicz, D. & Litynska, A. Identification of proteins bearing beta1-6 branched N-glycans in human melanoma cell lines from different progression stages by tandem mass spectrometry analysis. *Biochimica et biophysica acta* **1770**, 1427-1435 (2007).
112. Pochec, E., Litynska, A., Amoresano, A. & Casbarra, A. Glycosylation profile of integrin alpha 3 beta 1 changes with melanoma progression. *Biochimica et biophysica acta* **1643**, 113-123 (2003).
113. Ciolczyk-Wierzbička, D., Gil, D., Hoja-Lukowicz, D., Litynska, A. & Laidler, P. Carbohydrate moieties of N-cadherin from human melanoma cell lines. *Acta biochimica Polonica* **49**, 991-998 (2002).
114. Hoja-Lukowicz, D. *et al.* L1CAM from human melanoma carries a novel type of N-glycan with Galbeta1-4Galbeta1- motif. Involvement of N-linked glycans in migratory and invasive behaviour of melanoma cells. *Glycoconjugate journal* (2012).
115. Ciolczyk-Wierzbička, D. *et al.* The structure of the oligosaccharides of N-cadherin from human melanoma cell lines. *Glycoconjugate journal* **20**, 483-492 (2004).
116. Janik, M. E., Przybylo, M., Pochec, E., Pokrywka, M. & Litynska, A. Effect of alpha3beta1 and alphavbeta3 integrin glycosylation on interaction of melanoma cells with vitronectin. *Acta biochimica Polonica* **57**, 55-61 (2010).
117. Kawano, T., Takasaki, S., Tao, T. W. & Kobata, A. N-linked sugar chains of mouse B16 melanoma cells and their low-metastasizing variant selected by wheat germ agglutinin. *Glycobiology* **1**, 375-385 (1991).
118. Laidler, P. *et al.* Characterization of glycosylation and adherent properties of melanoma cell lines. *Cancer immunology, immunotherapy : CII* **55**, 112-118 (2006).
119. Litynska, A. *et al.* Comparison of the lectin-binding pattern in different human melanoma cell lines. *Melanoma research* **11**, 205-212 (2001).
120. Passaniti, A. & Hart, G. W. Cell surface sialylation and tumor metastasis. Metastatic potential of B16 melanoma variants correlates with their relative numbers of specific penultimate oligosaccharide structures. *The Journal of biological chemistry* **263**, 7591-7603 (1988).
121. Reddy, B. V. & Kalraiya, R. D. Sialylated beta1,6 branched N-oligosaccharides modulate adhesion, chemotaxis and motility of melanoma cells: Effect on invasion and

- spontaneous metastasis properties. *Biochimica et biophysica acta* **1760**, 1393-1402 (2006).
122. Thies, A., Moll, I., Berger, J. & Schumacher, U. Lectin binding to cutaneous malignant melanoma: HPA is associated with metastasis formation. *British journal of cancer* **84**, 819-823 (2001).
 123. Yoshimura, M., Ihara, Y., Matsuzawa, Y. & Taniguchi, N. Aberrant glycosylation of E-cadherin enhances cell-cell binding to suppress metastasis. *The Journal of biological chemistry* **271**, 13811-13815 (1996).
 124. Litynska, A., Przybylo, M., Hoja-Lukowicz, D., Pochec, E., Kremser, M., Ciolczyk-Wierzicka, D., Labedz, M., Laidler, P. Protein Glycosylation as Marker of Melanoma Progression. *Current Cancer Therapy Reviews* **4** (2008).
 125. Harvey, D. J. *et al.* Fragmentation of negative ions from N-linked carbohydrates, part 4. Fragmentation of complex glycans lacking substitution on the 6-antenna. *Journal of mass spectrometry : JMS* **45**, 528-535 (2010).
 126. Campbell, M. P. *et al.* Validation of the curation pipeline of UniCarb-DB: Building a global glycan reference MS/MS repository. *Biochimica et biophysica acta* (2013).
 127. Maio, M. Melanoma as a model tumour for immuno-oncology. *Annals of oncology : official journal of the European Society for Medical Oncology / ESMO* **23 Suppl 8**, viii10-14 (2012).
 128. Korn, E. L. *et al.* Meta-analysis of phase II cooperative group trials in metastatic stage IV melanoma to determine progression-free and overall survival benchmarks for future phase II trials. *Journal of clinical oncology : official journal of the American Society of Clinical Oncology* **26**, 527-534 (2008).
 129. Przybylo, M. & Litynska, A. Glycans in melanoma screening. Part 1. The role of beta1,6-branched N-linked oligosaccharides in melanoma. *Biochemical Society transactions* **39**, 370-373 (2011).
 130. Herlyn, M. & Shih, I. M. Interactions of melanocytes and melanoma cells with the microenvironment. *Pigment cell research / sponsored by the European Society for Pigment Cell Research and the International Pigment Cell Society* **7**, 81-88 (1994).
 131. Li, G. & Herlyn, M. Dynamics of intercellular communication during melanoma development. *Molecular medicine today* **6**, 163-169 (2000).
 132. Hsu, M. Y. *et al.* E-cadherin expression in melanoma cells restores keratinocyte-mediated growth control and down-regulates expression of invasion-related adhesion receptors. *The American journal of pathology* **156**, 1515-1525 (2000).
 133. Sers, C., Kirsch, K., Rothbacher, U., Riethmuller, G. & Johnson, J. P. Genomic organization of the melanoma-associated glycoprotein MUC18: implications for the evolution of the immunoglobulin domains. *Proceedings of the National Academy of Sciences of the United States of America* **90**, 8514-8518 (1993).
 134. Haass, N. K. & Herlyn, M. Normal human melanocyte homeostasis as a paradigm for understanding melanoma. *J Invest Dermatol Symp Proc* **10**, 153-163 (2005).
 135. Taniguchi, N. *et al.* Implication of GnT-V in cancer metastasis: a glycomic approach for identification of a target protein and its unique function as an angiogenic cofactor. *Glycoconjugate journal* **18**, 859-865 (2001).
 136. Hoja-Lukowicz, D. *et al.* L1CAM from human melanoma carries a novel type of N-glycan with Galbeta1-4Galbeta1- motif. Involvement of N-linked glycans in migratory and invasive behaviour of melanoma cells. *Glycoconjugate journal* **30**, 205-225 (2013).
 137. Rapanotti, M. C. *et al.* Sequential molecular analysis of circulating MCAM/MUC18 expression: a promising disease biomarker related to clinical outcome in melanoma. *Archives of dermatological research* **306**, 527-537 (2014).
 138. Zhang, H. *et al.* CD146 is a potential marker for the diagnosis of malignancy in cervical and endometrial cancer. *Oncology letters* **5**, 1189-1194 (2013).

139. Wu, G. J. *et al.* Expression of a human cell adhesion molecule, MUC18, in prostate cancer cell lines and tissues. *The Prostate* **48**, 305-315 (2001).
140. Shih, I. M. The role of CD146 (Mel-CAM) in biology and pathology. *The Journal of pathology* **189**, 4-11 (1999).
141. Lehmann, J. M., Riethmuller, G. & Johnson, J. P. MUC18, a marker of tumor progression in human melanoma, shows sequence similarity to the neural cell adhesion molecules of the immunoglobulin superfamily. *Proceedings of the National Academy of Sciences of the United States of America* **86**, 9891-9895 (1989).
142. Shih, I. M., Speicher, D., Hsu, M. Y., Levine, E. & Herlyn, M. Melanoma cell-cell interactions are mediated through heterophilic Mel-CAM/ligand adhesion. *Cancer research* **57**, 3835-3840 (1997).
143. Thies, A. *et al.* The developmentally regulated neural crest-associated glycotope HNK-1 predicts metastasis in cutaneous malignant melanoma. *The Journal of pathology* **203**, 933-939 (2004).
144. Zamze, S. *et al.* A family of novel, acidic N-glycans in Bowes melanoma tissue plasminogen activator have L2/HNK-1-bearing antennae, many with sulfation of the fucosylated chitobiose core. *European journal of biochemistry / FEBS* **268**, 4063-4078 (2001).
145. Shih, I. M., Elder, D. E., Speicher, D., Johnson, J. P. & Herlyn, M. Isolation and functional characterization of the A32 melanoma-associated antigen. *Cancer research* **54**, 2514-2520 (1994).
146. Herlyn, M. & Fukunaga-Kalabis, M. What is a good model for melanoma? *The Journal of investigative dermatology* **130**, 911-912 (2010).
147. Bubka, M., Link-Lenczowski, P., Janik, M., Pochec, E. & Litynska, A. Overexpression of N-acetylglucosaminyltransferases III and V in human melanoma cells. Implications for MCAM N-glycosylation. *Biochimie* **103**, 37-49 (2014).
148. Lee, A. *et al.* Rat liver membrane glycoproteome: enrichment by phase partitioning and glycoprotein capture. *Journal of proteome research* **8**, 770-781 (2009).
149. Przybylo, M., Pochec, E., Link-Lenczowski, P. & Litynska, A. Beta1-6 branching of cell surface glycoproteins may contribute to uveal melanoma progression by up-regulating cell motility. *Molecular vision* **14**, 625-636 (2008).
150. Litynska, A. *et al.* Does glycosylation of melanoma cells influence their interactions with fibronectin? *Biochimie* **88**, 527-534 (2006).
151. Chan, A. L. *et al.* A novel sialylated N-acetylgalactosamine-containing oligosaccharide is the major complex-type structure present in Bowes melanoma tissue plasminogen activator. *Glycobiology* **1**, 173-185 (1991).
152. Ferreira, S. A., Vasconcelos, J. L., Cavalcanti, C. L., Rego, M. J. & Beltrao, E. I. Sialic acid differential expression in non-melanoma skin cancer biopsies. *Med Mol Morphol* **46**, 198-202 (2013).
153. <http://www.who.int/en/>.
154. Mactier, S. *et al.* Protein signatures correspond to survival outcomes of AJCC stage III melanoma patients. *Pigment cell & melanoma research* **27**, 1106-1116 (2014).
155. Gould Rothberg, B. E., Bracken, M. B. & Rimm, D. L. Tissue biomarkers for prognosis in cutaneous melanoma: a systematic review and meta-analysis. *Journal of the National Cancer Institute* **101**, 452-474 (2009).
156. Tembe, V. *et al.* MicroRNA and mRNA expression profiling in metastatic melanoma reveal associations with BRAF mutation and patient prognosis. *Pigment cell & melanoma research* **28**, 254-266 (2015).
157. Winnepenninckx, V. *et al.* Gene expression profiling of primary cutaneous melanoma and clinical outcome. *Journal of the National Cancer Institute* **98**, 472-482 (2006).

158. Hardesty, W. M., Kelley, M. C., Mi, D., Low, R. L. & Caprioli, R. M. Protein signatures for survival and recurrence in metastatic melanoma. *Journal of proteomics* **74**, 1002-1014 (2011).
159. Bironaite, D., Nesland, J. M., Dalen, H., Risberg, B. & Bryne, M. N-Glycans influence the in vitro adhesive and invasive behaviour of three metastatic cell lines. *Tumour biology : the journal of the International Society for Oncodevelopmental Biology and Medicine* **21**, 165-175 (2000).
160. Kaufman, K. L. *et al.* Surface antigen profiles of leukocytes and melanoma cells in lymph node metastases are associated with survival in AJCC stage III melanoma patients. *Clinical & experimental metastasis* (2014).
161. Kakavand, H., Scolyer, R. A., Thompson, J. F. & Mann, G. J. Identification of new prognostic biomarkers for Stage III metastatic melanoma patients. *Oncoimmunology* **2**, e25564 (2013).
162. Thijssen, V. L., Heusschen, R., Caers, J. & Griffioen, A. W. Galectin expression in cancer diagnosis and prognosis: A systematic review. *Biochimica et biophysica acta* **1855**, 235-247 (2015).
163. Dennis, J. W. & Laferte, S. Tumor cell surface carbohydrate and the metastatic phenotype. *Cancer metastasis reviews* **5**, 185-204 (1987).
164. Green, E. D. & Baenziger, J. U. Asparagine-linked oligosaccharides on lutropin, follitropin, and thyrotropin. II. Distributions of sulfated and sialylated oligosaccharides on bovine, ovine, and human pituitary glycoprotein hormones. *The Journal of biological chemistry* **263**, 36-44 (1988).
165. Hirano, K., Matsuda, A., Shirai, T. & Furukawa, K. Expression of LacdiNAc groups on N-glycans among human tumors is complex. *BioMed research international* **2014**, 981627 (2014).
166. Dell, A. *et al.* Structural analysis of the oligosaccharides derived from glycodeclin, a human glycoprotein with potent immunosuppressive and contraceptive activities. *The Journal of biological chemistry* **270**, 24116-24126 (1995).
167. Anugraham, M. *et al.* Specific glycosylation of membrane proteins in epithelial ovarian cancer cell lines: glycan structures reflect gene expression and DNA methylation status. *Molecular & cellular proteomics : MCP* **13**, 2213-2232 (2014).
168. Do, K. Y., Do, S. I. & Cummings, R. D. Differential expression of LacdiNAc sequences (GalNAc beta 1-4GlcNAc-R) in glycoproteins synthesized by Chinese hamster ovary and human 293 cells. *Glycobiology* **7**, 183-194 (1997).
169. Machado, E. *et al.* N-Glycosylation of total cellular glycoproteins from the human ovarian carcinoma SKOV3 cell line and of recombinantly expressed human erythropoietin. *Glycobiology* **21**, 376-386 (2011).
170. Che, M. I. *et al.* beta1, 4-N-acetylgalactosaminyltransferase III modulates cancer stemness through EGFR signaling pathway in colon cancer cells. *Oncotarget* **5**, 3673-3684 (2014).
171. Peracaula, R. *et al.* Glycosylation of human pancreatic ribonuclease: differences between normal and tumor states. *Glycobiology* **13**, 227-244 (2003).
172. Fukushima, K., Satoh, T., Baba, S. & Yamashita, K. alpha1,2-Fucosylated and beta-N-acetylgalactosaminylated prostate-specific antigen as an efficient marker of prostatic cancer. *Glycobiology* **20**, 452-460 (2010).
173. Kitamura, N. *et al.* Prognostic significance of reduced expression of beta-N-acetylgalactosaminylated N-linked oligosaccharides in human breast cancer. *International journal of cancer. Journal international du cancer* **105**, 533-541 (2003).
174. Hsu, W. M. *et al.* B4GALNT3 expression predicts a favorable prognosis and suppresses cell migration and invasion via beta(1) integrin signaling in neuroblastoma. *The American journal of pathology* **179**, 1394-1404 (2011).

References

175. Albino, A. P., Lloyd, K. O., Houghton, A. N., Oettgen, H. F. & Old, L. J. Heterogeneity in surface antigen and glycoprotein expression of cell lines derived from different melanoma metastases of the same patient. Implications for the study of tumor antigens. *The Journal of experimental medicine* **154**, 1764-1778 (1981).
176. Kremser, M. E. *et al.* Characterisation of alpha3beta1 and alpha(v)beta3 integrin N-oligosaccharides in metastatic melanoma WM9 and WM239 cell lines. *Biochimica et biophysica acta* **1780**, 1421-1431 (2008).

Appendix 1: Patient clinical information

Tumour_ID	Person_Sex	Stage_at_Bank	Prognosis_TimeSinceLNMet(days)	Tum_NumNodesInv	Tum_Extranodal	Tum_Necrosis
196	Male	Stage III	658	1	no	5%
259	Female	Stage III	1888	1	no	0%
179	Male	Stage III	714	2	yes	0%
61	Female	Stage III	176	4	yes	50%
88	Female	Stage III	3650	2	no	20%
53	Male	Stage III	2408	2	yes	5%
322	Male	Stage III	189	2	no	0
148	Male	Stage IV	430	3	no	5%
175	Male	Stage IV	384	7	yes	40%
313	Female	Stage IV	215	10	yes	10%

Tumour_ID	Tum_NonTumour.	Tum_BRAFmut	Tum_NRASmut	Tum_PIK3CAmut	Tum_EGFRmut	Prognosis_Time Overall	Prim_Site
196	10%	Y	Y	N	N	3273	Abdomen
259	30%	N	Y	N	N	3716	Upper Arm
179	5%	N	N	N	N	1114	Acral - Toe
61	20%	Y	N	N	N	2239	Occult
88	20%	N	N	N	N	3684	Lower Leg
53	10%	N	Y	N	N	3137	Upper Arm
322	10%	Y	N	N	N	734	Upper Leg
148	50%	N	N	N	N	1081	Lower Arm
175	10%	N	Y	N	Y	616	Back
313	5%	N	Y	N	N	831	Upper Arm

Tumour_ID	Prim_Stage	Prim_Istage	Prim_NStage	Prim_Breslow	Prim_Clar	Prim_Histol	Prim_UIC
196	Stage I	T2 (0.76 - 1.5 OR level III)	N0 (No regional node metastasis)	1	4	SSM	No
259	Stage II	T3a (1.51 - 3.0 mm)	N0 (No regional node metastasis)	2.5	4	SSM	No
179	Stage III	T3b (3.01 - 4.0 mm) TX (Primary cannot be assessed)	N0 (No regional node metastasis)	4	5	Acral Lentiginous	Yes
61	Stage III		N1 (Metastasis <= 3 cm)	NA	NA	Not Known	
88	Stage III	T4b (satellites <2cm away)	N1 (Metastasis <= 3 cm)	4.5	4	NM	No
53	Stage II	T4a (> 4.0 mm OR level V)	N0 (No regional node metastasis)	6.2	5	SSM	No
322	Stage II	T4a (> 4.0 mm OR level V)	N0 (No regional node metastasis)	4.5	4	SSM	Yes
148	Stage II	T3a (1.51 - 3.0 mm)	N0 (No regional node metastasis)	2.2	4	SSM	No
175	Stage III	T3a (1.51 - 3.0 mm)	N1 (Metastasis <= 3 cm)	2.3	3	SSM	Yes
313	Stage II	T3a (1.51 - 3.0 mm)	N0 (No regional node metastasis)	2.3	4	NM	Yes

Appendix 2: Ethics approval

Macquarie University Mail - External Approval Noted- Packer (Ref: 5201200519)

29/03/2015 7:27 pm


MACQUARIE
University

Jodie Abrahams <jodie.abrahams@mq.edu.au>

External Approval Noted- Packer (Ref: 5201200519)

Ethics Secretariat <ethics.secretariat@mq.edu.au>
 To: Prof Nicki Packer <nicki.packer@mq.edu.au>
 Cc: Ms Jodie Abrahams <jodie.abrahams@mq.edu.au>

Tue, Jul 3, 2012 at 10:13 AM

Dear Prof Packer

Re: "Glycosylation and melanoma"

The above application was considered by the Executive of the Human Research Ethics Committee. In accordance with section 5.5 of the National Statement on Ethical Conduct in Human Research (2007) the Executive noted the final approval from the NSW Health Sydney Local Health Network and your right to proceed under their authority.

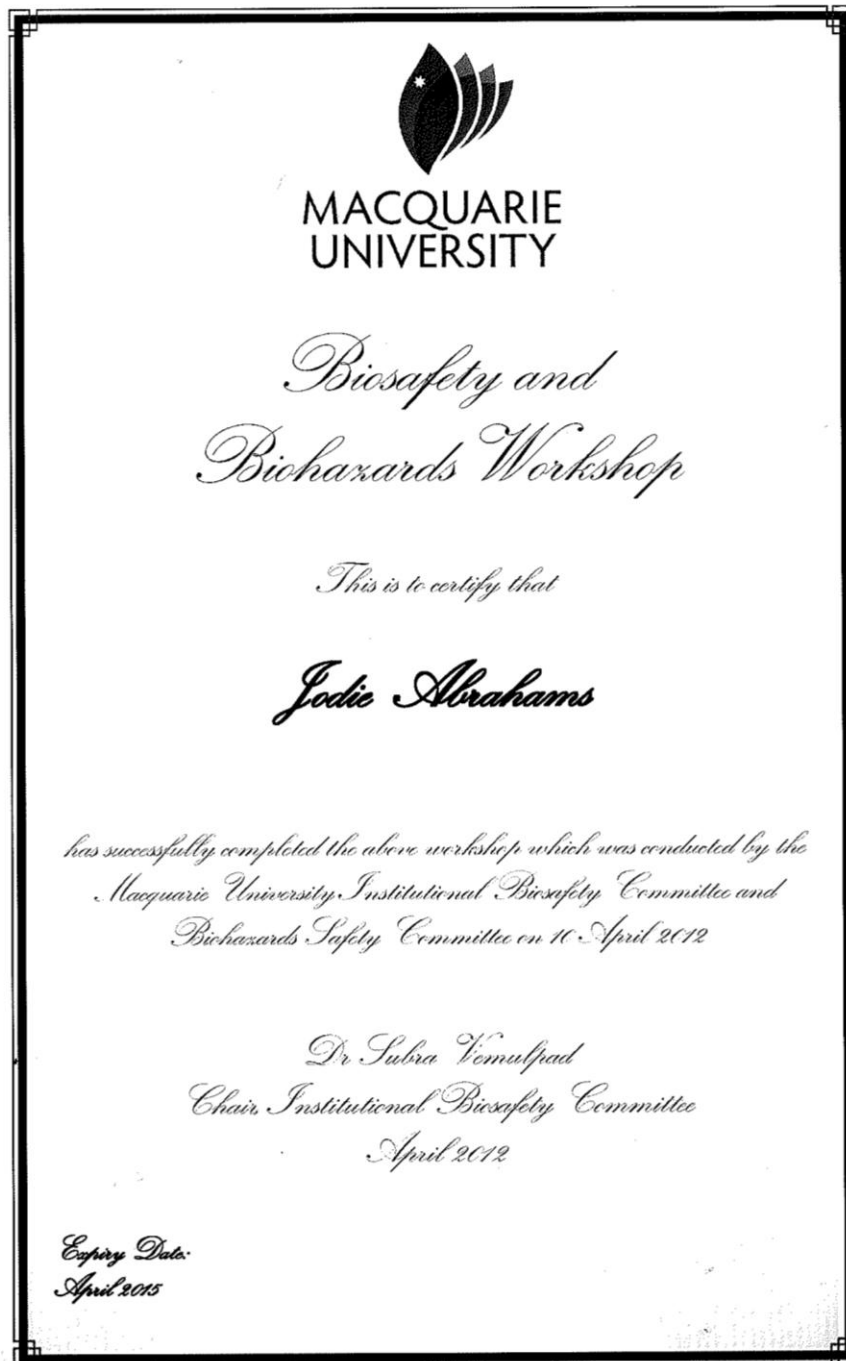
Please do not hesitate to contact the Ethics Secretariat if you have any questions or concerns.

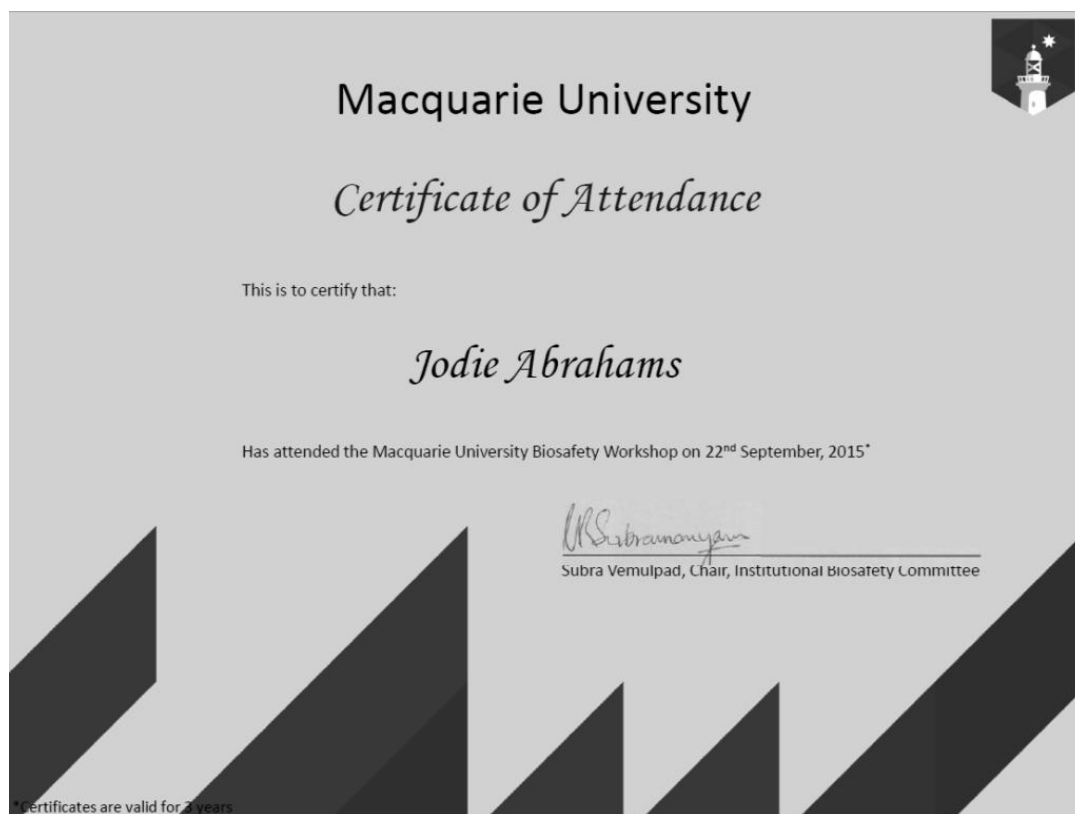
Please retain a copy of this email as this is your official notification of external approval being noted.



Yours sincerely

Dr Karolyn White
 Director of Research Ethics
 Chair, Human Research Ethics Committee

Appendix 3: Biosafety approval





SECTION A		Biohazard Risk Assessment Form – NON GMO		Notification Number:
 		LJK270412EHA		
Investigator completing assessment:	Liisa Kautto Jodie Abrahams, Shi Xian Edward Moh	Date of assessment:	27/04/2012	
Department:	CBIM S	Name of Supervisor submitting this assessment:	Prof. Nicolle Packer	
Contact number/email:	*9257/6955 liisa.kautto@mq.edu.au, jodie.abrahams@mq.edu.au			
Reason for this assessment				
<input checked="" type="checkbox"/> New research <input type="checkbox"/> New information relating to existing research <input type="checkbox"/> other _____				
Exact location(s) of research:				
E8C323 APAF PC2 cell culture laboratory, E8C320 normal laboratory				
Control measures: Eliminate risk <input type="checkbox"/> Substitute the hazard <input type="checkbox"/> Isolate the hazard <input checked="" type="checkbox"/> Implement engineering controls <input checked="" type="checkbox"/> Administration <input checked="" type="checkbox"/> (e.g. Training) PPE <input checked="" type="checkbox"/>				
PC2 and biological waste disposal training received				
Supporting documents which must be read in conjunction with this assessment. (e.g. Safe Working Procedures, Safety Data Sheets, Guidelines/Protocols)				
What is the type of the biological material?				
Bacteria <input type="checkbox"/> Fungi <input type="checkbox"/> Virus <input type="checkbox"/> Cell Line <input checked="" type="checkbox"/> Tissue <input checked="" type="checkbox"/> Parasite <input type="checkbox"/> Animal <input type="checkbox"/> Plant <input type="checkbox"/> Soil <input type="checkbox"/> Toxin <input type="checkbox"/> Prions <input type="checkbox"/> Nucleic Acid <input type="checkbox"/> other _____				
What is the name of the biological agent?				
ATCC Cell lines HCT116 (colon cancer), OCI-AML (leukemia), A549 (Lung cancer), and HL-60 (leukemia), tissue samples obtained from melanoma patients				
Rat heart and liver tissue obtained from MQ hospital research group				
List the Personal Protective Equipment required:				
Gloves <input checked="" type="checkbox"/> Nitrile _____ (e.g. chemical resistant) Eye protection <input checked="" type="checkbox"/> _____ (e.g. safety glasses/goggles) Clothing _____ <input checked="" type="checkbox"/> (e.g. button up lab coat/coveralls/apron)				
Footwear <input checked="" type="checkbox"/> _____ (e.g. Enclosed/Gumboots/overshoe covers) Respiratory Protection <input type="checkbox"/> _____ (e.g. PF2 face mask) Other <input type="checkbox"/> _____				

The University does not hold risk group 4 microorganisms

What are the risks associated with this Biological Agent. (Can be more than one risk group depending on method)			
Risk Group	Details of Biohazards	Biosafety level	Risk Reduction Measures (must be followed by the researcher)
Group 1- Low Individual and community risk (Microorganism that is unlikely to cause human, plant or animal disease)	Human cell lines, well characterised, provided by Patrys Ltd, originally from ATCC collection (HCT116 [ATCC CCL-247], OCI-AML1 originally obtained from the Ontario Cancer Institute (Toronto, Canada)], A549 [ATCC CCL185], HL-60 [ATCC CCL-240]) Rat heart and liver tissue obtained after been euthanized prior to disposal from healthy, clinical research rat kept in animal house	PC2 APAF cell culture room EBC323 (because of high risk of cell lines get contamination from us)	<ol style="list-style-type: none"> Standard laboratory procedures will be followed in accordance with Laboratory Microbiological Standards AS/NZ 2243:3:2010 and university guidelines (see supporting documents - Section A above) and include spillage and emergency response. Investigator has attended university Biosafety training course (see 3) Supervisor identified in Section A confirms that the investigator has received appropriate training and instruction or has adequate supervision and understands safe laboratory practice according to AS/NZ 2243:3:2010 and university guidelines (see supporting documents - Section A above)
Group 2- Moderate individual risk, limited community risk (Microorganism that is unlikely to be a significant risk to laboratory workers, the community/livestock/environment. Laboratory exposures may cause infection but effective treatment and preventative measures are available and the risk of spread is limited).	Human tissue samples (patient tested for HIV, Hepatitis A, B) collected and provided by collaborators Patrys Ltd, Melbourne and Westmead Institute for Cancer Research, Westmead Hospital.	PC2 APAF cell culture room EBC323	<ol style="list-style-type: none"> Standard laboratory procedures will be followed in accordance with Laboratory Microbiological Standards AS/NZ 2243:3:2010 and university guidelines which are appropriate for Risk Group 2 (see supporting documents - Section A above) and include spillage and emergency response. Investigator has attended university Biosafety training course (see 3) Supervisor identified in Section A confirms that the investigator has received appropriate training and instruction or has adequate supervision and understands safe laboratory practice according to AS/NZ 2243:3:2010 and university guidelines (see supporting documents - Section A above)
Group 3 -High individual risk, limited community risk (Microorganisms that usually causes serious human or animal disease and may present a significant risk to laboratory workers. It could present a limited to moderate risk if spread in the community or the environment, but there are usually effective preventative measures or treatment available).			<ol style="list-style-type: none"> Standard laboratory procedures will be followed in accordance with Laboratory Microbiological Standards AS/NZ 2243:3:2010 and university guidelines which are appropriate for Risk Group 3 (see supporting documents - Section A above) and include spillage and emergency response. Investigator has attended university Biosafety training course (see 3) Supervisor identified in Section A confirms that the investigator has received appropriate training and instruction or has adequate supervision

Source: Manager, Health & Safety

Created: March 2012

Document No: 68

Revised: N/A

Version No: 1

Hardcopies of this document are considered uncontrolled.
Please refer to the Health & Safety internet site for latest version.

Page 2 of 4

Source: Manager, Health & Safety
Created: March 2012
Document No: 68
Revised: N/A
Version No: 1

centrifugation and detergent addition steps. All waste generated such as tips, tubes will be disposed into biohazard waste bags and will be autoclaved prior dispose.
Lab bench will be sterilised after work with 70% ethanol

SECTION B



Biohazard Safety Committee – Risk Assessment Decision

Notification Number: LK270412EHA

Important Information

For non GMO investigations email this assessment to biohazard@mq.edu.au for approval by the Biohazard Safety Committee.

Individual Responsibilities

By submitting this assessment the **Supervisor** identified in Section A, confirms that any supporting documents, training, guidance, instruction or protocols issued by the University will be followed so far as reasonably practicable to ensure the work is carried out without risk to health, safety or the environment. The named **Supervisor** confirms that the investigator has received appropriate training and instruction or will have adequate supervision and understands safe laboratory practice according to [AS/NZS 2243:3:2010](#) and university guidelines.

Decision to be completed by the Biohazard Safety Committee:

The Committee has agreed that this risk assessment is sufficient for investigations to commence? Yes ☒ No ☐ Further action required ☒

Further Action/Comments:

- Remove "glassware will be decontaminated with 70% ethanol" under the cell culture heading.
- Use sodium hypochlorite to soak contaminated glassware prior to washing

Name of Approver (Committee Rep):	Michael Gillings (Chairperson, Biohazard Committee)
Extension and email address:	Michael.gillings@mq.edu.au ext: 8199
Date Approved and submitted to Health and Safety Unit:	4 th September, 2012

Hardcopies of this document are considered uncontrolled.

Please refer to the Health & Safety internet site for latest version.

Source: Manager, Health & Safety
Created: March 2012
Document No: 68
Revised: N/A
Version No: 1

